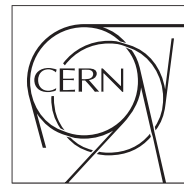




The Compact Muon Solenoid Experiment  
**Analysis Note**

The content of this note is intended for CMS internal use and distribution only



October 31, 2012

# Search for Direct Stop Quark Pair Production in the Single Lepton Channel at 8 TeV

L. Bauerdick, K. Burkett, I. Fisk, Y. Gao, O. Gutsche, B. Hooberman, S. Jindariani, J. Linacre, V. Martinez Outschoorn

*Fermilab National Accelerator Laboratory, Batavia, USA*

C. Campagnari, A. George, F. Golf, D. Kovalevsky, V. Krutelyov

*University of California, Santa Barbara, Santa Barbara, USA*

G. Cerati, M. D'Alfonso, D. Evans, R. Kelley, I. MacNeill, S. Padhi, Y. Tu, F. Würthwein, V. Welke, A. Yagil, J. Yoo

*University of California, San Diego, San Diego, USA*

## Abstract

This note describes a search for direct stop quark pair production in the single lepton channel using  $9.7 \text{ fb}^{-1}$  of pp collision data at  $\sqrt{s} = 8 \text{ TeV}$  taken with the CMS detector in 2012. A search for an excess of events over the Standard Model prediction is performed in a sample with a single isolated electron or muon, several jets including a b-tagged jet, missing transverse energy, and large transverse mass.

# Contents

<b>1</b>	<b>Introduction</b>	<b>3</b>
<b>2</b>	<b>Overview and Strategy for Background Determination</b>	<b>3</b>
2.1	$\ell +$ jets background . . . . .	4
2.2	Dilepton background . . . . .	5
2.3	Other backgrounds . . . . .	5
2.4	Future improvements . . . . .	6
<b>3</b>	<b>Data Samples</b>	<b>6</b>
<b>4</b>	<b>Event Selection</b>	<b>8</b>
4.1	Single Lepton Selection . . . . .	8
4.2	Isolated track veto . . . . .	8
4.3	Signal Region Selection . . . . .	8
4.4	Control Region Selection . . . . .	9
4.5	Definition of $M_T$ peak region . . . . .	10
4.6	Default $t\bar{t}$ MC sample . . . . .	10
4.7	MC Corrections . . . . .	10
4.7.1	Corrections to Jets and $E_T^{\text{miss}}$ . . . . .	10
4.8	Lepton Selection Efficiency Measurements . . . . .	10
4.9	Trigger Efficiency Measurements . . . . .	16
<b>5</b>	<b>Control Region Studies</b>	<b>18</b>
5.1	W+Jets MC Modelling Validation from CR1 . . . . .	18
5.2	Single Lepton Top MC Modelling Validation from CR2 . . . . .	23
5.3	Dilepton studies in CR4 . . . . .	25
5.3.1	Modeling of Additional Hard Jets in Top Dilepton Events . . . . .	25
5.3.2	Validation of the “Physics” Modelling of the $t\bar{t} \rightarrow \ell\ell$ MC in CR4 . . . . .	28
5.4	Test of control region with isolated track in CR5 . . . . .	31
<b>6</b>	<b>Other Backgrounds</b>	<b>35</b>
<b>7</b>	<b>Tail-to-Peak ratio for lepton + jets top and W events</b>	<b>35</b>
<b>8</b>	<b>Background Prediction</b>	<b>37</b>
<b>9</b>	<b>Systematic Uncertainties on the Background</b>	<b>41</b>
9.1	Statistical uncertainties on the event counts in the $M_T$ peak regions . . . . .	41
9.2	Uncertainty from the choice of $M_T$ peak region . . . . .	41
9.3	Uncertainty on the $W+jets$ cross-section and the rare MC cross-sections . . . . .	41

9.4	Tail-to-peak ratios for lepton + jets top and W events . . . . .	41
9.5	Uncertainty on extra jet radiation for dilepton background . . . . .	42
9.6	Uncertainty from MC statistics . . . . .	42
9.7	Uncertainty on the $t\bar{t} \rightarrow \ell\ell$ Background . . . . .	42
9.7.1	Check of the impact of Signal Contamination . . . . .	44
9.7.2	Check of the uncertainty on the $t\bar{t} \rightarrow \ell\ell$ Background . . . . .	44
9.8	Uncertainty from the isolated track veto . . . . .	50
9.8.1	Isolated Track Veto: Tag and Probe Studies . . . . .	50
9.9	Summary of uncertainties . . . . .	54
<b>10</b>	<b>Results</b>	<b>56</b>
<b>11</b>	<b>Limits</b>	<b>60</b>
<b>12</b>	<b>Conclusion</b>	<b>69</b>
<b>A</b>	<b>Performance of the Isolation Requirement</b>	<b>70</b>
<b>B</b>	<b>Example BG prediction calculation</b>	<b>72</b>
B.1	Central value of dilepton background . . . . .	72
B.2	Central value of the $t\bar{t} \rightarrow \ell + \text{jets}$ background . . . . .	72
B.3	Central value for the $W + \text{jets}$ background . . . . .	73
B.4	Central value for the rare backgrounds . . . . .	73
<b>C</b>	<b>Additional CR Data and MC Comparisons</b>	<b>74</b>
<b>D</b>	<b>Control Region Plots Summary</b>	<b>79</b>
D.1	CR4: $\geq 1$ b-tag, exactly 2 leptons . . . . .	79
D.2	CR5: $\geq 1$ b-tag, 1 lepton + 1 isolated track . . . . .	80
D.3	CR1: 0 b-tags, exactly 1 lepton . . . . .	81
D.4	CR2: 0 b-tags, exactly 2 leptons . . . . .	82
<b>E</b>	<b>Signal Kinematics</b>	<b>83</b>
<b>F</b>	<b>Model dependence of the signal acceptance</b>	<b>85</b>
<b>G</b>	<b>Glossary of abbreviations</b>	<b>85</b>

# 1 Introduction

This note presents a search for the production of supersymmetric (SUSY) stop quark pairs in events with a single isolated lepton, several jets, missing transverse energy, and large transverse mass. We use a data sample corresponding to an integrated luminosity of  $9.7 \text{ fb}^{-1}$ . This search is of theoretical interest because of the critical role played by the stop quark in solving the hierarchy problem in SUSY models. This solution requires that the stop quark be light, less than a few hundred GeV and hence within reach for direct pair production. We focus on two decay modes  $\tilde{t} \rightarrow t\chi_1^0$  and  $\tilde{t} \rightarrow b\chi_1^+$  which are expected to have large branching fractions if they are kinematically accessible, leading to:

- $pp \rightarrow \tilde{t}\bar{t} \rightarrow t\bar{t}\chi_1^0\chi_1^0$ , and
- $pp \rightarrow \tilde{t}\bar{t} \rightarrow b\bar{b}\chi_1^+\chi_1^- \rightarrow b\bar{b}W^+W^-\chi_1^0\chi_1^0$ .

Both of these signatures contain high transverse momentum ( $p_T$ ) jets including two b-jets, and missing transverse energy ( $E_T^{\text{miss}}$ ) due to the invisible  $\chi_1^0$  lightest SUSY particles (LSP's). In addition, the presence of two W bosons leads to a large branching fraction to the single lepton final state. Hence we require the presence of exactly one isolated, high  $p_T$  electron or muon, which provides significant suppression of several backgrounds that are present in the all-hadronic channel. The largest backgrounds for this signature are semi-leptonic  $t\bar{t}$  and  $W+\text{jets}$ . These backgrounds contain a single leptonically-decaying W boson, and the transverse mass ( $M_T$ ) of the lepton-neutrino system has a kinematic endpoint requiring  $M_T < M_W$ . For signal stop quark events, the presence of additional LSP's in the final states allows the  $M_T$  to exceed  $M_W$ . Hence we search for an excess of events with large  $M_T$ . The dominant background in this kinematic region is dilepton  $t\bar{t}$  where one of the leptons is not identified, since the presence of two neutrinos from leptonically-decaying W bosons allows the  $M_T$  to exceed  $M_W$ . Backgrounds are estimated from Monte Carlo (MC) simulation, with careful validation and determination of scale factors (where necessary) and corresponding uncertainties based on data control samples.

The expected stop quark pair production cross section (see Fig. 1) varies between 18 pb for  $m_{\tilde{t}} = 200 \text{ GeV}$  and 0.09 pb for  $m_{\tilde{t}} = 500 \text{ GeV}$  [1]. The critical challenge of this analysis is due to the fact that for light stop quarks ( $m_{\tilde{t}} \approx m_t$ ), the production cross section is large but the kinematic distributions, in particular  $M_T$ , are very similar to SM  $t\bar{t}$  production. In this regime it becomes very difficult to distinguish the signal and background. For large stop quark mass the kinematic distributions differ from those in SM  $t\bar{t}$  production, but the cross section decreases rapidly, reducing the signal-to-background ratio.

## 2 Overview and Strategy for Background Determination

We are searching for a  $t\bar{t}\chi_1^0\chi_1^0$  or  $WbW\bar{b}\chi_1^0\chi_1^0$  final state (after top decay in the first mode, the final states are actually the same). So to first order this is “ $t\bar{t}$ + extra  $E_T^{\text{miss}}$ ”.

We work in the  $\ell+\text{jets}$  final state, where the main background is  $t\bar{t}$ . We look for  $E_T^{\text{miss}}$  inconsistent with  $W \rightarrow \ell\nu$ . We do this by concentrating on the  $\ell\nu$  transverse mass ( $M_T$ ), since except for resolution and W-off-shell effects,  $M_T < M_W$  for  $W \rightarrow \ell\nu$ . Thus, the initial analysis is simply a counting experiment in the tail of the  $M_T$  distribution.

The event selection is one-and-only-one high  $p_T$  isolated lepton, four or more jets, and an  $E_T^{\text{miss}}$  cut. At least one of the jets has to be b tagged to reduce  $W+\text{jets}$ . The event sample is then dominated by  $t\bar{t}$ , but there are also contributions from  $W+\text{jets}$ , single top, dibosons, as well as rare SM processes such as  $ttW$ .

The  $t\bar{t}$  events in the  $M_T$  tail can be broken up into two categories: (i)  $t\bar{t} \rightarrow \ell+\text{jets}$ , and (ii)  $t\bar{t} \rightarrow \ell^+\ell^-$  where one of the two leptons is not found by the second-lepton-veto (here the second lepton can be a hadronically decaying  $\tau$ ). For a reasonable  $M_T$  cut, say  $M_T > 150 \text{ GeV}$ , the dilepton background is approximately 70% of the total. This is because in dileptons there are two neutrinos from W decay, thus  $M_T$  is not bounded by  $M_W$ . This is a very important point: while it is true that we are looking in the tail of  $M_T$ , the bulk of the background events end up there not because of some exotic  $E_T^{\text{miss}}$  reconstruction failure, but because of well understood physics processes. This means that the background estimate can be taken from Monte Carlo (MC) after carefully accounting for possible data/MC differences.

The search is performed in a number of Signal Regions (SRs) defined by minimum requirements on  $E_T^{\text{miss}}$  and  $M_T$ . The SRs are defined in Section 4.3.

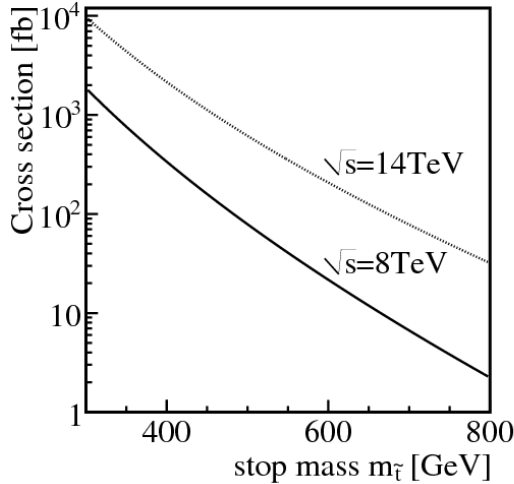


Figure 1: The stop quark pair production cross section as a function of the stop quark mass [2].

- 51 In Section 5 we will describe the analysis of various Control Regions (CRs) that are used to test the  
 52 Monte Carlo model and, if necessary, to extract data/MC scale factors. In this section we give a general  
 53 description of the procedure. The details of how the final background prediction is assembled are given  
 54 in Section 8.
- 55 One general point is that in order to minimize systematic uncertainties, the MC background predictions  
 56 are whenever possible normalized to the bulk of the  $t\bar{t}$  data, i.e. events passing all of the requirements  
 57 but with  $M_T \approx 80$  GeV. This (mostly) removes uncertainties due to  $\sigma(t\bar{t})$ , lepton ID, trigger efficiency,  
 58 luminosity, etc.

## 59 2.1 $\ell +$ jets background

- 60 The  $\ell +$  jets background is dominated by  $t\bar{t} \rightarrow \ell +$  jets, but also includes some  $W +$  jets as well as single  
 61 top. The MC input used in the background estimation is the ratio of the number of events with  $M_T$  in  
 62 the signal region to the number of events with  $M_T \approx 80$  GeV. This ratio is (possibly) corrected by a  
 63 data/MC scale factor obtained from a study of CRs, as outlined below.
- 64 Note that the ratio described above is actually different for  $t\bar{t}$ /single top and  $W +$  jets. This is because  
 65 in  $W$  events there is a significant contribution to the  $M_T$  tail from very off-shell  $W$ s. This contribution  
 66 is much smaller in top events because  $M(\ell\nu)$  cannot exceed  $M_{top} - M_b$ . Therefore the large  $M_T$  tail in  
 67  $t\bar{t}$ /single top is dominated by jet resolution effects, while for  $W +$  jets events the large  $M_T$  tail is dominated  
 68 by off-shell  $W$  production.
- 69 For  $W +$  jets the ability of the Monte Carlo to model this ratio ( $R_{wjet}$ ) is validated in a sample of  $\ell +$  jets  
 70 enriched in  $W +$  jets by the application of a b-veto. The equivalent ratio for top events ( $R_{top}$ ) is tested  
 71 in a sample of well identified  $Z \rightarrow \ell\ell$  with one lepton added to the  $E_T^{\text{miss}}$  calculation. This sample is well  
 72 suited to testing the resolution effects on the  $M_T$  tail, since off-shell effects are eliminated by the  $Z$ -mass  
 73 requirement. However, this test is unfortunately statistically limited and its usefulness is limited to event

74 selections with modest  $E_T^{\text{miss}}$  requirements.

75 Note that the fact that the ratios are different for  $t\bar{t}$ /single top and  $W +$  jets introduces a systematic  
76 uncertainty in the background calculation because one needs to know the relative fractions of these two  
77 components in the  $M_T \approx 80$  GeV lepton + jets sample.

## 78 2.2 Dilepton background

79 To suppress dilepton backgrounds, we veto events with an isolated track of  $p_T > 10$  GeV (see Sec. 4.2  
80 for details). Being the common feature for electron, muon, and one-prong tau decays, this veto is highly  
81 efficient for rejecting  $t\bar{t}$  to dilepton events. The remaining dilepton background can be classified into the  
82 following categories:

- 83     • lepton is out of acceptance ( $|\eta| > 2.5$ )
- 84     • lepton has  $p_T < 10$  GeV, and is inside the acceptance
- 85     • lepton has  $p_T > 10$  GeV, is inside the acceptance, but survives the additional isolated track veto

86 The last category includes 1-prong and 3-prong hadronic tau decays, as well as electrons and muons either  
87 from direct W decay or via  $W \rightarrow \tau \rightarrow \ell$  decay that fail the isolation requirement. We note that at present  
88 we do not attempt to veto 3-prong tau decays as they are about 15% of the total dilepton background  
89 according to the MC.

90 The high  $M_T$  dilepton background predictions come from MC, but their rate is normalized to the  $M_T \approx 80$   
91 GeV peak. In order to perform this normalization in data, the rare background events in the  $M_T$  peak  
92 are subtracted off. This also introduces a systematic uncertainty.

93 There are two types of effects that can influence the MC dilepton prediction: physics effects and instru-  
94 mental effects. We discuss these next, starting from physics.

95 First of all, many of our  $t\bar{t}$  MC samples (e.g. MadGraph) have  $\text{BR}(W \rightarrow \ell\nu) = \frac{1}{9} = 0.1111$ . PDG says  
96  $\text{BR}(W \rightarrow \ell\nu) = 0.1080 \pm 0.0009$ . This difference matters, so the  $t\bar{t}$  MC must be corrected to account for  
97 this.

98 Second, our selection is  $\ell + 4$  or more jets. A dilepton event passes the selection only if there are two  
99 additional jets from ISR, or one jet from ISR and one jet which is reconstructed from the unidentified  
100 lepton, e.g., a three-prong tau. Therefore, all MC dilepton  $t\bar{t}$  samples used in the analysis must have  
101 their jet multiplicity corrected (if necessary) to agree with what is seen in  $t\bar{t}$  data. We use a data control  
102 sample of well identified dilepton events with  $E_T^{\text{miss}}$  and at least one jet (including at least one b-tag) as  
103 a template to “adjust” the  $N_{jet}$  distribution of the  $t\bar{t} \rightarrow$  dileptons MC samples.

104 The final physics effect has to do with the modeling of  $t\bar{t}$  production and decay. Different MC models  
105 could in principle result in different BG predictions. Therefore we use several different  $t\bar{t}$  MC samples  
106 using different generators and different parameters, to test the stability of the dilepton BG prediction.  
107 All these predictions, **after** corrections for branching ratio and  $N_{jet}$  dependence, are compared to each  
108 other. The spread is a measure of the systematic uncertainty associated with the  $t\bar{t}$  generator modeling.

109 The main instrumental effect is associated with the efficiency of the isolated track veto. We use tag-  
110 and-probe to compare the isolated track veto performance in  $Z + 4$  jets data and MC. Note that the  
111 performance of the isolated track veto is not exactly the same on  $e/\mu$  and on one prong hadronic tau  
112 decays. This is because the pions from one-prong taus are often accompanied by  $\pi^0$ 's that can then  
113 result in extra tracks due to photon conversions. We let the simulation take care of that. Note that JES  
114 uncertainties are effectively “calibrated away” by the  $N_{jet}$  rescaling described above.

## 115 2.3 Other backgrounds

116 Other backgrounds are  $tW$ ,  $ttV$ , dibosons, tribosons, and Drell Yan. These are small. They are taken  
117 from MC with appropriate scale factors for trigger efficiency, and reweighting to match the distribution  
118 of reconstructed primary vertices in data.

119 **2.4 Future improvements**

120 Finally, there are possible improvements to this basic analysis strategy that can be added in the future:

- 121 • Move from counting experiment to shape analysis. But first, we need to get the counting experiment  
122 under control.
- 123 • Add an explicit three prong tau veto
- 124 • Do something to require that three of the jets in the event be consistent with  $t \rightarrow Wb, W \rightarrow q\bar{q}$ .  
125 This could help reject some of the dilepton BG in the search for  $\tilde{t} \rightarrow t\chi^0$ , but is not applicable to  
126 the  $\tilde{t} \rightarrow b\chi^+$  search.
- 127 • Consider the  $M(\ell b)$  variable, which is not bounded by  $M_{top}$  in  $\tilde{t} \rightarrow b\chi^+$

128 **3 Data Samples**

129 The datasets used for this analysis are summarized in Tables 1 (data) and 2 (MC). The total integrated  
130 luminosity is  $9.7 \text{ fb}^{-1}$  after applying the official good run list. The main  $t\bar{t}$  Monte Carlo sample is gen-  
131 erated with Powheg since this sample has the largest number of events, though samples with alternative  
132 generators such as Madgraph are also used for the derivation of systematic uncertainties in the  $t\bar{t}$  back-  
133 ground prediction. The triggers used to select both the signal and control samples are also summarized  
134 in Table 3.

Dataset Name
Single Lepton Samples
/SingleElectron/Run2012A-13Jul2012-v1/AOD
/SingleMu/Run2012A-13Jul2012-v1/AOD
/SingleElectron/Run2012B-13Jul2012-v1/AOD
/SingleMu/Run2012B-13Jul2012-v1/AOD
/SingleElectron/Run2012C-PromptReco-v1/AOD
/SingleMu/Run2012C-PromptReco-v1/AOD
/SingleElectron/Run2012C-PromptReco-v2/AOD
/SingleMu/Run2012C-PromptReco-v2/AOD
Dilepton Samples (only used for dilepton control region)
/DoubleElectron/Run2012A-13Jul2012-v1/AOD
/DoubleMu/Run2012A-13Jul2012-v1/AOD
/MuEG/Run2012A-13Jul2012-v1/AOD
/DoubleElectron/Run2012B-13Jul2012-v1/AOD
/DoubleMu/Run2012B-13Jul2012-v1/AOD
/MuEG/Run2012B-13Jul2012-v1/AOD
/DoubleElectron/Run2012C-PromptReco-v1/AOD
/DoubleMu/Run2012C-PromptReco-v1/AOD
/MuEG/Run2012C-PromptReco-v1/AOD
/DoubleElectron/Run2012C-PromptReco-v2/AOD
/DoubleMu/Run2012C-PromptReco-v2/AOD
/MuEG/Run2012C-PromptReco-v2/AOD

Table 1: Summary of data datasets used.

With Pileup: Processed dataset name is (53) Summer12_DR53X-PU_S10_START53_V7A-v*/AODSIM (52) Summer12-START52_V9_FSIM-v*/AODSIM		
Description	Primary Dataset Name	cross-section [pb]
$t\bar{t}$	/TT_CTE10_TuneZ2Star_8TeV-powheg-tauola (53)	225.2
$W \rightarrow \ell\nu$	/WJetsToLNu_TuneZ2Star_8TeV-madgraph-tauola (53)	37509
$W \rightarrow \ell\nu+3$ jets	/W3JetsToLNu_TuneZ2Star_8TeV-madgraph-tauola (53)	640
$W \rightarrow \ell\nu+\geq 4$ jets	/W4JetsToLNu_TuneZ2Star_8TeV-madgraph-tauola (53)	264
WW	/WWJetsTo2L2Nu_TuneZ2star_8TeV-madgraph-tauola (53)	5.8
WZ	/WZJetsTo3LNu_TuneZ2_8TeV-madgraph-tauola (53)	1.1
ZZ	/WZJetsTo2L2Q_TuneZ2star_8TeV-madgraph-tauola (53)	1.1
	/ZZJetsTo2L2Nu_TuneZ2star_8TeV-madgraph-tauola (53)	0.4
	/ZZJetsTo4L_TuneZ2star_8TeV-madgraph-tauola (53)	0.2
	/ZZJetsTo2L2Q_TuneZ2star_8TeV-madgraph-tauola (53)	2.4
$t$ ( $s$ -chan)	/T_TuneZ2Star_s-channel_8TeV-powheg-tauola (53)	3.9
$\bar{t}$ ( $s$ -chan)	/Tbar_TuneZ2Star_s-channel_8TeV-powheg-tauola (53)	1.8
$t$ ( $t$ -chan)	/T_TuneZ2Star_t-channel_8TeV-powheg-tauola (53)	55.5
$\bar{t}$ ( $t$ -chan)	/Tbar_TuneZ2Star_t-channel_8TeV-powheg-tauola (53)	30.0
$tW$	/T_TuneZ2Star_tW-channel-DR_8TeV-powheg-tauola (53)	11.2
$t\bar{W}$	/Tbar_TuneZ2Star_tW-channel-DR_8TeV-powheg-tauola (53)	11.2
$Z/\gamma^* \rightarrow \ell\ell$	/DYJetsToLL_TuneZ2Star_M-50_8TeV-madgraph-tarball (53)	3532.8
$Z/\gamma^* \rightarrow \ell\ell+\geq 4$ jets	/DY4JetsToLL_TuneZ2Star_M-50_8TeV-madgraph-tarball (53)	27.6
$t\bar{t}W$	/TTW_TuneZ2Star_8TeV-madgraph (53)	0.23
$t\bar{t}Z$	/TTZ_TuneZ2Star_8TeV-madgraph (53)	0.21
$t\bar{t}\gamma$	/TTGJets_TuneZ2Star_8TeV-madgraph (53)	0.65
WWW	/WWWW_TuneZ2Star_8TeV-madgraph (53)	0.082
WWZ	/WWZNoGstar_TuneZ2Star_8TeV-madgraph (53)	0.063
WZZ	/WZZNoGstar_TuneZ2Star_8TeV-madgraph (53)	0.019
ZZZ	/ZZZNoGstar_TuneZ2Star_8TeV-madgraph (53)	0.019
$\tilde{t}\tilde{t} \rightarrow t\bar{t}\chi_1^0\chi_1^0$	/SMS-T2tt_FineBin_Mstop-225to1200_mLSP-0to1000_8TeV-Pythia6Z (52)	scan
$\tilde{t}\tilde{t} \rightarrow b\bar{b}\chi_1^+\chi_1^-$	/SMS-T2bw_FineBin_Mstop-100to600_mLSP-0to500_8TeV-Pythia6Z (52)	scan
<hr/>		
$t\bar{t}$	/TTJets_MassiveBinDECAY_TuneZ2Star_8TeV-madgraph-tauola (53)	225.2
$t\bar{t}$ ( $Q^2 \times 2$ )	/TTjets_TuneZ2Star_scaleup_8TeV-madgraph-tauola (53)	225.2
$t\bar{t}$ ( $Q^2 \times 0.5$ )	/TTjets_TuneZ2Star_scaledown_8TeV-madgraph-tauola (53)	225.2
$t\bar{t}$ ( $x_q > 40$ GeV)	/TTjets_TuneZ2Star_matchingup_8TeV-madgraph-tauola (53)	225.2
$t\bar{t}$ ( $x_q > 10$ GeV)	/TTjets_TuneZ2Star_matchingdown_8TeV-madgraph-tauola (53)	225.2
$t\bar{t}$ ( $m_{top} = 178.5$ GeV)	/TTJets_TuneZ2Star_mass178.5_8TeV-madgraph-tauola (53)	225.2
$t\bar{t}$ ( $m_{top} = 166.5$ GeV)	/TTJets_TuneZ2Star_mass166.5_8TeV-madgraph-tauola (53)	225.2

Table 2: Summary of Monte Carlo datasets used.

Triggers
Single Muon Sample
HLT_IsoMu24_v*
HLT_IsoMu24_eta2p1_v*
Single Electron Sample
HLT_Ele27_WP80_v*
Dilepton Sample (only used for dilepton control regions)
HLT_Mu17_Mu8_v*
HLT_Mu17_Ele8_CaloIdT_CaloIsoVL_TrkIdVL_TrkIsoVL_v*
HLT_Mu8_Ele17_CaloIdT_CaloIsoVL_TrkIdVL_TrkIsoVL_v*
HLT_Ele17_CaloIdT_CaloIsoVL_TrkIdVL_TrkIsoVL_Ele8_CaloIdT_CaloIsoVL_TrkIdVL_TrkIsoVL_v*

Table 3: Summary of triggers used.

## 135 4 Event Selection

136 Here we define the selections of leptons, jets, and  $E_T^{\text{miss}}$ . We also describe our measurements of the lepton  
137 and trigger efficiency. The analysis uses several different Control Regions (CRs) in addition to the Signal  
138 Regions (SRs). All of these different regions are defined in this section. This section also includes some  
139 information on the basic MC corrections that we apply.

### 140 4.1 Single Lepton Selection

141 The single lepton selection is based on the following criteria, starting from the requirements described on  
142 [https://twiki.cern.ch/twiki/bin/viewauth/CMS/SUSYstop#SINGLE\\_LEPTON\\_CHANNEL](https://twiki.cern.ch/twiki/bin/viewauth/CMS/SUSYstop#SINGLE_LEPTON_CHANNEL) (re-  
143 vision r20)

- 144 • satisfy the trigger requirement (see Table 3). Note that the analysis triggers are inclusive single  
145 lepton triggers. Dilepton triggers are used only for the dilepton control region.

- 146 • select events with one high  $p_T$  electron or muon, requiring

- 147 –  $p_T > 30 \text{ GeV}/c$  and  $|\eta| < 1.4442(2.1)$  for electrons (muons). The restriction to the barrel for  
148 electrons is motivated by an observed excess of events with large  $M_T$  with endcap electrons  
149 in the b-veto control region, and does not significantly reduce the signal acceptance since the  
150 leptons tend to be central.
- 151 – muon ID criteria is based on the 2012 POG recommended tight working point
- 152 – electron ID criteria is based on the 2012 POG recommended medium working point
- 153 – PF-based isolation ( $\Delta R < 0.3$ ) relative isolation  $< 0.15$  and absolute isolation  $< 5 \text{ GeV}$ . PU  
154 corrections are performed with the  $\Delta\beta$  scheme for muons and effective-area fastjet rho scheme  
155 for electrons (as recommended by the relevant POGs).
- 156 –  $|p_T(\text{PF}_{\text{lep}}) - p_T(\text{RECO}_{\text{lep}})| < 10 \text{ GeV}$
- 157 –  $E/p_{\text{in}} < 4$  (electrons only)
- 158 – We remove electron events with  $E_T^{\text{miss}} > 50 \text{ GeV}$  and  $M_T > 100 \text{ GeV}$  with at least one crystal  
159 in the supercluster with laser correction  $> 2$ .<sup>1)</sup>

- 160 • require at least 4 PF jets in the event with  $p_T > 30 \text{ GeV}$  within  $|\eta| < 2.5$  out of which at least 1  
161 satisfies the CSV medium working point b-tagging requirement

- 162 • require moderate  $E_T^{\text{miss}} > 50 \text{ GeV}$  (type1-corrected pfmet with  $\phi$  corrections applied as described  
163 in Sec. 4.7.1).

- 164 • Isolated track veto, see Section 4.2

### 165 4.2 Isolated track veto

166 The isolated track veto is intended to remove top dilepton events. Looking for an isolated track is an  
167 effective way of identifying  $W \rightarrow e$ ,  $W \rightarrow \mu$ ,  $W \rightarrow \tau \rightarrow \ell$ , and  $W \rightarrow \tau \rightarrow h^\pm + n\pi^0$ . The requirements  
168 on the track are

- 169 •  $P_T > 10 \text{ GeV}$
- 170 • Relative track isolation  $< 10\%$  computed from charged PF candidates with  $d_Z < 0.05 \text{ cm}$  from the  
171 primary vertex.

### 172 4.3 Signal Region Selection

173 The signal regions (SRs) are selected to improve the sensitivity for the single lepton requirements and  
174 cover a range of scalar top scenarios. The  $M_T$  and  $E_T^{\text{miss}}$  variables are used to define the signal regions  
175 and the requirements are listed in Table 4.

<sup>1)</sup> This is an ad-hoc removal based on run-event numbers, since the problem was found very recently and the filter was not available when we processed the events.

Signal Region	Minimum $M_T$ [GeV]	Minimum $E_T^{\text{miss}}$ [GeV]
SRA	150	100
SRB	120	150
SRC	120	200
SRD	120	250
SRE	120	300
SRF	120	350
SRG	120	400

Table 4: Signal region definitions based on  $M_T$  and  $E_T^{\text{miss}}$  requirements. These requirements are applied in addition to the baseline single lepton selection.

Table 5 shows the expected number of SM background yields for the SRs. A few stop signal yields for four values of the parameters are also shown for comparison. The signal regions with looser requirements are sensitive to lower stop masses  $M(\tilde{t})$ , while those with tighter requirements are more sensitive to higher  $M(\tilde{t})$ . Kinematic distributions for a few sample signal points can be found in Appendix E.

Sample	SRA	SRB	SRC	SRD	SRE	SRF	SRG
$t\bar{t} \rightarrow \ell\ell$	$619 \pm 9$	$366 \pm 7$	$127 \pm 4$	$44 \pm 2$	$17 \pm 1$	$7 \pm 1$	$4 \pm 1$
$t\bar{t} \rightarrow \ell + \text{jets} \& \text{single top } (1\ell)$	$95 \pm 3$	$67 \pm 3$	$15 \pm 1$	$6 \pm 1$	$2 \pm 1$	$1 \pm 1$	$1 \pm 0$
$W + \text{jets}$	$29 \pm 2$	$15 \pm 2$	$6 \pm 1$	$3 \pm 1$	$1 \pm 0$	$0 \pm 0$	$0 \pm 0$
Rare	$59 \pm 3$	$38 \pm 3$	$16 \pm 2$	$8 \pm 1$	$4 \pm 1$	$2 \pm 0$	$1 \pm 0$
Total	$802 \pm 10$	$486 \pm 8$	$164 \pm 5$	$62 \pm 3$	$23 \pm 2$	$10 \pm 1$	$6 \pm 1$
Yield UL (optimistic)	$147$ (10%)	$94$ (10%)	$47$ (15%)	$25$ (20%)	$14$ (25%)	$8.6$ (30%)	$7.5$ (50%)
Yield UL (pessimistic)	$200$ (15%)	$152$ (20%)	$64$ (25%)	$30$ (30%)	$15$ (35%)	$9.7$ (50%)	$8.2$ (100%)
$T2tt$ $m(\text{stop}) = 250$ $m(\chi^0) = 0$	$315 \pm 18$	$193 \pm 14$	$53 \pm 8$	$13 \pm 4$	$2 \pm 2$	$0 \pm 0$	$0 \pm 0$
$T2tt$ $m(\text{stop}) = 300$ $m(\chi^0) = 50$	$296 \pm 11$	$236 \pm 10$	$88 \pm 6$	$28 \pm 3$	$10 \pm 2$	$2 \pm 1$	$0 \pm 0$
$T2tt$ $m(\text{stop}) = 300$ $m(\chi^0) = 100$	$128 \pm 7$	$93 \pm 6$	$29 \pm 3$	$10 \pm 2$	$5 \pm 1$	$2 \pm 1$	$1 \pm 1$
$T2tt$ $m(\text{stop}) = 350$ $m(\chi^0) = 0$	$224 \pm 6$	$206 \pm 6$	$119 \pm 4$	$52 \pm 3$	$20 \pm 2$	$8 \pm 1$	$3 \pm 1$
$T2tt$ $m(\text{stop}) = 450$ $m(\chi^0) = 0$	$71 \pm 2$	$71 \pm 2$	$53 \pm 1$	$36 \pm 1$	$21 \pm 1$	$11 \pm 1$	$5 \pm 0$

Table 5: Expected SM background contributions and signal yields for a few sample points, including both muon and electron channels. This is “dead reckoning” MC with no correction. It is meant only as a general guide. The uncertainties are statistical only. The signal yield expected upper limits are also shown for two values of the total background systematic uncertainty, indicated in parentheses.

#### 4.4 Control Region Selection

Control regions (CRs) are used to validate the background estimation procedure and derive systematic uncertainties for some contributions. The CRs are selected to have similar kinematics to the SRs, but have a different requirement in terms of number of b-tags and number of leptons, thus enhancing them in different SM contributions. The four CRs used in this analysis are summarized in Table 6.

Selection Criteria	exactly 1 lepton	exactly 2 leptons	1 lepton + isolated track
0 b-tags	CR1) W+Jets dominated: Validate W+Jets $M_T$ tail	CR2) apply Z-mass constraint $\rightarrow$ Z+Jets dominated: Validate $t\bar{t} \rightarrow \ell + \text{jets}$ $M_T$ tail comparing data vs. MC “pseudo- $M_T$ ”	CR3) not used
$\geq 1$ b-tags	SIGNAL REGION	CR4) Apply Z-mass veto $\rightarrow$ $t\bar{t} \rightarrow \ell\ell$ dominated: Validate “physics” modelling of $t\bar{t} \rightarrow \ell\ell$	CR5) $t\bar{t} \rightarrow \ell\ell$ , $t\bar{t} \rightarrow \ell\tau$ and $t\bar{t} \rightarrow \ell\text{fake}$ dominated: Validate $\tau$ and fake lepton modeling/detector effects in $t\bar{t} \rightarrow \ell\ell$

Table 6: Summary of signal and control regions.

185 **4.5 Definition of  $M_T$  peak region**

186 This region is defined as  $50 < M_T < 80$  GeV.

187 **4.6 Default  $t\bar{t}$  MC sample**

188 Our default  $t\bar{t}$  MC sample is Powheg.

189 **4.7 MC Corrections**

190 All MC samples are corrected for trigger efficiency. In the case of single lepton selections, we apply the  
191  $p_T$  and  $\eta$ -dependent scale factors that we measure ourselves, see Section 4.9. In the case of dilepton  
192 selections that require the dilepton triggers, we apply overall scale factors of 0.95, 0.88, and 0.92 for  $ee$ ,  
193  $\mu\mu$ , and  $e\mu$  respectively [3].

194 The leptonic branching fraction used in some of the  $t\bar{t}$  MC samples differs from the value listed in the  
195 PDG ( $10.80 \pm 0.09$ )%. Table 7 summarizes the branching fractions used in the generation of the various  
196  $t\bar{t}$  MC samples. For  $t\bar{t}$  samples with the incorrect leptonic branching fraction, event weights are applied  
197 based on the number of true leptons and the ratio of the corrected and incorrect branching fractions.

$t\bar{t}$ Sample - Event Generator	Leptonic Branching Fraction
Madgraph	0.111
MC@NLO	0.111
Pythia	0.108
Powheg	0.108

Table 7: Leptonic branching fractions for the various  $t\bar{t}$  samples used in the analysis. The  $t\bar{t}$  MC samples produced with Madgraph and MC@NLO has a branching fraction that is almost 3% higher than the PDG value.

198 All  $t\bar{t}$  dilepton samples are corrected (when needed and appropriate) in order to have the correct jet  
199 multiplicity distribution. This correction procedure is described in Section 5.3.1.

200 **4.7.1 Corrections to Jets and  $E_T^{\text{miss}}$**

201 The official recommendations from the Jet/MET group are used for the data and MC samples. In  
202 particular, the jet energy corrections (JEC) are updated using the official recipe. L1FastL2L3Residual  
203 (L1FastL2L3) corrections are applied for data (MC), based on the global tags GR.R\_52\_V9 (START52\_V9B)  
204 for data (MC). In addition, these jet energy corrections are propagated to the  $E_T^{\text{miss}}$  calculation, following  
205 the official prescription for deriving the Type I corrections.

206 Events with anomalous “rho” pile-up corrections are excluded from the sample since these can correspond  
207 to events with unphysically large  $E_T^{\text{miss}}$  and  $M_T$ . In addition, the recommended MET filters are applied.  
208 A correction to remove the  $\phi$  modulation in  $E_T^{\text{miss}}$  is also applied to the data.

209 **4.8 Lepton Selection Efficiency Measurements**

210 In this section we measure the identification and isolation efficiencies for muons and electrons in data  
211 and MC using tag-and-probe studies. The tag is required to pass the full offline analysis selection and  
212 have  $p_T > 30$  GeV,  $|\eta| < 2.1$ , and be matched to the single lepton trigger, HLT\_IsoMu24(\_eta2p1) for  
213 muons and HLT\_Ele27\_WP80 for electrons. The probe is required to have  $|\eta| < 2.1$  and  $p_T > 20$  GeV. To  
214 measure the identification efficiency we require the probe to pass the isolation requirement, to measure  
215 the isolation efficiency we require the probe to pass the identification requirement.

216 The tag-probe pair is required to have opposite-sign and an invariant mass in the range 76–106 GeV.  
217 In order to suppress lepton pairs from sources other than Z boson decays, we require the event to have  
218  $E_T^{\text{miss}} < 30$  GeV and no b-tagged jets (CSV loose working point).

219 The muon efficiencies are summarized in Table 8 for inclusive events (i.e. no jet requirements). These  
220 efficiencies are displayed in Fig. 2 for several different jet multiplicity requirements. We currently observe

221 good agreement for muons with  $p_T$  up to about 300 GeV. For high  $p_T$  muons we observe a source of  
222 background in the data with large impact parameters, which we suppress by requiring muon  $d_0 < 0.02$  cm  
223 and  $d_Z < 0.5$  cm. The electron efficiencies are summarized in Table 9 for inclusive events (i.e. no jet  
224 requirements). These efficiencies are displayed in Fig. 3 for several different jet multiplicity requirements.  
225 In general we observe good agreement between the data and MC identification and isolation efficiencies.  
226 We do not correct the MC for differences in lepton efficiency. In the background calculation, we do  
227 not take any systematics due to lepton selection efficiency uncertainties. This is because all backgrounds  
228 except the rare MC background are normalized to the  $M_T$  peak, thus the lepton identification uncertainty  
229 cancels out. For the rare MC these uncertainties are negligible compared to the assumed cross-section  
230 uncertainty (Section 6).

Table 8: Summary of the data and MC muon identification and isolation efficiencies measured with tag-and-probe studies.

MC ID $p_T$ range [GeV]	$ \eta  < 0.8$	$0.8 <  \eta  < 1.5$	$1.5 <  \eta  < 2.1$
20 - 30	0.9672 $\pm$ 0.0005	0.9640 $\pm$ 0.0006	0.9471 $\pm$ 0.0008
30 - 40	0.9684 $\pm$ 0.0002	0.9657 $\pm$ 0.0003	0.9446 $\pm$ 0.0004
40 - 50	0.9704 $\pm$ 0.0002	0.9687 $\pm$ 0.0002	0.9432 $\pm$ 0.0004
50 - 60	0.9684 $\pm$ 0.0005	0.9640 $\pm$ 0.0005	0.9414 $\pm$ 0.0009
60 - 80	0.9678 $\pm$ 0.0009	0.9640 $\pm$ 0.0010	0.9354 $\pm$ 0.0018
80 - 100	0.9709 $\pm$ 0.0021	0.9642 $\pm$ 0.0027	0.9234 $\pm$ 0.0051
100 - 150	0.9679 $\pm$ 0.0029	0.9654 $\pm$ 0.0035	0.9261 $\pm$ 0.0069
150 - 200	0.9643 $\pm$ 0.0069	0.9568 $\pm$ 0.0088	0.9045 $\pm$ 0.0198
200 - 300	0.9647 $\pm$ 0.0116	0.9388 $\pm$ 0.0171	0.8906 $\pm$ 0.0390
300 - 10000	1.0000 $\pm$ 0.0000	1.0000 $\pm$ 0.0000	1.0000 $\pm$ 0.0000

MC ISO $p_T$ range [GeV]	$ \eta  < 0.8$	$0.8 <  \eta  < 1.5$	$1.5 <  \eta  < 2.1$
20 - 30	0.8966 $\pm$ 0.0007	0.9153 $\pm$ 0.0008	0.9298 $\pm$ 0.0009
30 - 40	0.9610 $\pm$ 0.0002	0.9632 $\pm$ 0.0003	0.9707 $\pm$ 0.0003
40 - 50	0.9876 $\pm$ 0.0001	0.9897 $\pm$ 0.0001	0.9912 $\pm$ 0.0002
50 - 60	0.9921 $\pm$ 0.0002	0.9927 $\pm$ 0.0003	0.9939 $\pm$ 0.0003
60 - 80	0.9927 $\pm$ 0.0004	0.9937 $\pm$ 0.0004	0.9947 $\pm$ 0.0005
80 - 100	0.9920 $\pm$ 0.0012	0.9921 $\pm$ 0.0013	0.9932 $\pm$ 0.0016
100 - 150	0.9898 $\pm$ 0.0017	0.9923 $\pm$ 0.0017	0.9933 $\pm$ 0.0022
150 - 200	0.9901 $\pm$ 0.0037	0.9922 $\pm$ 0.0039	0.9950 $\pm$ 0.0050
200 - 300	0.9919 $\pm$ 0.0057	1.0000 $\pm$ 0.0000	0.9828 $\pm$ 0.0171
300 - 10000	1.0000 $\pm$ 0.0000	1.0000 $\pm$ 0.0000	1.0000 $\pm$ 0.0000

DATA ID $p_T$ range [GeV]	$ \eta  < 0.8$	$0.8 <  \eta  < 1.5$	$1.5 <  \eta  < 2.1$
20 - 30	0.9530 $\pm$ 0.0005	0.9517 $\pm$ 0.0006	0.9369 $\pm$ 0.0008
30 - 40	0.9556 $\pm$ 0.0003	0.9519 $\pm$ 0.0003	0.9362 $\pm$ 0.0005
40 - 50	0.9584 $\pm$ 0.0002	0.9558 $\pm$ 0.0003	0.9355 $\pm$ 0.0004
50 - 60	0.9540 $\pm$ 0.0005	0.9487 $\pm$ 0.0006	0.9314 $\pm$ 0.0010
60 - 80	0.9536 $\pm$ 0.0010	0.9466 $\pm$ 0.0012	0.9307 $\pm$ 0.0019
80 - 100	0.9505 $\pm$ 0.0028	0.9414 $\pm$ 0.0035	0.9289 $\pm$ 0.0053
100 - 150	0.9472 $\pm$ 0.0038	0.9454 $\pm$ 0.0045	0.9149 $\pm$ 0.0079
150 - 200	0.9628 $\pm$ 0.0073	0.9675 $\pm$ 0.0089	0.8950 $\pm$ 0.0217
200 - 300	0.9463 $\pm$ 0.0157	0.9290 $\pm$ 0.0206	0.8889 $\pm$ 0.0468
300 - 10000	0.9412 $\pm$ 0.0404	1.0000 $\pm$ 0.0000	0.4000 $\pm$ 0.2191

DATA ISO $p_T$ range [GeV]	$ \eta  < 0.8$	$0.8 <  \eta  < 1.5$	$1.5 <  \eta  < 2.1$
20 - 30	0.8939 $\pm$ 0.0007	0.9144 $\pm$ 0.0008	0.9361 $\pm$ 0.0008
30 - 40	0.9598 $\pm$ 0.0002	0.9646 $\pm$ 0.0003	0.9744 $\pm$ 0.0003
40 - 50	0.9870 $\pm$ 0.0001	0.9901 $\pm$ 0.0001	0.9920 $\pm$ 0.0002
50 - 60	0.9912 $\pm$ 0.0002	0.9933 $\pm$ 0.0002	0.9953 $\pm$ 0.0003
60 - 80	0.9920 $\pm$ 0.0004	0.9934 $\pm$ 0.0005	0.9956 $\pm$ 0.0005
80 - 100	0.9926 $\pm$ 0.0011	0.9933 $\pm$ 0.0013	0.9955 $\pm$ 0.0014
100 - 150	0.9913 $\pm$ 0.0016	0.9949 $\pm$ 0.0015	0.9965 $\pm$ 0.0017
150 - 200	0.9969 $\pm$ 0.0022	0.9974 $\pm$ 0.0026	0.9944 $\pm$ 0.0055
200 - 300	1.0000 $\pm$ 0.0000	1.0000 $\pm$ 0.0000	1.0000 $\pm$ 0.0000
300 - 10000	1.0000 $\pm$ 0.0000	1.0000 $\pm$ 0.0000	1.0000 $\pm$ 0.0000

Scale Factor ID $p_T$ range [GeV]	$ \eta  < 0.8$	$0.8 <  \eta  < 1.5$	$1.5 <  \eta  < 2.1$
20 - 30	0.9853 $\pm$ 0.0007	0.9872 $\pm$ 0.0009	0.9893 $\pm$ 0.0012
30 - 40	0.9868 $\pm$ 0.0003	0.9857 $\pm$ 0.0005	0.9911 $\pm$ 0.0007
40 - 50	0.9877 $\pm$ 0.0003	0.9866 $\pm$ 0.0004	0.9918 $\pm$ 0.0006
50 - 60	0.9851 $\pm$ 0.0007	0.9841 $\pm$ 0.0009	0.9894 $\pm$ 0.0014
60 - 80	0.9853 $\pm$ 0.0014	0.9820 $\pm$ 0.0017	0.9949 $\pm$ 0.0028
80 - 100	0.9790 $\pm$ 0.0036	0.9763 $\pm$ 0.0046	1.0059 $\pm$ 0.0080
100 - 150	0.9786 $\pm$ 0.0049	0.9793 $\pm$ 0.0059	0.9879 $\pm$ 0.0113
150 - 200	0.9984 $\pm$ 0.0104	1.0112 $\pm$ 0.0131	0.9894 $\pm$ 0.0323
200 - 300	0.9810 $\pm$ 0.0201	0.9896 $\pm$ 0.0284	0.9981 $\pm$ 0.0684
300 - 10000	0.9412 $\pm$ 0.0404	1.0000 $\pm$ 0.0000	0.4000 $\pm$ 0.2191

Scale Factor ISO $p_T$ range [GeV]	$ \eta  < 0.8$	$0.8 <  \eta  < 1.5$	$1.5 <  \eta  < 2.1$
20 - 30	0.9970 $\pm$ 0.0012	0.9989 $\pm$ 0.0012	1.0068 $\pm$ 0.0013
30 - 40	0.9987 $\pm$ 0.0004	1.0014 $\pm$ 0.0004	1.0038 $\pm$ 0.0005
40 - 50	0.9994 $\pm$ 0.0002	1.0004 $\pm$ 0.0002	1.0008 $\pm$ 0.0002
50 - 60	0.9991 $\pm$ 0.0003	1.0006 $\pm$ 0.0003	1.0013 $\pm$ 0.0004
60 - 80	0.9993 $\pm$ 0.0006	0.9997 $\pm$ 0.0006	1.0009 $\pm$ 0.0008
80 - 100	1.0006 $\pm$ 0.0016	1.0012 $\pm$ 0.0018	1.0023 $\pm$ 0.0022
100 - 150	1.0015 $\pm$ 0.0023	1.0027 $\pm$ 0.0023	1.0032 $\pm$ 0.0028
150 - 200	1.0068 $\pm$ 0.0044	1.0053 $\pm$ 0.0047	0.9994 $\pm$ 0.0075
200 - 300	1.0081 $\pm$ 0.0058	1.0000 $\pm$ 0.0000	1.0175 $\pm$ 0.0177
300 - 10000	1.0000 $\pm$ 0.0000	1.0000 $\pm$ 0.0000	1.0000 $\pm$ 0.0000

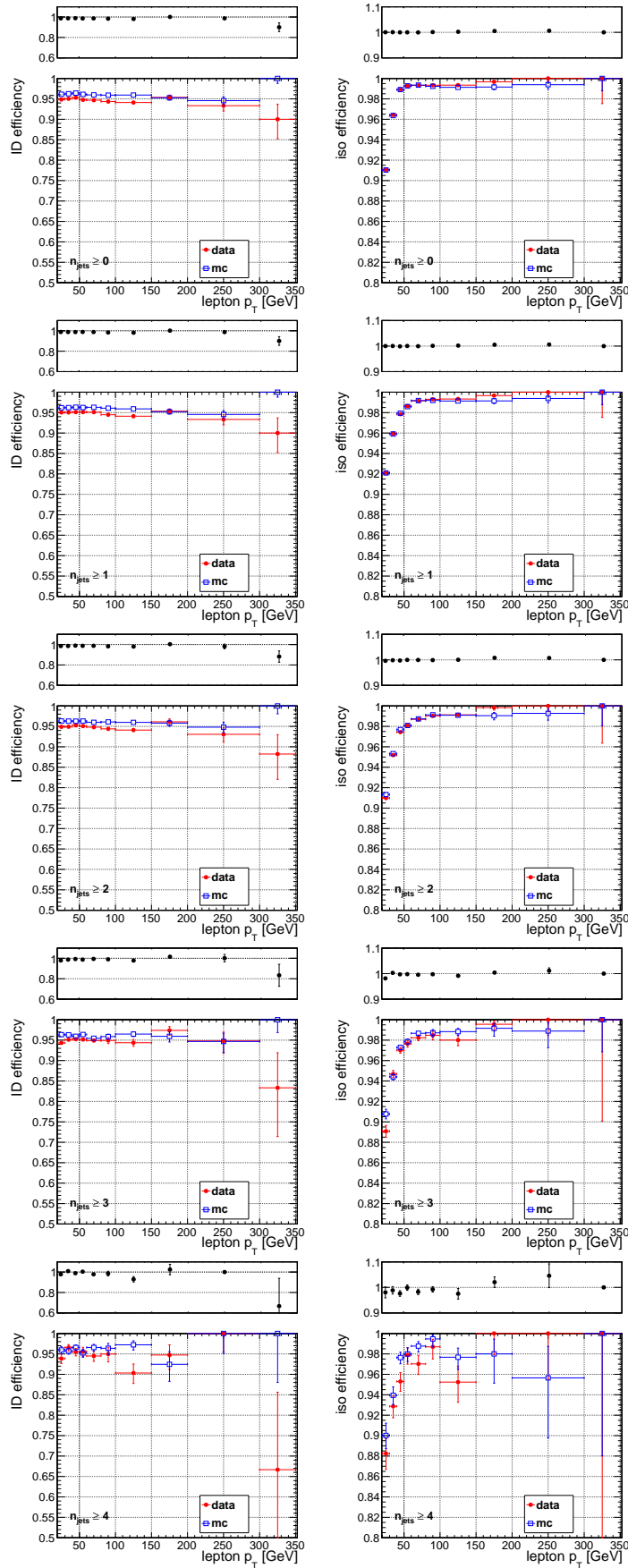


Figure 2: Comparison of the muon identification and isolation efficiencies in data and MC for various jet multiplicity requirements.

Table 9: Summary of the data and MC electron identification and isolation efficiencies measured with tag-and-probe studies.

MC ID		
$p_T$ range [GeV]	$ \eta  < 1.5$	$1.5 <  \eta  < 2.1$
20 - 30	0.8156 $\pm$ 0.0008	0.6565 $\pm$ 0.0019
30 - 40	0.8670 $\pm$ 0.0004	0.7450 $\pm$ 0.0010
40 - 50	0.8922 $\pm$ 0.0003	0.7847 $\pm$ 0.0008
50 - 60	0.9023 $\pm$ 0.0006	0.7956 $\pm$ 0.0018
60 - 80	0.9097 $\pm$ 0.0011	0.8166 $\pm$ 0.0034
80 - 100	0.9203 $\pm$ 0.0028	0.8196 $\pm$ 0.0090
100 - 150	0.9162 $\pm$ 0.0037	0.8378 $\pm$ 0.0117
150 - 200	0.9106 $\pm$ 0.0087	0.8111 $\pm$ 0.0292
200 - 300	0.9304 $\pm$ 0.0119	0.9153 $\pm$ 0.0363
300 - 10000	0.8684 $\pm$ 0.0388	0.8000 $\pm$ 0.1789
MC ISO		
$p_T$ range [GeV]	$ \eta  < 1.5$	$1.5 <  \eta  < 2.1$
20 - 30	0.9245 $\pm$ 0.0006	0.9466 $\pm$ 0.0011
30 - 40	0.9682 $\pm$ 0.0002	0.9741 $\pm$ 0.0004
40 - 50	0.9876 $\pm$ 0.0001	0.9883 $\pm$ 0.0002
50 - 60	0.9909 $\pm$ 0.0002	0.9912 $\pm$ 0.0005
60 - 80	0.9916 $\pm$ 0.0004	0.9930 $\pm$ 0.0008
80 - 100	0.9915 $\pm$ 0.0010	0.9908 $\pm$ 0.0025
100 - 150	0.9929 $\pm$ 0.0012	0.9894 $\pm$ 0.0035
150 - 200	0.9919 $\pm$ 0.0029	0.9932 $\pm$ 0.0068
200 - 300	0.9953 $\pm$ 0.0033	1.0000 $\pm$ 0.0000
300 - 10000	1.0000 $\pm$ 0.0000	1.0000 $\pm$ 0.0000
DATA ID		
$p_T$ range [GeV]	$ \eta  < 1.5$	$1.5 <  \eta  < 2.1$
20 - 30	0.8145 $\pm$ 0.0008	0.6528 $\pm$ 0.0018
30 - 40	0.8676 $\pm$ 0.0004	0.7462 $\pm$ 0.0010
40 - 50	0.8955 $\pm$ 0.0003	0.7922 $\pm$ 0.0008
50 - 60	0.9049 $\pm$ 0.0006	0.8072 $\pm$ 0.0018
60 - 80	0.9110 $\pm$ 0.0011	0.8212 $\pm$ 0.0035
80 - 100	0.9156 $\pm$ 0.0028	0.8358 $\pm$ 0.0091
100 - 150	0.9257 $\pm$ 0.0036	0.8507 $\pm$ 0.0116
150 - 200	0.9186 $\pm$ 0.0084	0.8929 $\pm$ 0.0292
200 - 300	0.9106 $\pm$ 0.0149	0.7576 $\pm$ 0.0746
300 - 10000	0.9400 $\pm$ 0.0336	1.0000 $\pm$ 0.0000
DATA ISO		
$p_T$ range [GeV]	$ \eta  < 1.5$	$1.5 <  \eta  < 2.1$
20 - 30	0.9201 $\pm$ 0.0006	0.9419 $\pm$ 0.0011
30 - 40	0.9667 $\pm$ 0.0002	0.9734 $\pm$ 0.0004
40 - 50	0.9872 $\pm$ 0.0001	0.9892 $\pm$ 0.0002
50 - 60	0.9904 $\pm$ 0.0002	0.9922 $\pm$ 0.0004
60 - 80	0.9923 $\pm$ 0.0004	0.9916 $\pm$ 0.0009
80 - 100	0.9914 $\pm$ 0.0010	0.9921 $\pm$ 0.0024
100 - 150	0.9945 $\pm$ 0.0011	1.0000 $\pm$ 0.0000
150 - 200	0.9908 $\pm$ 0.0031	1.0000 $\pm$ 0.0000
200 - 300	0.9941 $\pm$ 0.0042	1.0000 $\pm$ 0.0000
300 - 10000	0.9792 $\pm$ 0.0206	1.0000 $\pm$ 0.0000
Scale Factor ID		
$p_T$ range [GeV]	$ \eta  < 1.5$	$1.5 <  \eta  < 2.1$
20 - 30	0.9987 $\pm$ 0.0014	0.9944 $\pm$ 0.0040
30 - 40	1.0007 $\pm$ 0.0006	1.0015 $\pm$ 0.0019
40 - 50	1.0036 $\pm$ 0.0005	1.0096 $\pm$ 0.0015
50 - 60	1.0029 $\pm$ 0.0010	1.0146 $\pm$ 0.0031
60 - 80	1.0014 $\pm$ 0.0018	1.0057 $\pm$ 0.0060
80 - 100	0.9949 $\pm$ 0.0043	1.0197 $\pm$ 0.0158
100 - 150	1.0104 $\pm$ 0.0057	1.0154 $\pm$ 0.0198
150 - 200	1.0087 $\pm$ 0.0134	1.1008 $\pm$ 0.0535
200 - 300	0.9786 $\pm$ 0.0203	0.8277 $\pm$ 0.0879
300 - 10000	1.0824 $\pm$ 0.0619	1.2500 $\pm$ 0.2795
Scale Factor ISO		
$p_T$ range [GeV]	$ \eta  < 1.5$	$1.5 <  \eta  < 2.1$
20 - 30	0.9952 $\pm$ 0.0009	0.9950 $\pm$ 0.0016
30 - 40	0.9984 $\pm$ 0.0003	0.9992 $\pm$ 0.0006
40 - 50	0.9996 $\pm$ 0.0002	1.0009 $\pm$ 0.0003
50 - 60	0.9995 $\pm$ 0.0003	1.0009 $\pm$ 0.0006
60 - 80	1.0006 $\pm$ 0.0005	0.9985 $\pm$ 0.0012
80 - 100	0.9999 $\pm$ 0.0014	1.0013 $\pm$ 0.0035
100 - 150	1.0016 $\pm$ 0.0016	1.0108 $\pm$ 0.0036
150 - 200	0.9989 $\pm$ 0.0042	1.0068 $\pm$ 0.0069
200 - 300	0.9987 $\pm$ 0.0053	1.0000 $\pm$ 0.0000
300 - 10000	0.9792 $\pm$ 0.0206	1.0000 $\pm$ 0.0000

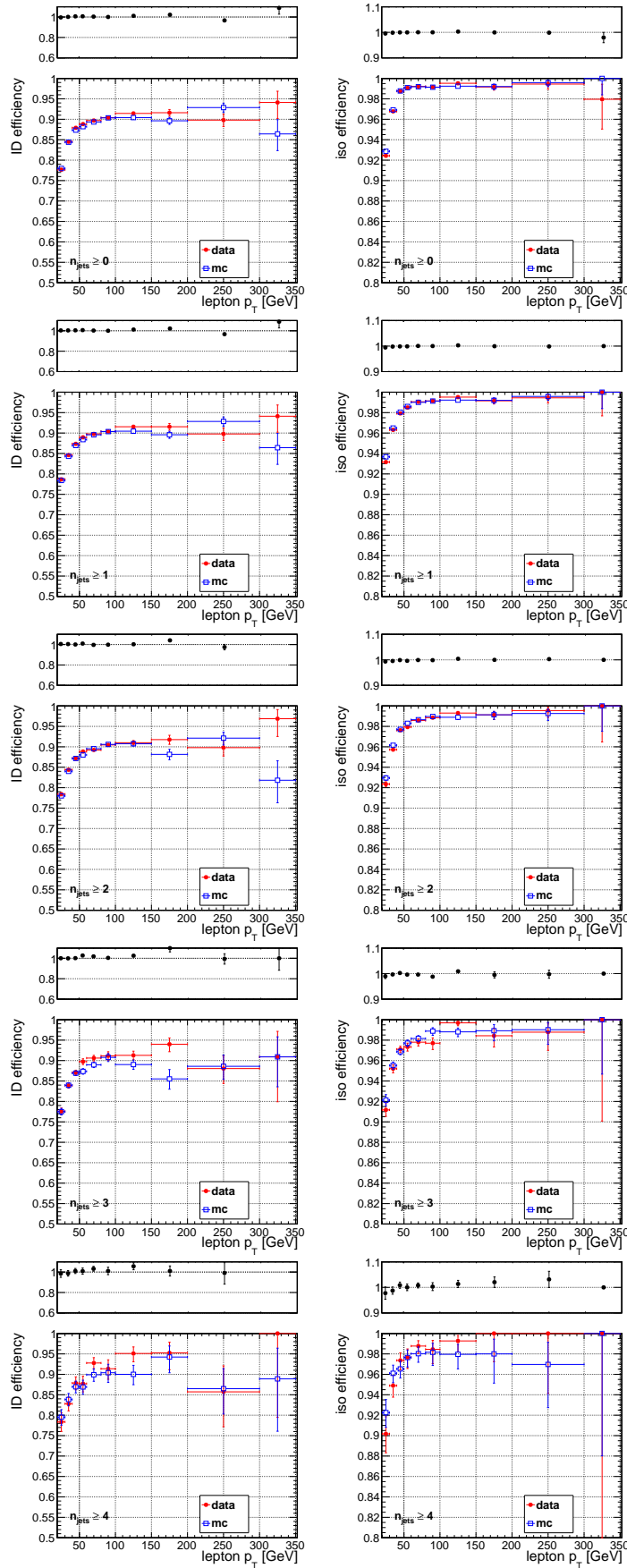


Figure 3: Comparison of the electron identification and isolation efficiencies in data and MC for various jet multiplicity requirements.

## 231 4.9 Trigger Efficiency Measurements

- 232 In this section we measure the efficiencies of the single lepton triggers, HLT\_IsoMu24(\_eta2p1) for muons  
 233 and HLT\_Ele27\_WP80 for electrons, using a tag-and-probe approach. The tag is required to pass the  
 234 full offline analysis selection and have  $p_T > 30$  GeV,  $|\eta| < 2.1$ , and be matched to the single lepton  
 235 trigger. The probe is also required to pass the full offline analysis selection and have  $|\eta| < 2.1$ , but the  
 236  $p_T$  requirement is relaxed to 20 GeV in order to measure the  $p_T$  turn-on curve. The tag-probe pair is  
 237 required to have opposite-sign and an invariant mass in the range 76–106 GeV.
- 238 The measured trigger efficiencies are displayed in Fig. 4 and summarized in Table 10 (muons) and Table 11  
 239 (electrons). These trigger efficiencies are applied to the MC when used to predict data yields selected by  
 240 single lepton triggers.

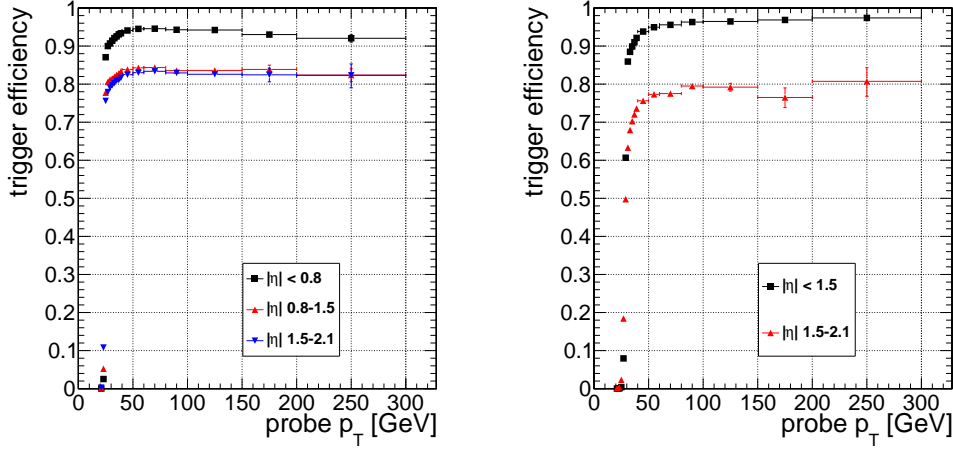


Figure 4: Efficiency for the single muon trigger HLT\_IsoMu24(\_eta2p1) (left) and single electron trigger HLT\_Ele27\_WP80 (right) as a function of lepton  $p_T$ , for several bins in lepton  $|\eta|$ .

Table 10: Summary of the single muon trigger efficiency HLT\_IsoMu24(\_eta2p1). Uncertainties are statistical.

$p_T$ range [GeV]	$ \eta  < 0.8$	$0.8 <  \eta  < 1.5$	$1.5 <  \eta  < 2.1$
20 - 22	$0.00 \pm 0.000$	$0.00 \pm 0.000$	$0.00 \pm 0.000$
22 - 24	$0.03 \pm 0.001$	$0.05 \pm 0.001$	$0.11 \pm 0.002$
24 - 26	$0.87 \pm 0.002$	$0.78 \pm 0.002$	$0.76 \pm 0.003$
26 - 28	$0.90 \pm 0.001$	$0.81 \pm 0.002$	$0.78 \pm 0.002$
28 - 30	$0.91 \pm 0.001$	$0.81 \pm 0.002$	$0.79 \pm 0.002$
30 - 32	$0.91 \pm 0.001$	$0.81 \pm 0.001$	$0.80 \pm 0.002$
32 - 34	$0.92 \pm 0.001$	$0.82 \pm 0.001$	$0.80 \pm 0.002$
34 - 36	$0.93 \pm 0.001$	$0.82 \pm 0.001$	$0.81 \pm 0.001$
36 - 38	$0.93 \pm 0.001$	$0.83 \pm 0.001$	$0.81 \pm 0.001$
38 - 40	$0.93 \pm 0.001$	$0.83 \pm 0.001$	$0.82 \pm 0.001$
40 - 50	$0.94 \pm 0.000$	$0.84 \pm 0.000$	$0.82 \pm 0.001$
50 - 60	$0.95 \pm 0.000$	$0.84 \pm 0.001$	$0.83 \pm 0.001$
60 - 80	$0.95 \pm 0.001$	$0.84 \pm 0.002$	$0.83 \pm 0.002$
80 - 100	$0.94 \pm 0.002$	$0.84 \pm 0.004$	$0.83 \pm 0.006$
100 - 150	$0.94 \pm 0.003$	$0.84 \pm 0.005$	$0.83 \pm 0.008$
150 - 200	$0.93 \pm 0.006$	$0.84 \pm 0.011$	$0.82 \pm 0.018$
>200	$0.92 \pm 0.010$	$0.82 \pm 0.017$	$0.82 \pm 0.031$

Table 11: Summary of the single electron trigger efficiency HLT\_Ele27\_WP80. Uncertainties are statistical.

$p_T$ range [GeV]	$ \eta  < 1.5$	$1.5 <  \eta  < 2.1$
20 - 22	$0.00 \pm 0.000$	$0.00 \pm 0.000$
22 - 24	$0.00 \pm 0.000$	$0.00 \pm 0.001$
24 - 26	$0.00 \pm 0.000$	$0.02 \pm 0.001$
26 - 28	$0.08 \pm 0.001$	$0.18 \pm 0.003$
28 - 30	$0.61 \pm 0.002$	$0.50 \pm 0.004$
30 - 32	$0.86 \pm 0.001$	$0.63 \pm 0.003$
32 - 34	$0.88 \pm 0.001$	$0.68 \pm 0.003$
34 - 36	$0.90 \pm 0.001$	$0.70 \pm 0.002$
36 - 38	$0.91 \pm 0.001$	$0.72 \pm 0.002$
38 - 40	$0.92 \pm 0.001$	$0.74 \pm 0.002$
40 - 50	$0.94 \pm 0.000$	$0.76 \pm 0.001$
50 - 60	$0.95 \pm 0.000$	$0.77 \pm 0.002$
60 - 80	$0.96 \pm 0.001$	$0.78 \pm 0.003$
80 - 100	$0.96 \pm 0.002$	$0.80 \pm 0.008$
100 - 150	$0.96 \pm 0.002$	$0.79 \pm 0.010$
150 - 200	$0.97 \pm 0.004$	$0.76 \pm 0.026$
>200	$0.97 \pm 0.005$	$0.81 \pm 0.038$

## 241 5 Control Region Studies

242 The CR studies described in this Section are key to validating the background predictions. The CRs are  
 243 defined in Section 4.4.

244 CR1 and CR2 are designed to test the  $M_T$  tail in  $W+$  jets and  $t\bar{t}$  respectively. Note that, as explained  
 245 in Section 2.1, these tails are different in the two samples because the off-shell effects are much more  
 246 pronounced for  $W+$  jets (the s- and t-channel single top have the same  $M_T$  tail as  $t\bar{t}$ ). To put things in  
 247 perspective, keep in mind that these backgrounds are only about 15% of the total, see Table 5.

248 CR4 and CR5 address the dominant  $t\bar{t}$  dilepton background. In CR4 we test the  $M_T$  tail in well identified  
 249 dilepton events. In CR5 we test the same quantity, but in events where the second lepton is identified as  
 250 an isolated track. Clearly CR4 and CR5 overlap.

### 251 5.1 $W+$ -Jets MC Modelling Validation from CR1

252 The estimate of the uncertainty on this background is based on CR1, defined by applying the full signal  
 253 selection, including the isolated track veto, but requiring 0 b-tags (CSV medium working point as de-  
 254 scribed in Sec. 4). The sample is dominated by  $W+$ -jets and is thus used to validate the MC modelling  
 255 of this background.

256 In Table 12 we show the amount that we need to scale the  $W+$ -jets MC by in order to have agreement  
 257 between data and Monte Carlo in the  $M_T$  peak region, defined as  $50 < M_T < 80$  GeV, for the different  
 258 signal regions. (Recall, the signal regions have different  $E_T^{\text{miss}}$  requirements). These scale factors are not  
 259 terribly important, but it is reassuring that they are not too different from 1.

Sample	CR1PRESEL	CR1A	CR1B	CR1C	CR1D	CR1E	CR1F	CR1G
$\mu M_T$ -SF	$0.92 \pm 0.02$	$0.97 \pm 0.03$	$0.90 \pm 0.04$	$0.91 \pm 0.06$	$0.93 \pm 0.09$	$0.98 \pm 0.13$	$0.94 \pm 0.18$	$0.96 \pm 0.25$
$e M_T$ -SF	$0.94 \pm 0.02$	$0.90 \pm 0.04$	$0.84 \pm 0.05$	$0.80 \pm 0.07$	$0.83 \pm 0.10$	$0.77 \pm 0.13$	$0.86 \pm 0.20$	$0.87 \pm 0.29$

Table 12:  $M_T$  peak Data/MC scale factors applied to  $W+$ -jets samples. No scaling is made for back-  
 grounds from other processes. CR1PRESEL refers to a sample with  $E_T^{\text{miss}} > 50$  GeV. The uncertainties  
 are statistical only.

260 Next, in Fig 41, 6, and 7, we show plots of  $E_T^{\text{miss}}$  and then  $M_T$  for different  $E_T^{\text{miss}}$  requirements corre-  
 261 sponding to those defining our signal regions. It is clear that there are more events in the  $M_T$  tail than  
 262 predicted from MC. This implies that we need to rescale the MC  $W+$ -jets background in the tail region.

263 The rescaling is explored in Table 13, where we compare the data and MC yields in the  $M_T$  signal regions  
 264 and in a looser control region. Note that the MC is normalized in the  $M_T$  peak region by rescaling the  
 265  $W+$ -jets component according to Table 12.

266 We also derive data/MC scale factors. As shown in Table 13, these are derived in two different ways,  
 267 separately for muons and electrons and then combined, as follows:

- 268 • For the first three sets of scale factors, above the triple horizontal line, we calculate the scale factor  
 269 as the amount by which we would need to rescale **all** MC ( $W+$ -jets,  $t\bar{t}$ , single top, rare) in order  
 270 to have data-MC agreement in the  $M_T$  tail.
- 271 • For the next three set of scale factors, below the triple horizontal line, we calculate the scale factor  
 272 as the amount by which we would need to scale  $W+$ -jets keeping all other components fixed in order  
 273 to have data-MC agreement in the tail.

274 The true  $W+$ -jets scale factor is somewhere in between these two extremes. We also note that there is no  
 275 statistically significant difference between the electron and muon samples. We use these data to extract  
 276 a data/MC scale factor for  $W+$ -jets which will be used to rescale the  $W+$ -jets MC tail. This scale factor  
 277 is listed in the last line of the Table, and is called  $SFR_{w+jets}$ . It is calculated as follows.

- 278 • Separately for each signal region
- 279 • As the average of the two methods described above

Sample	CR1PRESEL	CR1A	CR1B	CR1C	CR1D	CR1E	CR1F	CR1G
$\mu$ MC	$480 \pm 22$	$173 \pm 5$	$114 \pm 4$	$40 \pm 2$	$16 \pm 1$	$8 \pm 1$	$4 \pm 1$	$2 \pm 1$
$\mu$ Data	629	238	139	45	12	8	3	2
$\mu$ Data/MC	$1.31 \pm 0.08$	$1.37 \pm 0.10$	$1.22 \pm 0.11$	$1.12 \pm 0.18$	$0.75 \pm 0.23$	$0.99 \pm 0.37$	$0.75 \pm 0.45$	$0.96 \pm 0.72$
e MC	$330 \pm 8$	$118 \pm 4$	$79 \pm 3$	$29 \pm 2$	$13 \pm 1$	$5 \pm 1$	$3 \pm 1$	$2 \pm 0$
e Data	473	174	100	36	16	5	5	2
e Data/MC	$1.43 \pm 0.07$	$1.47 \pm 0.12$	$1.27 \pm 0.14$	$1.23 \pm 0.22$	$1.26 \pm 0.34$	$1.07 \pm 0.51$	$1.80 \pm 0.91$	$1.26 \pm 0.97$
$\mu + e$ MC	$810 \pm 23$	$291 \pm 7$	$192 \pm 5$	$69 \pm 3$	$29 \pm 2$	$13 \pm 1$	$7 \pm 1$	$4 \pm 1$
$\mu + e$ Data	1102	412	239	81	28	13	8	4
$\mu + e$ Data/MC	$1.36 \pm 0.08$	$1.42 \pm 0.13$	$1.24 \pm 0.15$	$1.17 \pm 0.23$	$0.97 \pm 0.31$	$1.02 \pm 0.51$	$1.18 \pm 0.69$	$1.09 \pm 0.96$
$\mu$ W MC	$300 \pm 23$	$84 \pm 5$	$52 \pm 4$	$20 \pm 2$	$9 \pm 2$	$5 \pm 1$	$3 \pm 1$	$1 \pm 1$
$\mu$ W Data	449 ± 26	149 ± 16	78 ± 12	25 ± 7	5 ± 4	5 ± 3	2 ± 2	1 ± 1
$\mu$ W Data/MC	$1.50 \pm 0.14$	$1.77 \pm 0.21$	$1.49 \pm 0.26$	$1.25 \pm 0.38$	$0.56 \pm 0.39$	$0.98 \pm 0.62$	$0.60 \pm 0.73$	$0.94 \pm 1.14$
e W MC	$192 \pm 8$	$55 \pm 4$	$36 \pm 3$	$14 \pm 2$	$6 \pm 1$	$3 \pm 1$	$2 \pm 1$	$1 \pm 0$
e W Data	335 ± 22	111 ± 13	58 ± 10	20 ± 6	10 ± 4	3 ± 2	4 ± 2	1 ± 1
e W Data/MC	$1.74 \pm 0.14$	$2.02 \pm 0.29$	$1.58 \pm 0.32$	$1.49 \pm 0.50$	$1.50 \pm 0.70$	$1.10 \pm 0.80$	$2.27 \pm 1.55$	$1.51 \pm 1.96$
$\mu + e$ W MC	$493 \pm 24$	$139 \pm 6$	$89 \pm 5$	$33 \pm 3$	$16 \pm 2$	$8 \pm 1$	$4 \pm 1$	$2 \pm 1$
$\mu + e$ W Data	785 ± 59	260 ± 37	135 ± 28	45 ± 16	15 ± 9	8 ± 7	6 ± 5	3 ± 3
$\mu + e$ W Data/MC	$1.59 \pm 0.14$	$1.87 \pm 0.28$	$1.53 \pm 0.33$	$1.35 \pm 0.50$	$0.95 \pm 0.58$	$1.03 \pm 0.83$	$1.29 \pm 1.13$	$1.16 \pm 1.65$
$SFR_{wjet}$	$1.48 \pm 0.26$	$1.64 \pm 0.38$	$1.38 \pm 0.30$	$1.26 \pm 0.39$	$0.96 \pm 0.45$	$1.02 \pm 0.67$	$1.23 \pm 0.92$	$1.12 \pm 1.31$

Table 13: Yields in  $M_T$  tail comparing the MC prediction (after applying SFs) to data. CR1PRESEL refers to a sample with  $E_T^{\text{miss}} > 50$  GeV and  $M_T > 150$  GeV. See text for details.

280

- Including the statistical uncertainty
- Adding in quadrature to the uncertainty one-half of the deviation from 1.0

281

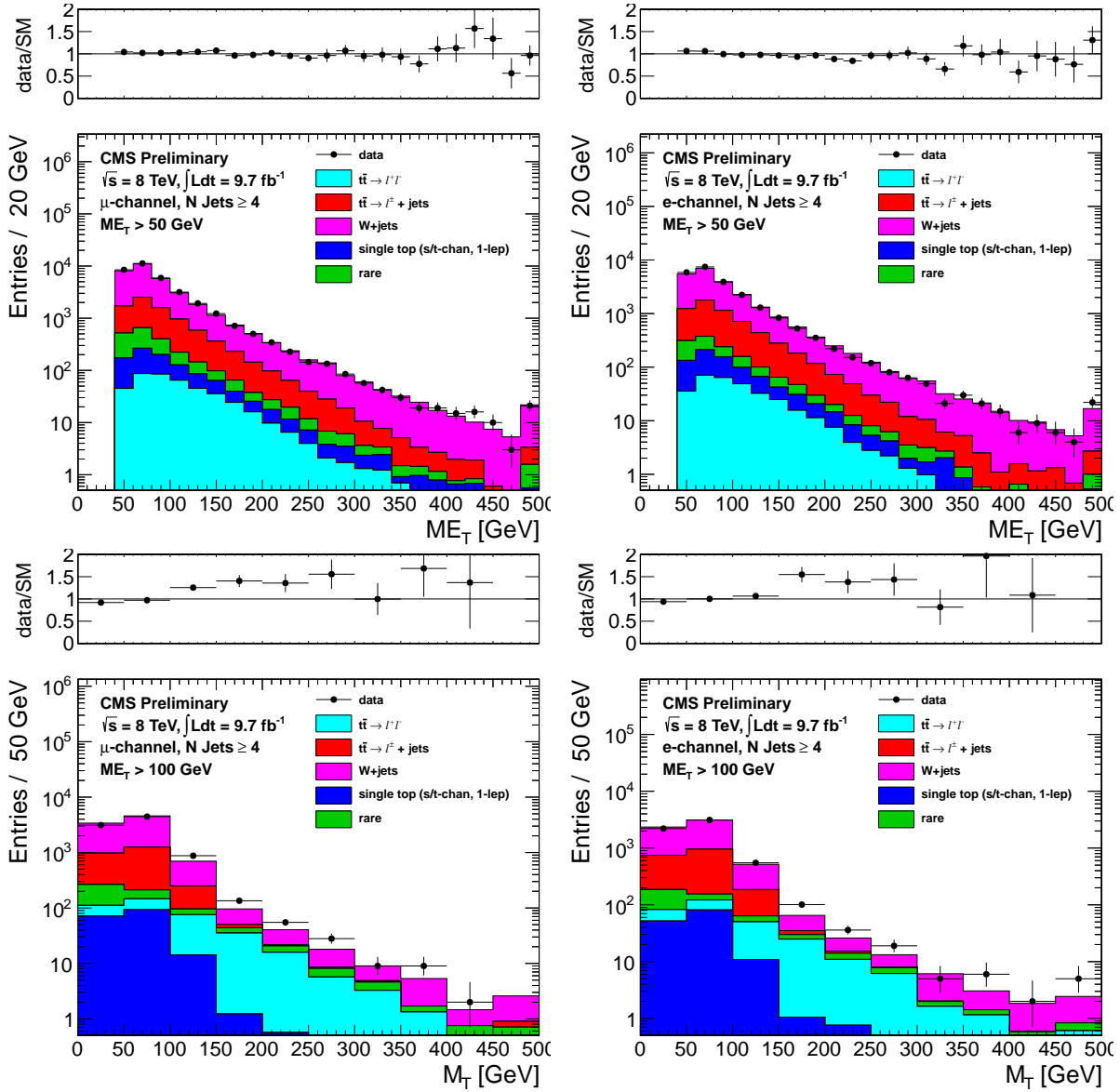


Figure 5: Comparison of the  $E_T^{\text{miss}}$  (top) and  $M_T$  for  $E_T^{\text{miss}} > 100$  (bottom) distributions in data vs. MC for events with a leading muon (left) and leading electron (right) satisfying the requirements of CR1.

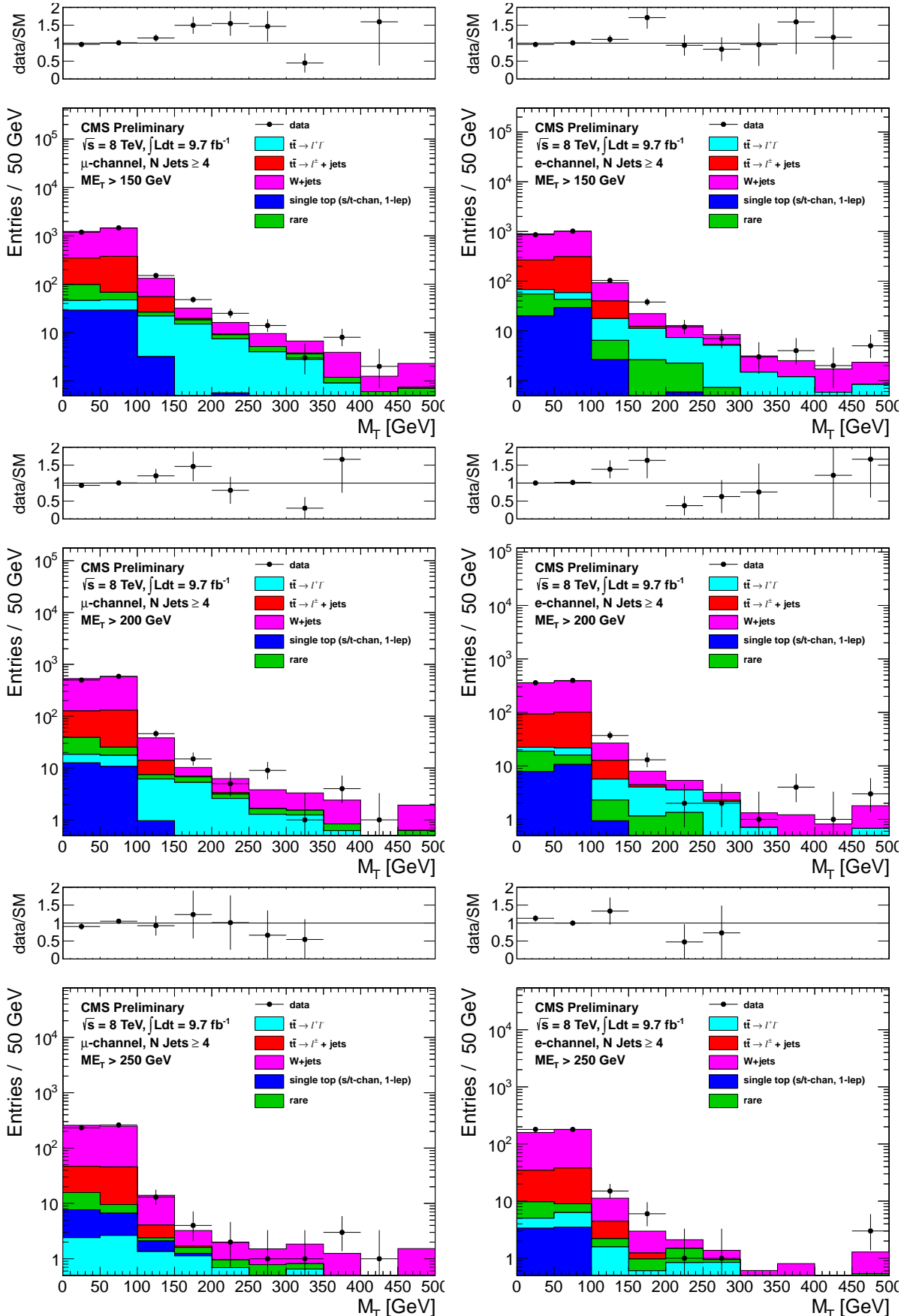


Figure 6: Comparison of the  $M_T$  distribution in data vs. MC for events with a leading muon (left) and leading electron (right) satisfying the requirements of CR1. The  $E_T^{\text{miss}}$  requirements used are 150 GeV (top), 200 GeV (middle) and 250 GeV (bottom).

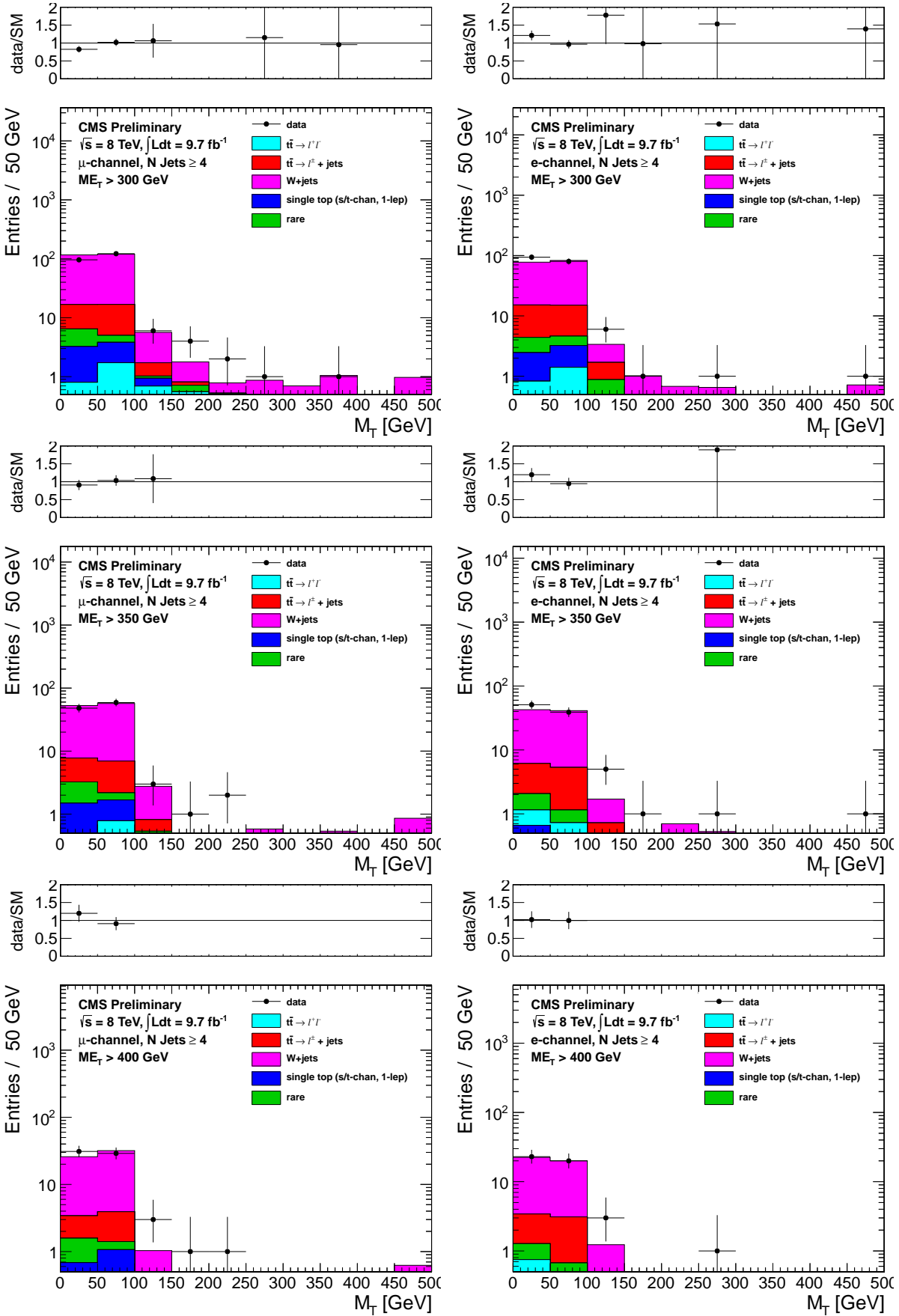


Figure 7: Comparison of the  $M_T$  distribution in data vs. MC for events with a leading muon (left) and leading electron (right) satisfying the requirements of CR1. The  $E_T^{\text{miss}}$  requirements used are 300 GeV (top), 350 GeV (middle) and 400 GeV (bottom).

## 282 5.2 Single Lepton Top MC Modelling Validation from CR2

283 The  $M_T$  tail for single-lepton top events ( $t\bar{t} \rightarrow \ell + \text{jets}$  and single top) is dominated by jet resolution  
 284 effects. The  $W$  cannot be far off-shell because  $M_W < M_{\text{top}}$ . The modeling of the  $M_T$  tail from jet  
 285 resolution effects can be studied using  $Z+\text{jets}$  data and MC samples. However, as we will show below,  
 286 this test is statistically limited and can only be performed for the  $E_T^{\text{miss}}$  requirements corresponding to  
 287 SRA and SRB.

288 Z events are selected by requiring exactly 2 good leptons (satisfying ID and isolation requirements) and  
 289 requiring the  $M_{\ell\ell}$  to be in the range  $81 - 101$  GeV. Events with additional isolated tracks are vetoed, as  
 290 in Section 4.2. To reduce  $t\bar{t}$  backgrounds, events with a CSV tag are removed. The positive lepton is  
 291 treated as a neutrino and so is added to the MET:  $E_T^{\text{miss}} \rightarrow p_T(\ell^+) + E_T^{\text{miss}}$ , and the  $M_T$  is recalculated  
 292 with the negative lepton:  $M_T(\ell^-, E_T^{\text{miss}})$ . The resulting “pseudo- $M_T$ ” is dominated by jet resolution  
 293 effects, since no off-shell Z production enters the sample due to the  $M_{\ell\ell}$  requirement. This section  
 294 describes how well the MC predicts the tail of “pseudo- $M_T$ ”.

295 The underlying distributions are shown in Fig. 42. We then perform the exact same type of Data/MC  
 296 comparison and analysis as described for CR1 in Section D.3. For CR1 we collected the data/MC tail  
 297 information in Table 13; the equivalent for CR2 is Table 14 (for CR2 the statistics are not sufficient to  
 298 split electrons and muons). The last line of Table 14 gives the data/MC scale factors for the  $t\bar{t}$  lepton  
 299 + jets  $M_T$  tail ( $SFR_{top}$ ). This is calculated in the same way as  $SFR_{wjets}$  of Table 13. Just as in CR1,  
 300 there is an excess of data in the tails, as reflected in the values of  $SFR_{top}$ . There are insufficient events  
 301 to derive scale factors for  $E_T^{\text{miss}} > 150$  GeV. As a result, the scale factors derived from CR2 are not  
 302 used for the central prediction of the single-lepton top background. They serve as a valuable cross check  
 303 of the predictions described in Section 7. The single lepton top predictions obtained for SRA and SRB  
 304 using the  $SFR_{top}$  values described here are consistent with the default predictions.

Sample	CR2PRESEL0	CR2PRESEL1	CR2A	CR2B
MC	$32 \pm 2$	$28 \pm 2$	$10 \pm 1$	$10 \pm 1$
Data	50	45	17	17
Data/MC	$1.56 \pm 0.24$	$1.63 \pm 0.27$	$1.68 \pm 0.45$	$1.74 \pm 0.48$
DY MC	$25 \pm 2$	$20 \pm 2$	$5 \pm 1$	$5 \pm 1$
DY Data	$42 \pm 7$	$38 \pm 7$	$12 \pm 4$	$12 \pm 4$
DY Data/MC	$1.73 \pm 0.32$	$1.85 \pm 0.37$	$2.37 \pm 0.96$	$2.58 \pm 1.16$
$SFR_{top}$	$1.64 \pm 0.40$	$1.74 \pm 0.46$	$2.02 \pm 0.68$	$2.16 \pm 0.75$

Table 14: Yields in  $M_T$  tail comparing the  $Z+\text{jets}$  MC prediction (after applying SFs) to data without subtracting the non- $Z+\text{jets}$  components (top table) and with subtracting the non- $Z+\text{jets}$  components (bottom table). CR2PRESEL refers to a sample with  $E_T^{\text{miss}} > 50$  GeV and  $M_T > 150$  GeV.

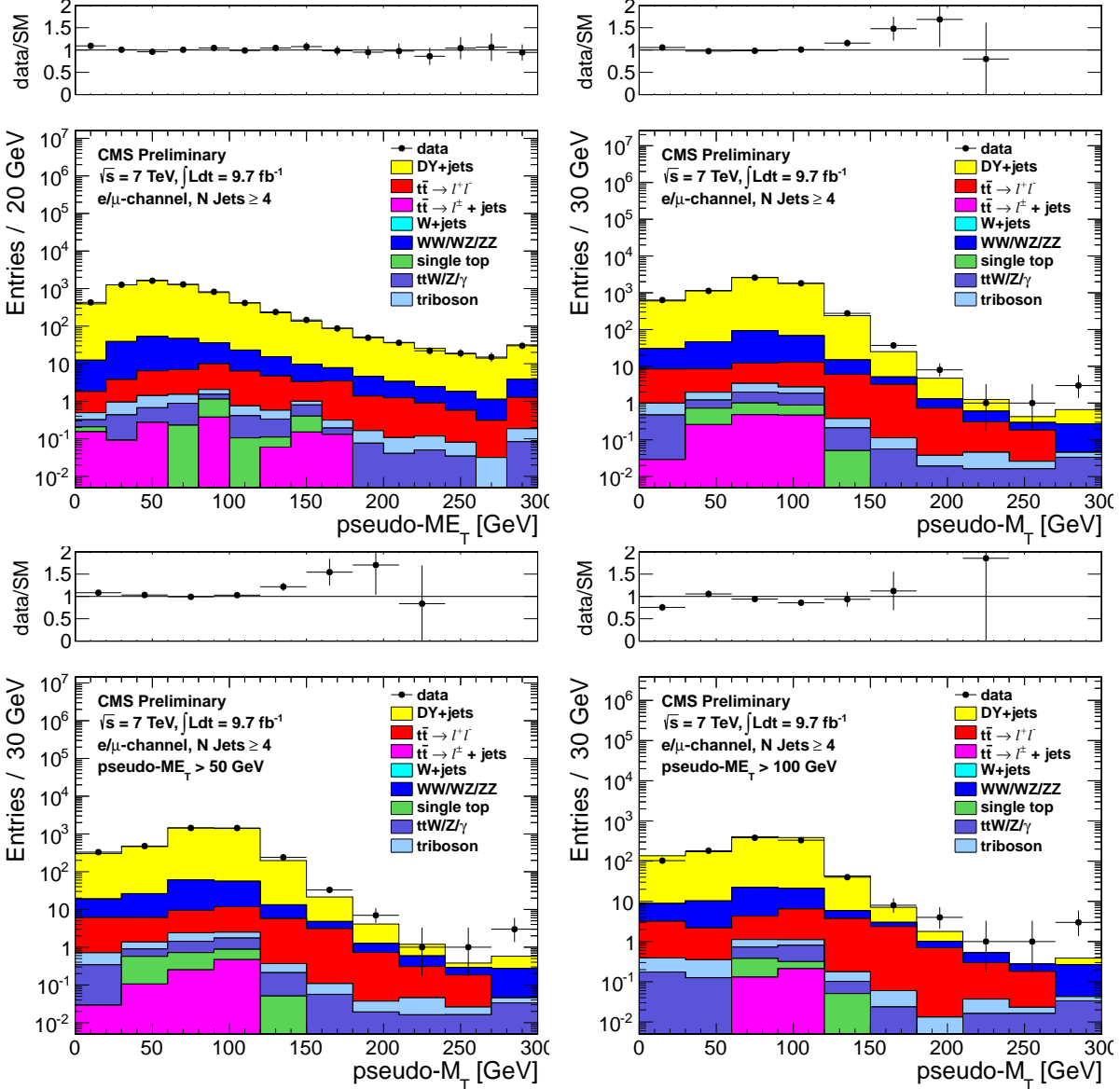


Figure 8: Comparison of the pseudo- $E_T^{\text{miss}}$  (top, left), pseudo- $M_T$  (top, right and bottom) distributions in data vs. MC for events satisfying the requirements of CR2, combining both the muon and electron channels. The pseudo- $M_T$  distributions are shown before any additional requirements (top, right) and after requiring pseudo- $E_T^{\text{miss}} > 50 \text{ GeV}$  (bottom, left) and pseudo- $E_T^{\text{miss}} > 100 \text{ GeV}$  (bottom, right).

305 **5.3 Dilepton studies in CR4**

306 **5.3.1 Modeling of Additional Hard Jets in Top Dilepton Events**

307 Dilepton  $t\bar{t}$  events have 2 jets from the top decays, so additional jets from radiation or higher order  
 308 contributions are required to enter the signal sample. In this Section we develop an algorithm to be  
 309 applied to all  $t\bar{t} \rightarrow \ell\ell$  MC samples to ensure that the distribution of extra jets is properly modelled.

310 The modeling of additional jets in  $t\bar{t}$  events is checked in a  $t\bar{t} \rightarrow \ell\ell$  control sample, selected by requiring

- 311 • exactly 2 electrons or muons with  $p_T > 20$  GeV
- 312 •  $E_T^{\text{miss}} > 50$  GeV
- 313 •  $\geq 1$  b-tagged jet
- 314 • Z-veto ( $|m_{\ell\ell} - 91| > 15$  GeV)

315 Figure 9 shows a comparison of the jet multiplicity distribution in data and MC for this two-lepton  
 316 control sample. After requiring at least 1 b-tagged jet, most of the events have 2 jets, as expected from  
 317 the dominant process  $t\bar{t} \rightarrow \ell\ell$ . There is also a significant fraction of events with additional jets. The  
 318 3-jet sample is mainly comprised of  $t\bar{t}$  events with 1 additional emission and similarly the  $\geq 4$ -jet sample  
 319 contains primarily  $t\bar{t} + \geq 2$  jet events.

320 It should be noted that in the case of  $t\bar{t} \rightarrow \ell\ell$  events with a single reconstructed lepton, the other lepton  
 321 may be mis-reconstructed as a jet. For example, a hadronic tau may be misidentified as a jet (since no  
 322  $\tau$  identification is used). In this case only 1 additional jet from radiation may suffice for a  $t\bar{t} \rightarrow \ell\ell$  event  
 323 to enter the signal sample. As a result, both the samples with  $t\bar{t} + 1$  jet and  $t\bar{t} + \geq 2$  jets are relevant for  
 324 estimating the top dilepton background in the signal region.

325 Table 15 shows scale factors ( $K_3$  and  $K_4$ ) used to correct the fraction of events with additional jets in  
 326 MC to the observed fraction in data. These scale factors are calculated from Fig. 9 as follows:

- 327 •  $N_2$  = data yield minus non-dilepton  $t\bar{t}$  MC yield for  $N_{\text{jets}} = 1$  or 2.
- 328 •  $N_3$  = data yield minus non-dilepton  $t\bar{t}$  MC yield for  $N_{\text{jets}} = 3$
- 329 •  $N_4$  = data yield minus non-dilepton  $t\bar{t}$  MC yield for  $N_{\text{jets}} \geq 4$
- 330 •  $M_2$  = dilepton  $t\bar{t}$  MC yield for  $N_{\text{jets}} = 1$  or 2
- 331 •  $M_3$  = dilepton  $t\bar{t}$  MC yield for  $N_{\text{jets}} = 3$
- 332 •  $M_4$  = dilepton  $t\bar{t}$  MC yield for  $N_{\text{jets}} \geq 4$

333 then

- 334 •  $SF_2 = N_2/M_2$
- 335 •  $SF_3 = N_3/M_3$
- 336 •  $SF_4 = N_4/M_4$
- 337 •  $K_3 = SF_3/SF_2$
- 338 •  $K_4 = SF_4/SF_2$

339 This insures that  $K_3 M_3 / (M_2 + K_3 M_3 + K_4 M_4) = N_3 / (N_2 + N_3 + N_4)$  and similarly for the  $\geq 4$  jet bin.

340 Table 15 also shows the values of  $K_3$  and  $K_4$  for different values of the  $E_T^{\text{miss}}$  cut in the control sample  
 341 definition. This demonstrates that there is no statistically significant dependence of  $K_3$  and  $K_4$  on the  
 342  $E_T^{\text{miss}}$  cut.

343 The factors  $K_3$  and  $K_4$  (derived with the 100 GeV  $E_T^{\text{miss}}$  cut) are applied to the  $t\bar{t} \rightarrow \ell\ell$  MC throughout  
 344 the entire analysis, i.e. whenever  $t\bar{t} \rightarrow \ell\ell$  MC is used to estimate or subtract a yield or distribution.

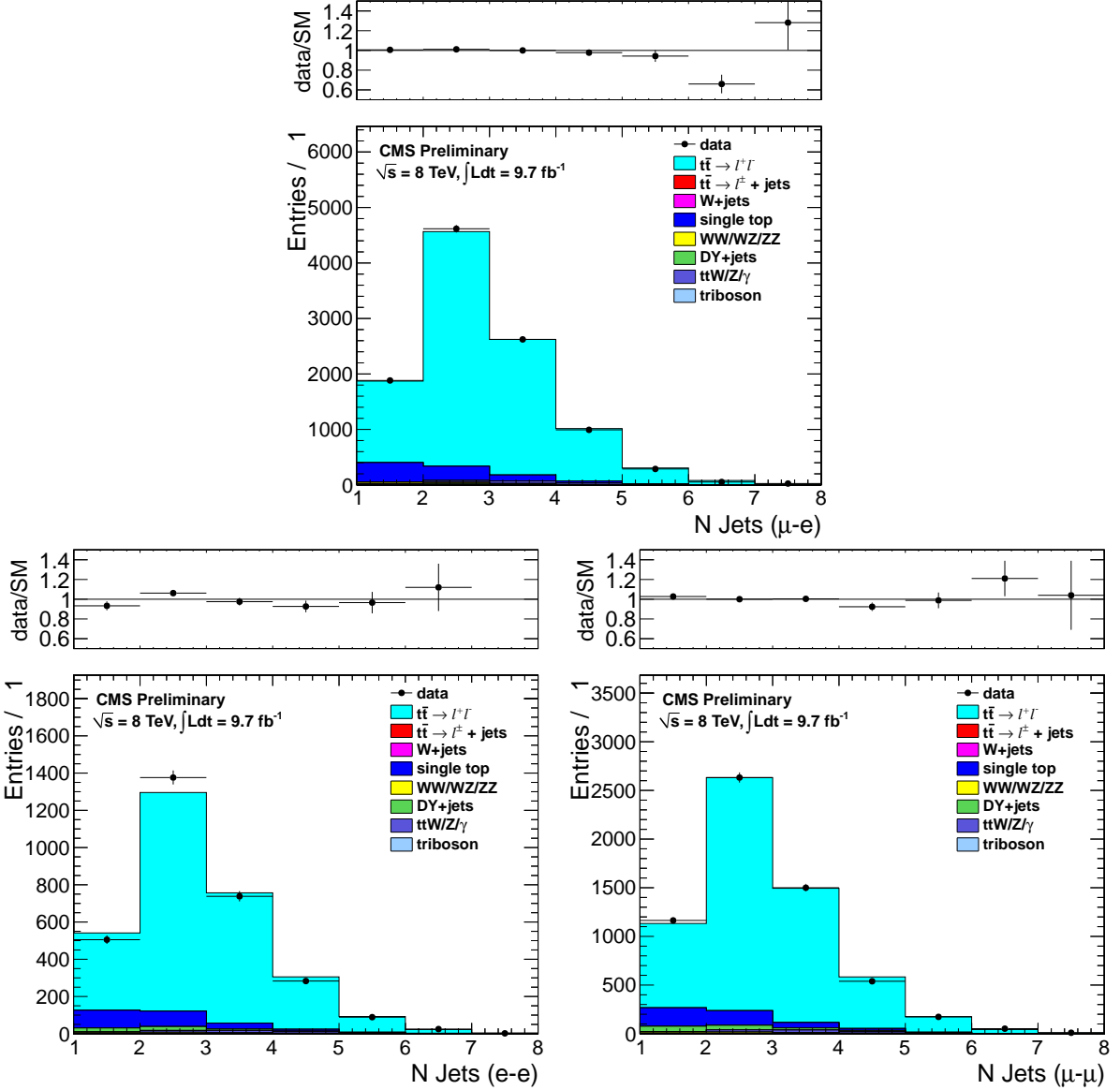


Figure 9: Comparison of the jet multiplicity distribution in data and MC for dilepton events in the  $e-\mu$  (top),  $e-e$  (bottom left) and  $\mu-\mu$  (bottom right) channels.

345 To be explicit, whenever Powheg is used, the Powheg  $K_3$  and  $K_4$  are used; whenever default MadGraph  
 346 is used, the MadGraph  $K_3$  and  $K_4$  are used, etc. In order to do so, it is first necessary to count the  
 347 number of additional jets from radiation and exclude leptons misidentified as jets. A jet is considered a  
 348 misidentified lepton if it is matched to a generator-level second lepton with sufficient energy to satisfy  
 349 the jet  $p_T$  requirement ( $p_T > 30$  GeV). Then  $t\bar{t} \rightarrow ll$  events that need two radiation jets to enter our  
 350 selection are scaled by  $K_4$ , while those that only need one radiation jet are scaled by  $K_3$ .

Sample	$E_T^{\text{miss}}$ cut for data/MC scale factors					
	50 GeV	100 GeV	150 GeV	200 GeV	250 GeV	300 GeV
N jets = 3	$K_3 = 0.98 \pm 0.02$	$K_3 = 1.01 \pm 0.03$	$K_3 = 1.00 \pm 0.08$	$K_3 = 1.03 \pm 0.18$	$K_3 = 1.29 \pm 0.51$	$K_3 = 1.58 \pm 1.23$
N jets $\geq 4$	$K_4 = 0.94 \pm 0.02$	$K_4 = 0.93 \pm 0.04$	$K_4 = 1.00 \pm 0.08$	$K_4 = 1.07 \pm 0.18$	$K_4 = 1.30 \pm 0.48$	$K_4 = 1.65 \pm 1.19$

Table 15: Data/MC scale factors used to account for differences in the fraction of events with additional hard jets from radiation in  $t\bar{t} \rightarrow \ell\ell$  events. The N jets = 3 scale factor,  $K_3$ , is sensitive to  $t\bar{t} + 1$  extra jet from radiation, while the N jets  $\geq 4$  scale factor,  $K_4$ , is sensitive to  $t\bar{t} + \geq 2$  extra jets from radiation. The values derived with the 100 GeV  $E_T^{\text{miss}}$  cut are applied to the  $t\bar{t} \rightarrow \ell\ell$  MC throughout the analysis.

351 **5.3.2 Validation of the “Physics” Modelling of the  $t\bar{t} \rightarrow \ell\ell$  MC in CR4**

- 352 As mentioned above,  $t\bar{t} \rightarrow$  dileptons where one of the leptons is somehow lost constitutes the main  
 353 background. The object of this test is to validate the  $M_T$  distribution of this background by looking at  
 354 the  $M_T$  distribution of well identified dilepton events. We construct a transverse mass variable from the  
 355 leading lepton and the  $E_T^{\text{miss}}$ . We distinguish between events with leading electrons and leading muons.  
 356 The  $t\bar{t}$  MC is corrected using the  $K_3$  and  $K_4$  factors from Section 5.3.1. It is also normalized to the  
 357 total data yield separately for the  $E_T^{\text{miss}}$  requirements of the various signal regions. These normalization  
 358 factors are listed in Table 16 and are close to unity.  
 359 The underlying  $E_T^{\text{miss}}$  and  $M_T$  distributions are shown in Figures 39 and 11. The data-MC agreement is  
 360 quite good. Quantitatively, this is also shown in Table 17. This is a **very** important Table. It shows that  
 361 for well identified  $t\bar{t} \rightarrow \ell\ell$ , the MC can predict the  $M_T$  tail. Since the main background is also  $t\bar{t} \rightarrow \ell\ell$   
 362 except with one “missed” lepton, this is a key test.

Sample	CR4PRESEL	CR4A	CR4B	CR4C	CR4D	CR4E	CR4F
$\mu$ Data/MC-SF	$1.01 \pm 0.03$	$0.96 \pm 0.04$	$0.99 \pm 0.07$	$1.05 \pm 0.13$	$0.91 \pm 0.20$	$1.10 \pm 0.34$	$1.50 \pm 0.67$
e Data/MC-SF	$0.99 \pm 0.03$	$0.99 \pm 0.05$	$0.91 \pm 0.08$	$0.84 \pm 0.13$	$0.70 \pm 0.18$	$0.73 \pm 0.29$	$0.63 \pm 0.38$

Table 16: Data/MC scale factors for total yields, applied to compare the shapes of the distributions. The uncertainties are statistical only.

Sample	CR4PRESEL	CR4A	CR4B	CR4C	CR4D	CR4E	CR4F
$\mu$ MC	$256 \pm 14$	$152 \pm 11$	$91 \pm 9$	$26 \pm 5$	$6 \pm 2$	$4 \pm 2$	$2 \pm 1$
$\mu$ Data	251	156	98	27	8	6	4
$\mu$ Data/MC SF	$0.98 \pm 0.08$	$1.02 \pm 0.11$	$1.08 \pm 0.16$	$1.04 \pm 0.28$	$1.29 \pm 0.65$	$1.35 \pm 0.80$	$2.10 \pm 1.72$
e MC	$227 \pm 13$	$139 \pm 11$	$73 \pm 8$	$21 \pm 4$	$5 \pm 2$	$2 \pm 1$	$1 \pm 1$
e Data	219	136	72	19	2	1	1
e Data/MC SF	$0.96 \pm 0.09$	$0.98 \pm 0.11$	$0.99 \pm 0.16$	$0.92 \pm 0.29$	$0.41 \pm 0.33$	$0.53 \pm 0.62$	$0.76 \pm 0.96$
$\mu+e$ MC	$483 \pm 19$	$291 \pm 16$	$164 \pm 13$	$47 \pm 7$	$11 \pm 3$	$6 \pm 2$	$3 \pm 2$
$\mu+e$ Data	470	292	170	46	10	7	5
$\mu+e$ Data/MC SF	$0.97 \pm 0.06$	$1.00 \pm 0.08$	$1.04 \pm 0.11$	$0.99 \pm 0.20$	$0.90 \pm 0.37$	$1.11 \pm 0.57$	$1.55 \pm 1.04$

Table 17: Yields in  $M_T$  tail comparing the MC prediction (after applying SFs) to data. The uncertainties are statistical only.

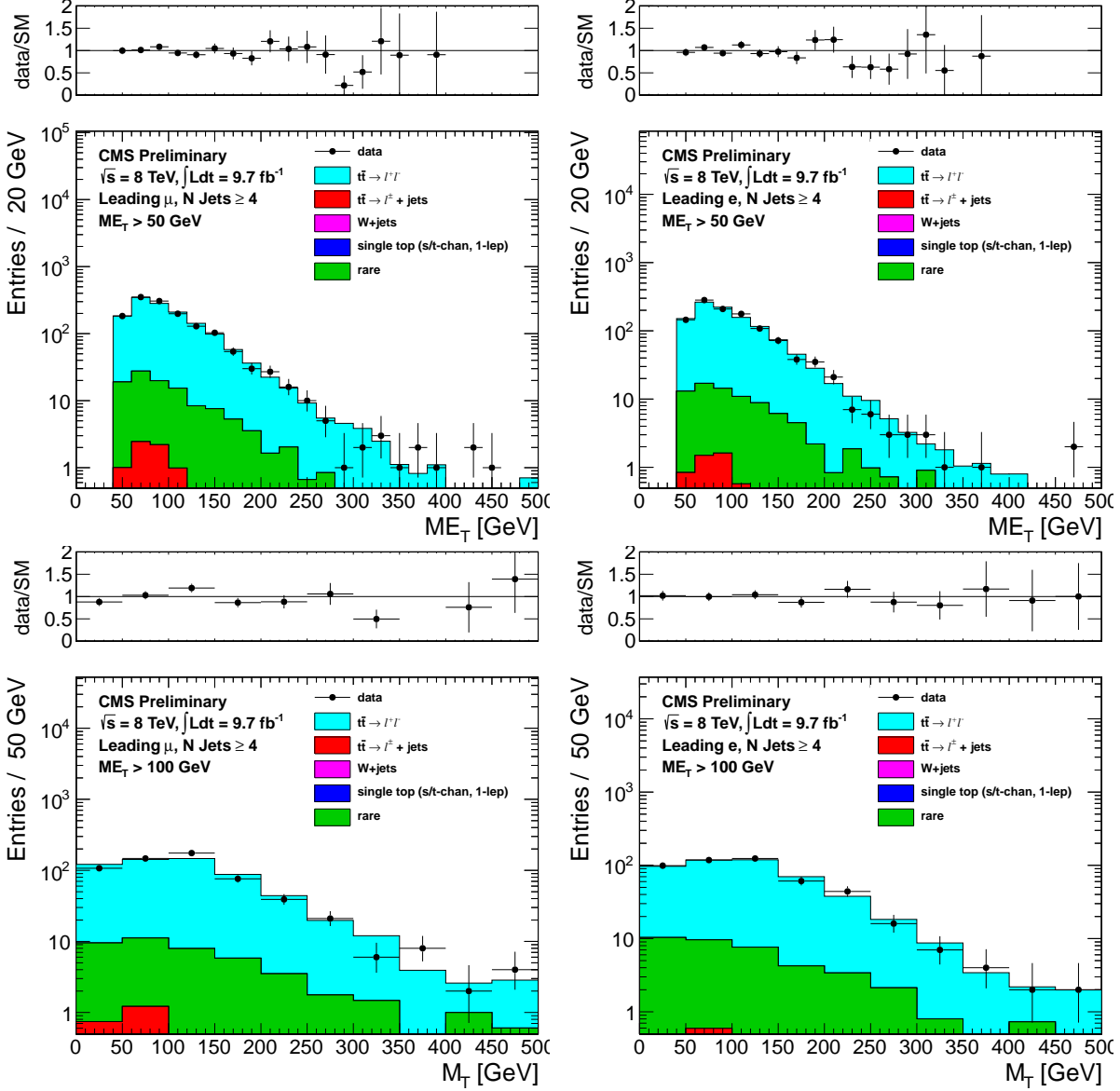


Figure 10: Comparison of the  $E_T^{\text{miss}}$  (top) and  $M_T$  for  $E_T^{\text{miss}} > 100$  (bottom) distributions in data vs. MC for events with a leading muon (left) and leading electron (right) satisfying the requirements of CR4.

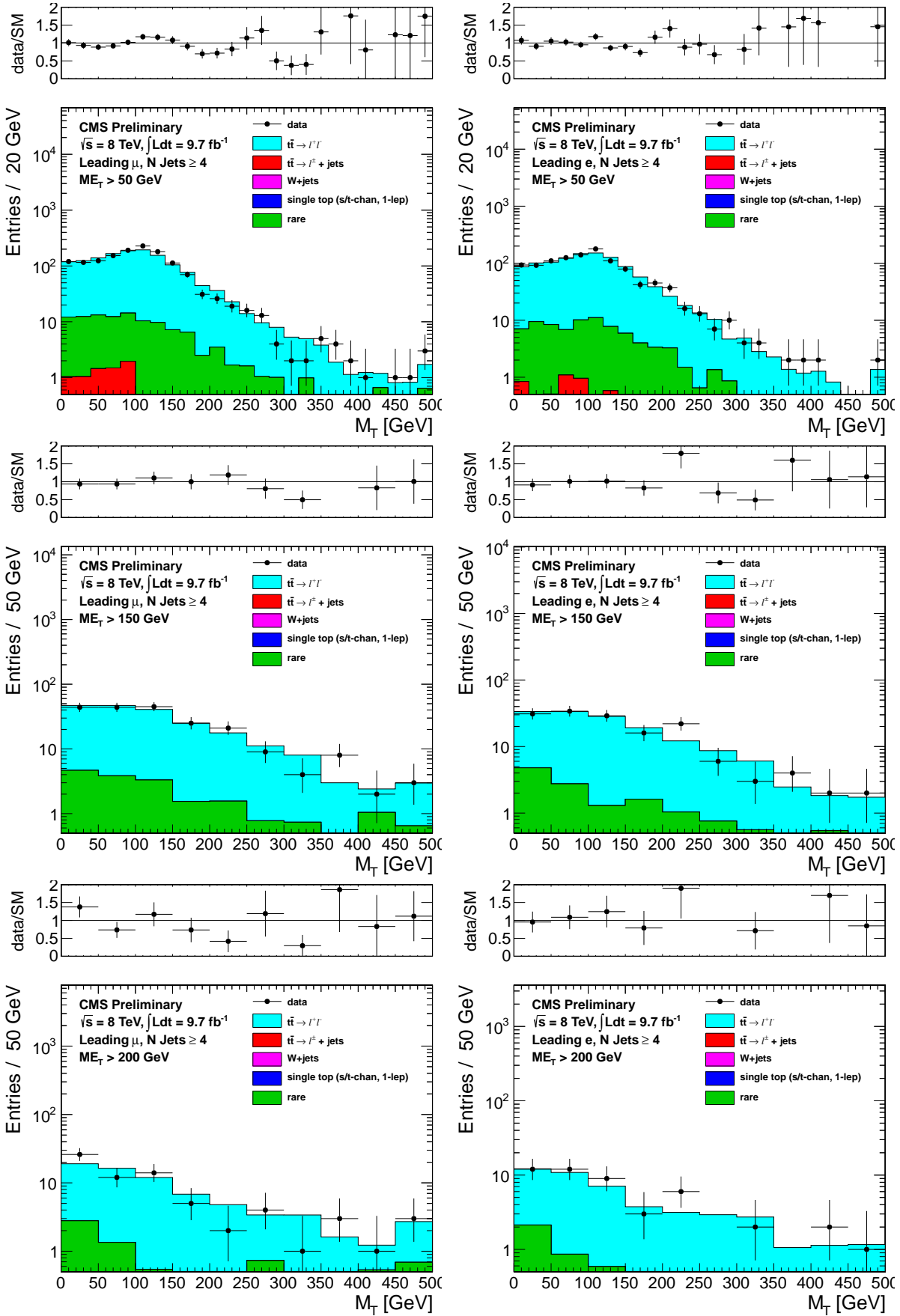


Figure 11: Comparison of the  $M_T$  distribution in data vs. MC for events with a leading muon (left) and leading electron (right) satisfying the requirements of CR4. The  $E_T^{\text{miss}}$  requirements used are 50 GeV (top), 200 GeV (middle) and 250 GeV (bottom).

## 363 5.4 Test of control region with isolated track in CR5

364 This CR consists of events that pass all cuts but fail the isolated track veto cut. These events (especially  
 365 in the tail of  $M_T$ ) are predominantly  $t\bar{t}$  dileptons. Thus the test in this control region is similar to that  
 366 performed in CR4 and described in Section 5.3.2. There is some non-trivial complementarity because  
 367 CR5 also includes events with taus and events with electrons or muons below the threshold of the CR4  
 368 selection. Also, this test is somewhat sensitive to the simulation of the track isolation requirement, since  
 369 the number of dilepton events in CR5 depends on the (in)efficiency of that cut.

370 In CR5 there is also a significant component of  $t\bar{t} \rightarrow \ell + \text{jets}$ , where one of the jets fluctuates to an isolated  
 371 track. This component dominates at low  $M_T$  and is not necessarily well reproduced quantitatively by  
 372 the simulation. This makes the normalization of the top MC a little bit tricky. We define a “pre-veto”  
 373 sample as the sample of events that pass all cuts without any isolated track requirements. This sample  
 374 is dominated by  $t\bar{t} \rightarrow \ell + \text{jets}$ . We normalize the dilepton component of the top MC to that sample. This  
 375 is done by normalizing the total  $t\bar{t}$  MC to the  $M_T$  peak region,  $50 < M_T < 80$  GeV in this sample.

376 Next we define a “post-veto” sample as the events that have an isolated track (note that we use the  
 377 term “post-veto” to refer to the application of the isolated track cut of the sample, which in this case  
 378 is an isolated track requirement). The  $t\bar{t} \rightarrow \ell + \text{jets}$  component is normalized in this sample, again by  
 379 normalizing to the  $M_T$  peak region. These normalization factors are summarized in Table 18.

380 The post-veto  $t\bar{t} \rightarrow \ell\ell$  is taken from MC, but with scale factor obtained by the normalization of the  
 381 “pre-veto” sample.

382 The underlying  $E_T^{\text{miss}}$  and  $M_T$  distributions are shown in Figures 40 and 13. The data-MC agreement  
 383 is quite good. Quantitatively, this is also shown in Table 19. This is the second key test of the  $t\bar{t} \rightarrow \ell\ell$   
 384 modeling

Sample	CR5PRESEL	CR5A	CR5B	CR5C	CR5D	CR5E	CR5F	CR5G
$\mu$ pre-veto $M_T$ -SF	$1.05 \pm 0.01$	$1.02 \pm 0.02$	$0.95 \pm 0.03$	$0.90 \pm 0.05$	$0.98 \pm 0.08$	$0.97 \pm 0.13$	$0.85 \pm 0.18$	$0.92 \pm 0.31$
$\mu$ post-veto $M_T$ -SF	$1.25 \pm 0.04$	$1.17 \pm 0.07$	$1.05 \pm 0.12$	$0.85 \pm 0.19$	$0.84 \pm 0.30$	$1.07 \pm 0.54$	$1.38 \pm 1.14$	$0.68 \pm 2.05$
e pre-veto $M_T$ -SF	$1.01 \pm 0.01$	$0.95 \pm 0.02$	$0.95 \pm 0.03$	$0.94 \pm 0.06$	$0.85 \pm 0.09$	$0.84 \pm 0.13$	$1.05 \pm 0.23$	$1.04 \pm 0.33$
e post-veto $M_T$ -SF	$1.21 \pm 0.04$	$1.12 \pm 0.07$	$1.25 \pm 0.14$	$1.17 \pm 0.27$	$2.01 \pm 0.64$	$1.71 \pm 0.99$	$2.79 \pm 2.04$	$0.81 \pm 1.58$

Table 18:  $M_T$  peak Data/MC scale factors. The pre-veto SFs are applied to the  $t\bar{t} \rightarrow \ell\ell$  sample, while  
 the post-veto SFs are applied to the single lepton samples. The raw MC is used for backgrounds from  
 rare processes. The uncertainties are statistical only.

Sample	CR5PRESEL	CR5A	CR5B	CR5C	CR5D	CR5E	CR5F	CR5G
$\mu$ MC	$490 \pm 9$	$299 \pm 7$	$155 \pm 6$	$49 \pm 3$	$19 \pm 2$	$7 \pm 1$	$3 \pm 1$	$2 \pm 1$
$\mu$ Data	514	311	167	57	12	4	2	1
$\mu$ Data/MC SF	$1.05 \pm 0.05$	$1.04 \pm 0.06$	$1.08 \pm 0.09$	$1.17 \pm 0.17$	$0.64 \pm 0.20$	$0.54 \pm 0.29$	$0.66 \pm 0.49$	$0.58 \pm 0.62$
e MC	$405 \pm 8$	$239 \pm 7$	$130 \pm 5$	$43 \pm 3$	$16 \pm 2$	$8 \pm 1$	$6 \pm 2$	$3 \pm 1$
e Data	427	248	120	38	14	4	3	2
e Data/MC SF	$1.06 \pm 0.06$	$1.04 \pm 0.07$	$0.93 \pm 0.09$	$0.89 \pm 0.16$	$0.86 \pm 0.25$	$0.52 \pm 0.28$	$0.54 \pm 0.35$	$0.76 \pm 0.60$
$\mu+e$ MC	$894 \pm 12$	$538 \pm 10$	$284 \pm 8$	$92 \pm 4$	$35 \pm 3$	$15 \pm 2$	$9 \pm 2$	$4 \pm 1$
$\mu+e$ Data	941	559	287	95	26	8	5	3
$\mu+e$ Data/MC SF	$1.05 \pm 0.04$	$1.04 \pm 0.05$	$1.01 \pm 0.07$	$1.04 \pm 0.12$	$0.74 \pm 0.16$	$0.53 \pm 0.20$	$0.58 \pm 0.29$	$0.69 \pm 0.43$

Table 19: Yields in  $M_T$  tail comparing the MC prediction (after applying SFs) to data. The uncertainties  
 are statistical only.

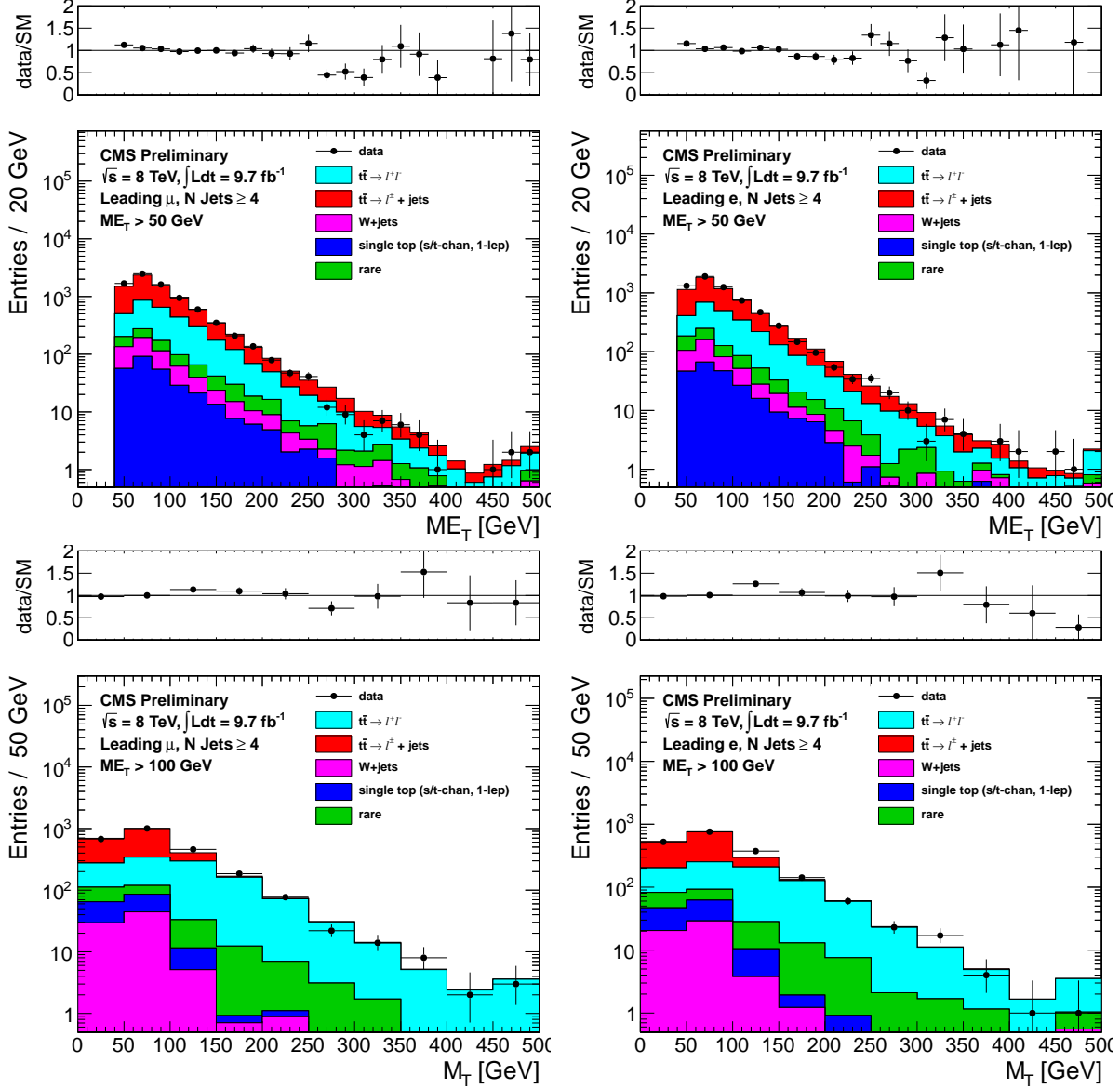


Figure 12: Comparison of the  $E_T^{\text{miss}}$  (top) and  $M_T$  for  $E_T^{\text{miss}} > 100$  (bottom) distributions in data vs. MC for events with a leading muon (left) and leading electron (right) satisfying the requirements of CR5.

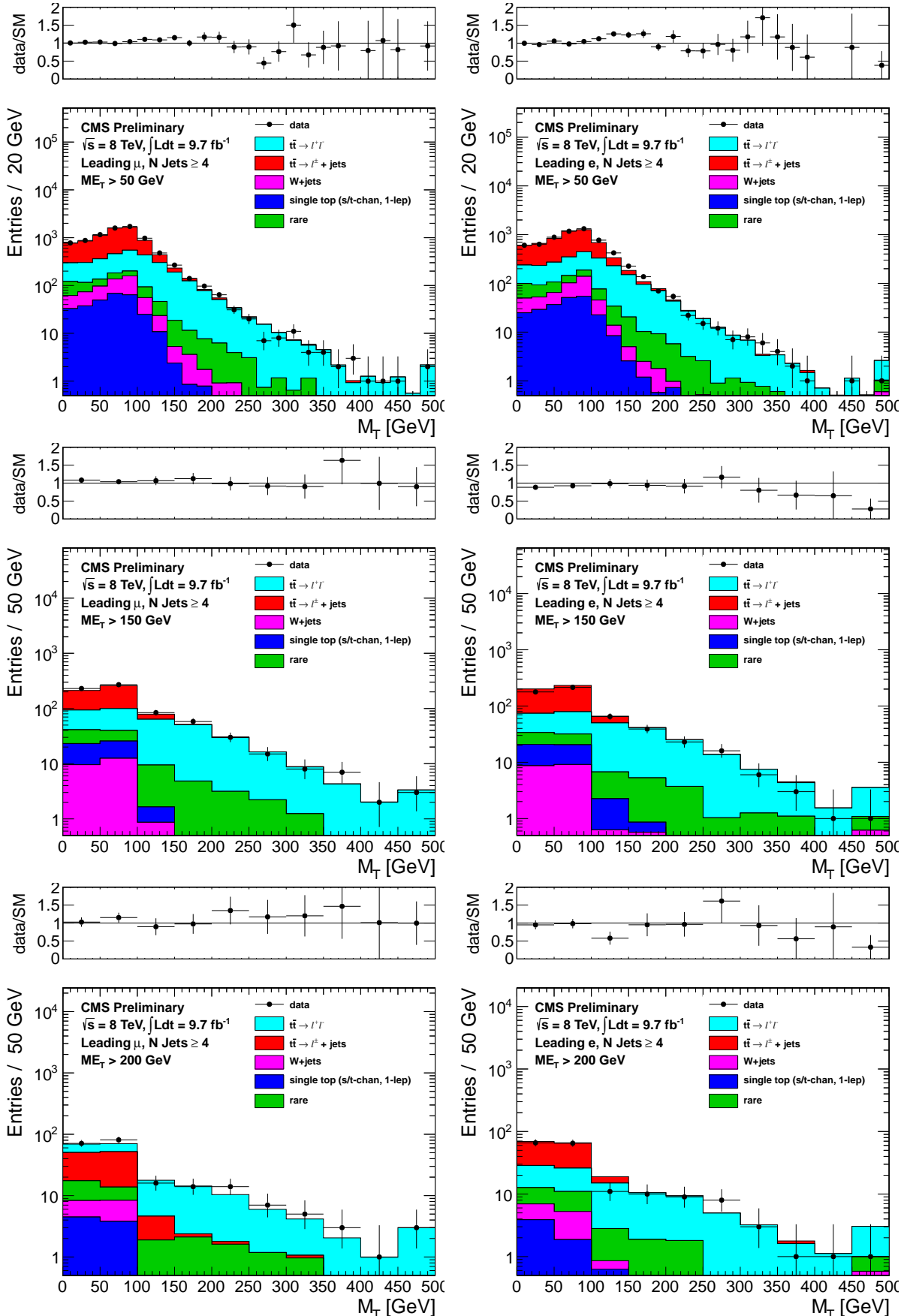


Figure 13: Comparison of the  $M_T$  distribution in data vs. MC for events with a leading muon (left) and leading electron (right) satisfying the requirements of CR5. The  $E_T^{\text{miss}}$  requirements used are 50 GeV (top), 150 GeV (middle) and 200 GeV (bottom).

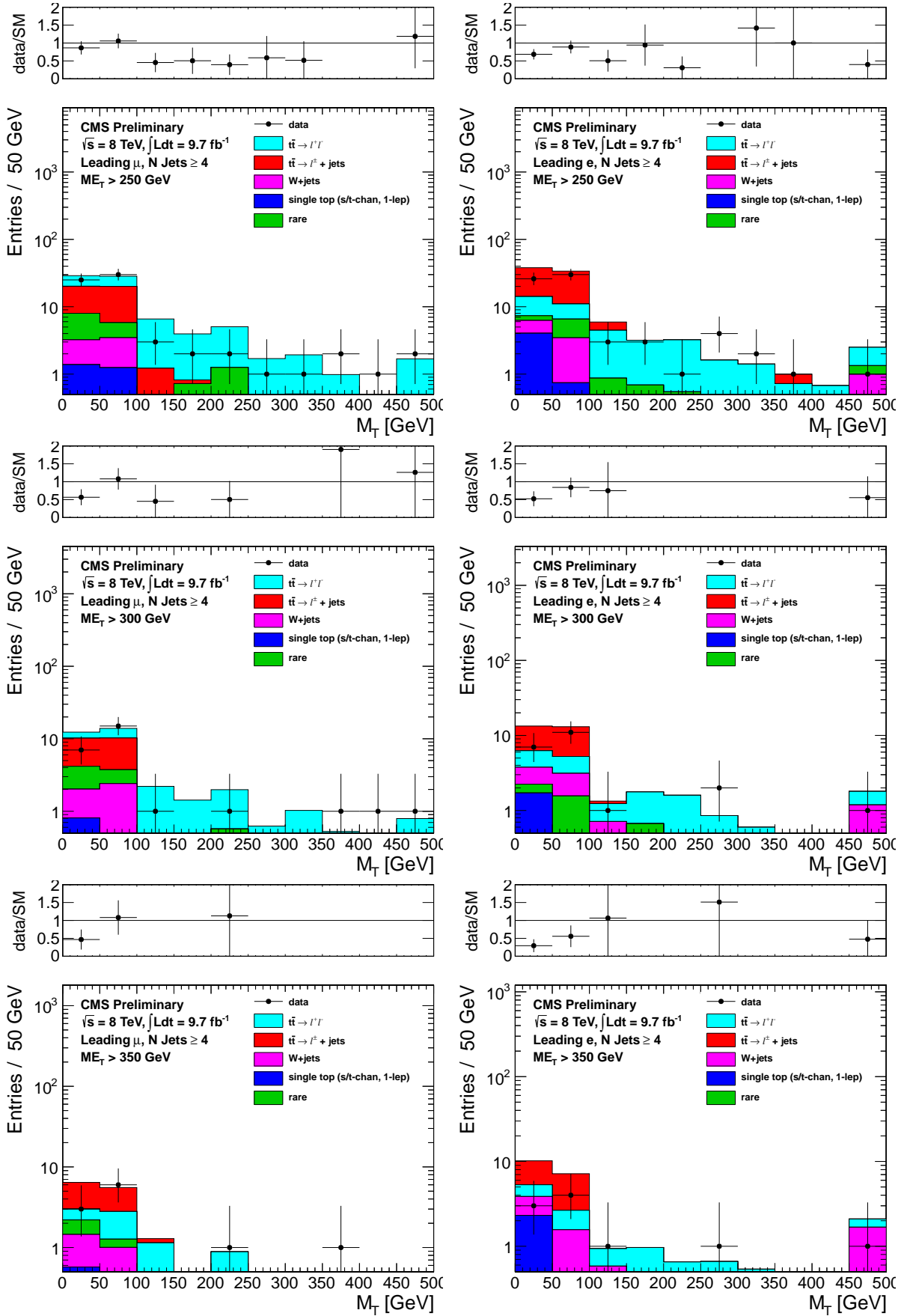


Figure 14: Comparison of the  $M_T$  distribution in data vs. MC for events with a leading muon (left) and leading electron (right) satisfying the requirements of CR5. The  $E_T^{\text{miss}}$  requirements used are 250 GeV (top), 300 GeV (middle) and 350 GeV (bottom).

## 385 6 Other Backgrounds

386 Additional background contributions from rare processes include

- 387 •  $t\bar{t}$  in association with a boson,  $t\bar{t} + WZ/\gamma^*$

388

- 389 •  $Z/\gamma^* + \text{Jets}$

390

- 391 • diboson,  $WW/WZ/ZZ$

392

- 393 • triboson,  $WWW/WWZ/WZZ/ZZZ$

394

- 395 • dilepton single top,  $tW$ .

396

397 These backgrounds are small, contributing at the  $\sim 5\%$  level and their predictions are taken from MC,  
 398 normalized to the corresponding cross sections. A 50% systematic uncertainty is assigned for all these  
 399 backgrounds. Note that these backgrounds are not double-counted because the contribution to the  $M_T$   
 400 peak region is subtracted off when deriving the  $M_T$  peak data/MC scale factors.

401 Backgrounds from QCD are expected to be small in the signal regions with large  $M_T$  and  $E_T^{\text{miss}}$ .

## 402 7 Tail-to-Peak ratio for lepton + jets top and W events

403 An important component of the background calculation is the ratio of the number of events with  $M_T$  in  
 404 the signal region to the number of events with  $50 < M_T < 80$  GeV. As discussed in Section 2.1, these  
 405 ratios are different for  $W+\text{jets}$  and top events.

Sample	SRA	SRB	SRC	SRD	SRE	SRF	SRG
Muons							
$R_{top}^{MC}$	$0.015 \pm 0.001$	$0.035 \pm 0.002$	$0.021 \pm 0.002$	$0.021 \pm 0.004$	$0.025 \pm 0.007$	$0.015 \pm 0.009$	$0.021 \pm 0.015$
$R_{wjet}^{MC}$	$0.040 \pm 0.001$	$0.071 \pm 0.003$	$0.062 \pm 0.004$	$0.064 \pm 0.006$	$0.065 \pm 0.009$	$0.067 \pm 0.012$	$0.065 \pm 0.016$
Electrons							
$R_{top}^{MC}$	$0.015 \pm 0.001$	$0.031 \pm 0.002$	$0.026 \pm 0.003$	$0.025 \pm 0.005$	$0.009 \pm 0.005$	$0.021 \pm 0.012$	$0.034 \pm 0.024$
$R_{wjet}^{MC}$	$0.040 \pm 0.002$	$0.075 \pm 0.004$	$0.067 \pm 0.005$	$0.063 \pm 0.007$	$0.061 \pm 0.010$	$0.067 \pm 0.015$	$0.070 \pm 0.021$

Table 20: Ratio of MC events in the  $M_T$ -tail over events in the  $M_T$ -peak for  $t\bar{t} \rightarrow \ell + \text{jets}$  (also used for 1-lepton single top) and  $W+\text{jets}$ . These are derived before applying the b-tagging requirement.

406 The MC values of these ratios are shown in Table 20. The e and  $\mu$  channel results are averaged before  
 407 corrections are made.

408 The MC value of  $R_{wjet}^{MC}$  is corrected based on the studies of CR1 (Section D.3), which lead to the data/MC  
 409 scale factor  $SFR_{wjet}$  (Table 13). The corrected  $R_{wjet}$  is thus given by  $R_{wjet}^{MC} \times SFR_{wjet}$ .

410 There is no similar scale factor to correct the MC value of  $R_{top}^{MC}$  due to the lack of events in CR2  
 411 (Section 5.2). We must therefore use a different procedure to derive a corrected value of  $R_{top}$ .

412 We start by defining optimistic (too small) and pessimistic (too large) predictions for  $R_{top}$ .

413 For the pessimistic prediction, we use the  $W+\text{jets}$  MC tail-to-peak ratio and data/MC scale factor,  $R_{wjet}^{MC}$   
 414 and  $SFR_{wjet}$  (i.e. the pessimistic prediction is the same as  $R_{wjet}$ ). This prediction is too large because  
 415 in  $W+\text{jets}$  events the  $M_T$  tail comes from off-shell Ws and resolution effects, while in top events to first  
 416 order only resolution effects matter.

417 For the optimistic prediction, we use the  $t\bar{t} \rightarrow \ell + \text{jets}$  MC tail-to-peak ratio  $R_{top}^{MC}$ , but take the  $W+\text{jets}$   
 418 data/MC scale factor  $SFR_{wjet}$ . This prediction is too small because the true top scale factor is to first

- order the same as for on-shell Ws, while  $SFR_{wjet}$  is a weighted average of the scale factor for on-shell Ws (which is  $> 1$ ) and the scale factor for off-shell Ws (which is close to 1 as it is well modeled by MC).  
The final prediction for  $R_{top}$  is given by the average of the optimistic and pessimistic predictions, and the systematic uncertainty is given by half the difference between the two.  
The corrected values of  $R_{wjet}$  and  $R_{top}$  and their uncertainties are given in Table 21.

Sample	SRA	SRB	SRC	SRD	SRE	SRF	SRG
$R_{top}$	$0.045 \pm 0.023$	$0.074 \pm 0.031$	$0.055 \pm 0.031$	$0.042 \pm 0.028$	$0.041 \pm 0.036$	$0.052 \pm 0.049$	$0.053 \pm 0.066$
$R_{wjet}$	$0.066 \pm 0.015$	$0.101 \pm 0.022$	$0.081 \pm 0.025$	$0.061 \pm 0.029$	$0.064 \pm 0.042$	$0.082 \pm 0.062$	$0.075 \pm 0.088$

Table 21: Corrected values of  $R_{wjet}$  and  $R_{top}$ . Both statistical and systematic uncertainties are included.

## 424 8 Background Prediction

425 Here we give the details of how we arrive at the background prediction in a given signal region. We con-  
 426 centrate on the method used to arrive at the central value of the background prediction. The systematic  
 427 uncertainties will be discussed in Section 9. The actual results for the BG prediction will be given in  
 428 Section 10.

429 As mentioned in Section 2, we normalize the main  $t\bar{t}$  background to the  $M_T$  peak. This is actually a  
 430 bit tricky because we want to minimize the effect of the isolated track veto on lepton + jets events,  
 431 which may not be terribly well reproduced. Thus, we define two normalization region in the  $M_T$  peak  
 432 ( $50 < M_T < 80$  GeV), one before and one after the application of the isolated track veto.

433 The event counts in pre-veto and post-veto normalization regions are given in Tables 22 and 23. The  
 434 data-MC agreement in these two tables is quite good, and this is certainly a good thing.

Sample	SRA	SRB	SRC	SRD	SRE	SRF	SRG
Muon							
$t\bar{t} \rightarrow \ell\ell$	$371 \pm 6$	$120 \pm 4$	$43 \pm 2$	$17 \pm 1$	$8 \pm 1$	$4 \pm 1$	$1 \pm 0$
$t\bar{t} \rightarrow \ell + \text{jets} \& \text{single top } (1\ell)$	$3666 \pm 21$	$1088 \pm 12$	$355 \pm 7$	$127 \pm 4$	$50 \pm 3$	$22 \pm 2$	$8 \pm 1$
$W+\text{jets}$	$316 \pm 8$	$113 \pm 5$	$46 \pm 3$	$21 \pm 2$	$11 \pm 1$	$5 \pm 1$	$2 \pm 1$
Rare	$117 \pm 5$	$48 \pm 3$	$16 \pm 2$	$6 \pm 1$	$2 \pm 1$	$1 \pm 0$	$1 \pm 0$
Total	$4470 \pm 24$	$1369 \pm 13$	$461 \pm 8$	$171 \pm 5$	$71 \pm 3$	$33 \pm 2$	$13 \pm 1$
Data	4538	1304	418	168	69	28	12
Electron							
$t\bar{t} \rightarrow \ell\ell$	$290 \pm 6$	$98 \pm 3$	$35 \pm 2$	$13 \pm 1$	$6 \pm 1$	$3 \pm 1$	$1 \pm 0$
$t\bar{t} \rightarrow \ell + \text{jets} \& \text{single top } (1\ell)$	$2899 \pm 19$	$861 \pm 10$	$282 \pm 6$	$104 \pm 4$	$42 \pm 2$	$16 \pm 2$	$8 \pm 1$
$W+\text{jets}$	$252 \pm 28$	$87 \pm 4$	$35 \pm 3$	$18 \pm 2$	$8 \pm 1$	$4 \pm 1$	$2 \pm 1$
Rare	$89 \pm 5$	$34 \pm 3$	$15 \pm 2$	$7 \pm 1$	$3 \pm 1$	$0 \pm 0$	$0 \pm 0$
Total	$3530 \pm 35$	$1079 \pm 12$	$367 \pm 7$	$142 \pm 5$	$60 \pm 3$	$24 \pm 2$	$11 \pm 1$
Data	3358	1022	346	122	51	25	12
Muon+Electron Combined							
$t\bar{t} \rightarrow \ell\ell$	$661 \pm 9$	$218 \pm 5$	$78 \pm 3$	$30 \pm 2$	$14 \pm 1$	$7 \pm 1$	$3 \pm 1$
$t\bar{t} \rightarrow \ell + \text{jets} \& \text{single top } (1\ell)$	$6565 \pm 28$	$1949 \pm 16$	$637 \pm 9$	$231 \pm 5$	$92 \pm 4$	$39 \pm 2$	$16 \pm 2$
$W+\text{jets}$	$568 \pm 29$	$199 \pm 6$	$81 \pm 4$	$38 \pm 3$	$19 \pm 2$	$9 \pm 1$	$4 \pm 1$
Rare	$206 \pm 7$	$82 \pm 4$	$31 \pm 3$	$14 \pm 2$	$5 \pm 1$	$2 \pm 0$	$1 \pm 0$
Total	$8000 \pm 42$	$2448 \pm 18$	$828 \pm 11$	$314 \pm 7$	$131 \pm 4$	$56 \pm 3$	$24 \pm 2$
Data	7896	2326	764	290	120	53	24

Table 22: Preveto MC and data yields in  $M_T$  peak region. The n-jets k-factors have been applied to the  $t\bar{t} \rightarrow \ell\ell$ . The uncertainties are statistical only. These MC and data yields are used to derive data/MC SFs, the pre-veto  $M_T$ -SFs, shown in Table 24.

Sample	SRA	SRB	SRC	SRD	SRE	SRF	SRG
Muon							
$t\bar{t} \rightarrow \ell\ell$	$139 \pm 4$	$46 \pm 2$	$16 \pm 1$	$7 \pm 1$	$3 \pm 1$	$1 \pm 0$	$1 \pm 0$
$t\bar{t} \rightarrow \ell + \text{jets} \& \text{single top } (1\ell)$	$3273 \pm 20$	$974 \pm 11$	$321 \pm 6$	$113 \pm 4$	$45 \pm 2$	$21 \pm 2$	$8 \pm 1$
$W + \text{jets}$	$294 \pm 8$	$105 \pm 5$	$42 \pm 3$	$19 \pm 2$	$10 \pm 1$	$5 \pm 1$	$2 \pm 1$
Rare	$83 \pm 4$	$34 \pm 3$	$11 \pm 1$	$4 \pm 1$	$2 \pm 1$	$1 \pm 0$	$1 \pm 0$
Total	$3789 \pm 22$	$1160 \pm 12$	$391 \pm 7$	$143 \pm 4$	$60 \pm 3$	$28 \pm 2$	$11 \pm 1$
Data	3790	1098	358	143	59	24	11
Electron							
$t\bar{t} \rightarrow \ell\ell$	$116 \pm 4$	$40 \pm 2$	$14 \pm 1$	$5 \pm 1$	$2 \pm 0$	$1 \pm 0$	$1 \pm 0$
$t\bar{t} \rightarrow \ell + \text{jets} \& \text{single top } (1\ell)$	$2595 \pm 18$	$774 \pm 10$	$258 \pm 6$	$97 \pm 4$	$40 \pm 2$	$15 \pm 1$	$7 \pm 1$
$W + \text{jets}$	$236 \pm 28$	$82 \pm 4$	$33 \pm 3$	$17 \pm 2$	$8 \pm 1$	$4 \pm 1$	$2 \pm 1$
Rare	$62 \pm 4$	$23 \pm 2$	$9 \pm 1$	$4 \pm 1$	$2 \pm 1$	$0 \pm 0$	$0 \pm 0$
Total	$3009 \pm 34$	$919 \pm 11$	$315 \pm 7$	$123 \pm 4$	$51 \pm 3$	$21 \pm 2$	$10 \pm 1$
Data	2788	837	288	92	39	19	10
Muon+Electron Combined							
$t\bar{t} \rightarrow \ell\ell$	$255 \pm 5$	$86 \pm 3$	$30 \pm 2$	$12 \pm 1$	$5 \pm 1$	$2 \pm 1$	$1 \pm 0$
$t\bar{t} \rightarrow \ell + \text{jets} \& \text{single top } (1\ell)$	$5869 \pm 27$	$1747 \pm 15$	$579 \pm 9$	$209 \pm 5$	$85 \pm 3$	$36 \pm 2$	$15 \pm 2$
$W + \text{jets}$	$529 \pm 29$	$188 \pm 6$	$75 \pm 4$	$36 \pm 3$	$18 \pm 2$	$9 \pm 1$	$4 \pm 1$
Rare	$145 \pm 6$	$58 \pm 4$	$21 \pm 2$	$8 \pm 1$	$3 \pm 1$	$1 \pm 0$	$1 \pm 0$
Total	$6797 \pm 40$	$2079 \pm 17$	$705 \pm 10$	$265 \pm 6$	$111 \pm 4$	$49 \pm 3$	$21 \pm 2$
Data	6578	1935	646	235	98	43	21

Table 23: MC and data yields in  $M_T$  peak region after full selection. The n-jets k-factors have been applied to the  $t\bar{t} \rightarrow \ell\ell$ . The uncertainties are statistical only. These MC and data yields are used to derive data/MC SFs, the post-veto  $M_T$ -SFs, shown in Table 24.

435 The dominant dilepton background is normalized to the pre-veto normalization region. A pre-veto scale  
 436 factor ( $SF_{pre}$ ) is defined as a common scale factors that needs to be applied to the  $t\bar{t}$ , single-top, and  $W+$   
 437 jets MC to make the data yield in the pre-veto normalization agree with the MC prediction (the small  
 438 rare MC component is held fixed). Then, the dilepton background prediction is obtained by multiplying  
 439 the dilepton BG Monte Carlo by  $SF_{pre}$ .

440 The  $t\bar{t}$  lepton + jet BG is normalized to post-veto normalization region. A post-veto scale factor ( $SF_{post}$ )  
 441 is defined in (almost) the same way as the pre-veto scale factor. The difference here is that this scale factor  
 442 applies only to the lepton + jets components and not the dilepton component, since that component is  
 443 already rescaled by  $SF_{pre}$ . This procedure minimizes the reliance on the understanding of the isolated  
 444 track veto.

445 The pre-veto and post-veto SF are shown in Table 24.

Sample	SRA	SRB	SRC	SRD	SRE	SRF	SRG
$\mu$ pre-veto $M_T$ -SF	$1.02 \pm 0.02$	$0.95 \pm 0.03$	$0.90 \pm 0.05$	$0.98 \pm 0.08$	$0.97 \pm 0.13$	$0.85 \pm 0.18$	$0.92 \pm 0.31$
$\mu$ post-veto $M_T$ -SF	$1.00 \pm 0.02$	$0.95 \pm 0.03$	$0.91 \pm 0.05$	$1.00 \pm 0.09$	$0.99 \pm 0.13$	$0.85 \pm 0.18$	$0.96 \pm 0.31$
$\mu$ veto $M_T$ -SF	$0.98 \pm 0.01$	$0.99 \pm 0.01$	$1.01 \pm 0.02$	$1.02 \pm 0.04$	$1.02 \pm 0.06$	$1.00 \pm 0.09$	$1.04 \pm 0.11$
e pre-veto $M_T$ -SF	$0.95 \pm 0.02$	$0.95 \pm 0.03$	$0.94 \pm 0.06$	$0.85 \pm 0.09$	$0.84 \pm 0.13$	$1.05 \pm 0.23$	$1.04 \pm 0.33$
e post-veto $M_T$ -SF	$0.92 \pm 0.02$	$0.91 \pm 0.03$	$0.91 \pm 0.06$	$0.74 \pm 0.08$	$0.75 \pm 0.13$	$0.91 \pm 0.22$	$1.01 \pm 0.33$
e veto $M_T$ -SF	$0.97 \pm 0.01$	$0.96 \pm 0.02$	$0.97 \pm 0.03$	$0.87 \pm 0.05$	$0.89 \pm 0.08$	$0.86 \pm 0.11$	$0.97 \pm 0.14$

Table 24:  $M_T$  peak Data/MC scale factors. The pre-veto SFs are applied to the  $t\bar{t} \rightarrow \ell\ell$  sample, while the post-veto SFs are applied to the single lepton samples. The veto SF is shown for comparison across channels. The raw MC is used for backgrounds from rare processes. The uncertainties are statistical only.

446 Then the  $t\bar{t}$  lepton + jet BG is obtained by taking the number of MC-predicted  $t\bar{t}$  lepton + jets in the  
 447 post-veto normalization region, scaling it by  $SF_{post}$ , and multiplying it by the corrected tail-to-peak ratio  
 448  $R_{top}$  of Table 21.

449 The single top background is obtained in exactly the same way as the  $t\bar{t}$  lepton + jet BG, using the same  
 450 tail-to-peak ratio. The  $W+$ jets background is done in a similar way, but using a different tail-to-peak  
 451 ratio ( $R_{wjets}$  of Table 21).

452 Other (small) backgrounds are taken straight from Monte Carlo, as described in Section 6.

Sample	SRA	SRB	SRC	SRD	SRE	SRF	SRG
Muon							
$t\bar{t} \rightarrow \ell\ell$	$326 \pm 6$	$193 \pm 5$	$66 \pm 3$	$23 \pm 2$	$9 \pm 1$	$4 \pm 1$	$2 \pm 1$
$t\bar{t} \rightarrow \ell + \text{jets} \& \text{single top } (1\ell)$	$54 \pm 3$	$38 \pm 2$	$8 \pm 1$	$3 \pm 1$	$1 \pm 1$	$1 \pm 0$	$0 \pm 0$
$W+\text{jets}$	$17 \pm 2$	$8 \pm 1$	$3 \pm 1$	$2 \pm 1$	$0 \pm 0$	$0 \pm 0$	$0 \pm 0$
Rare	$33 \pm 2$	$23 \pm 2$	$9 \pm 1$	$5 \pm 1$	$3 \pm 1$	$1 \pm 0$	$1 \pm 0$
Total	$430 \pm 7$	$262 \pm 6$	$86 \pm 3$	$33 \pm 2$	$14 \pm 1$	$6 \pm 1$	$4 \pm 1$
Electron							
$t\bar{t} \rightarrow \ell\ell$	$261 \pm 5$	$153 \pm 4$	$54 \pm 2$	$19 \pm 1$	$7 \pm 1$	$2 \pm 1$	$1 \pm 0$
$t\bar{t} \rightarrow \ell + \text{jets} \& \text{single top } (1\ell)$	$41 \pm 2$	$28 \pm 2$	$7 \pm 1$	$3 \pm 1$	$1 \pm 0$	$1 \pm 0$	$1 \pm 0$
$W+\text{jets}$	$11 \pm 2$	$7 \pm 1$	$3 \pm 1$	$2 \pm 1$	$0 \pm 0$	$0 \pm 0$	$0 \pm 0$
Rare	$26 \pm 2$	$16 \pm 2$	$7 \pm 1$	$3 \pm 1$	$1 \pm 0$	$0 \pm 0$	$0 \pm 0$
Total	$340 \pm 6$	$204 \pm 5$	$71 \pm 3$	$26 \pm 2$	$8 \pm 1$	$4 \pm 1$	$2 \pm 1$
Muon+Electron Combined							
$t\bar{t} \rightarrow \ell\ell$	$587 \pm 8$	$346 \pm 6$	$120 \pm 4$	$42 \pm 2$	$16 \pm 1$	$7 \pm 1$	$4 \pm 1$
$t\bar{t} \rightarrow \ell + \text{jets} \& \text{single top } (1\ell)$	$95 \pm 3$	$67 \pm 3$	$15 \pm 1$	$6 \pm 1$	$2 \pm 1$	$1 \pm 1$	$1 \pm 0$
$W+\text{jets}$	$29 \pm 2$	$15 \pm 2$	$6 \pm 1$	$3 \pm 1$	$1 \pm 0$	$0 \pm 0$	$0 \pm 0$
Rare	$59 \pm 3$	$38 \pm 3$	$16 \pm 2$	$8 \pm 1$	$4 \pm 1$	$2 \pm 0$	$1 \pm 0$
Total	$770 \pm 10$	$466 \pm 7$	$157 \pm 4$	$59 \pm 3$	$22 \pm 2$	$10 \pm 1$	$6 \pm 1$

Table 25: MC yields in  $M_T$  tail region after full selection. The n-jets k-factors have been applied to the  $t\bar{t} \rightarrow \ell\ell$ . The uncertainties are statistical only. Note these values are only used for the rare backgrounds prediction.

## 453 9 Systematic Uncertainties on the Background

454 In this Section we discuss the systematic uncertainty on the BG prediction. This prediction is assembled  
455 from the event counts in the peak region of the transverse mass distribution as well as Monte Carlo with  
456 a number of correction factors, as described previously. The final uncertainty on the prediction is built  
457 up from the uncertainties in these individual components. The calculation is done for each signal region,  
458 for electrons and muons separately.

459 The choice to normalize to the peak region of  $M_T$  has the advantage that some uncertainties, e.g., luminosity,  
460 cancel. It does however introduce complications because it couples some of the uncertainties in  
461 non-trivial ways. For example, the primary effect of an uncertainty on the rare MC cross-section is to  
462 introduce an uncertainty in the rare MC background estimate which comes entirely from MC. But this  
463 uncertainty also affects, for example, the  $t\bar{t} \rightarrow$  dilepton BG estimate because it changes the  $t\bar{t}$  normaliza-  
464 tion to the peak region (because some of the events in the peak region are from rare processes). These  
465 effects are carefully accounted for. The contribution to the overall uncertainty from each background  
466 source is tabulated in Section 9.9. Here we discuss the uncertainties one-by-one and comment on their  
467 impact on the overall result, at least to first order. Second order effects, such as the one described, are  
468 also included.

### 469 9.1 Statistical uncertainties on the event counts in the $M_T$ peak regions

470 These vary between 2% and 20%, depending on the signal region (different signal regions have different  
471  $E_T^{\text{miss}}$  requirements, thus they also have different  $M_T$  regions used as control). Since the major back-  
472 grounds, eg,  $t\bar{t}$  are normalized to the peak regions, this fractional uncertainty is pretty much carried  
473 through all the way to the end. There is also an uncertainty from the finite MC event counts in the  $M_T$   
474 peak regions. This is also included, but it is smaller.

475 Normalizing to the  $M_T$  peak has the distinct advantages that uncertainties on luminosity, cross-sections,  
476 trigger efficiency, lepton ID, cancel out. For the low statistics regions with high  $E_T^{\text{miss}}$  requirements, the  
477 price to pay in terms of event count is that statistical uncertainties start to become significant. In the  
478 future we may consider a different normalization strategy in the low statistics regions.

### 479 9.2 Uncertainty from the choice of $M_T$ peak region

480 This choice affects the scale factors of Table 24. If the  $M_T$  peak region is not well modelled, this would  
481 introduce an uncertainty.  
482 We have tested this possibility by recalculating the post-veto scale factors for a different choice of  $M_T$   
483 peak region ( $40 < M_T < 100$  GeV instead of the default  $50 < M_T < 80$  GeV). This is shown in Table 26.  
484 The two results for the scale factors are very compatible. We do not take any systematic uncertainty for  
485 this possible effect.

### 486 9.3 Uncertainty on the $W$ +jets cross-section and the rare MC cross-sections

487 These are taken as 50%, uncorrelated. The primary effect is to introduce a 50% uncertainty on the  $W$ +  
488 jets and rare BG background predictions, respectively. However they also have an effect on the other BGs  
489 via the  $M_T$  peak normalization in a way that tends to reduce the uncertainty. This is easy to understand:  
490 if the  $W$  cross-section is increased by 50%, then the  $W$  background goes up. But the number of  $M_T$  peak  
491 events attributed to  $t\bar{t}$  goes down, and since the  $t\bar{t}$  BG is scaled to the number of  $t\bar{t}$  events in the peak,  
492 the  $t\bar{t}$  BG goes down.

### 493 9.4 Tail-to-peak ratios for lepton + jets top and W events

494 The tail-to-peak ratios  $R_{top}$  and  $R_{wjet}$  are described in Section 7. The data/MC scale factors are studied  
495 in CR1 and CR2 (Sections D.3 and 5.2). Only the scale factor for  $W$ +jets,  $SFR_{wjet}$ , is used, and its  
496 uncertainty is given in Table 13. This uncertainty affects both  $R_{wjet}$  and  $R_{top}$ . The additional systematic  
497 uncertainty on  $R_{top}$  from the variation between optimistic and pessimistic scenarios is given in Section 7.

Sample	SRA	SRB	SRC	SRD	SRE	SRF	SRG
$50 \leq M_T \leq 80$							
$\mu$ pre-veto $M_T$ -SF	$1.02 \pm 0.02$	$0.95 \pm 0.03$	$0.90 \pm 0.05$	$0.98 \pm 0.08$	$0.97 \pm 0.13$	$0.85 \pm 0.18$	$0.92 \pm 0.31$
$\mu$ post-veto $M_T$ -SF	$1.00 \pm 0.02$	$0.95 \pm 0.03$	$0.91 \pm 0.05$	$1.00 \pm 0.09$	$0.99 \pm 0.13$	$0.85 \pm 0.18$	$0.96 \pm 0.31$
$\mu$ veto $M_T$ -SF	$0.98 \pm 0.01$	$0.99 \pm 0.01$	$1.01 \pm 0.02$	$1.02 \pm 0.04$	$1.02 \pm 0.06$	$1.00 \pm 0.09$	$1.04 \pm 0.11$
e pre-veto $M_T$ -SF	$0.95 \pm 0.02$	$0.95 \pm 0.03$	$0.94 \pm 0.06$	$0.85 \pm 0.09$	$0.84 \pm 0.13$	$1.05 \pm 0.23$	$1.04 \pm 0.33$
e post-veto $M_T$ -SF	$0.92 \pm 0.02$	$0.91 \pm 0.03$	$0.91 \pm 0.06$	$0.74 \pm 0.08$	$0.75 \pm 0.13$	$0.91 \pm 0.22$	$1.01 \pm 0.33$
e veto $M_T$ -SF	$0.97 \pm 0.01$	$0.96 \pm 0.02$	$0.97 \pm 0.03$	$0.87 \pm 0.05$	$0.89 \pm 0.08$	$0.86 \pm 0.11$	$0.97 \pm 0.14$
$40 \leq M_T \leq 100$							
$\mu$ pre-veto $M_T$ -SF	$1.02 \pm 0.01$	$0.97 \pm 0.02$	$0.91 \pm 0.05$	$0.95 \pm 0.06$	$0.97 \pm 0.10$	$0.80 \pm 0.14$	$0.74 \pm 0.22$
$\mu$ post-veto $M_T$ -SF	$1.00 \pm 0.01$	$0.96 \pm 0.02$	$0.90 \pm 0.04$	$0.98 \pm 0.07$	$1.00 \pm 0.11$	$0.80 \pm 0.15$	$0.81 \pm 0.24$
$\mu$ veto $M_T$ -SF	$0.98 \pm 0.01$	$0.99 \pm 0.01$	$0.99 \pm 0.02$	$1.03 \pm 0.03$	$1.03 \pm 0.05$	$1.01 \pm 0.08$	$1.09 \pm 0.09$
e pre-veto $M_T$ -SF	$0.97 \pm 0.01$	$0.93 \pm 0.02$	$0.94 \pm 0.04$	$0.81 \pm 0.06$	$0.86 \pm 0.10$	$0.95 \pm 0.17$	$1.06 \pm 0.26$
e post-veto $M_T$ -SF	$0.94 \pm 0.01$	$0.91 \pm 0.02$	$0.91 \pm 0.04$	$0.71 \pm 0.06$	$0.82 \pm 0.10$	$0.93 \pm 0.17$	$1.09 \pm 0.27$
e veto $M_T$ -SF	$0.97 \pm 0.01$	$0.98 \pm 0.01$	$0.97 \pm 0.02$	$0.88 \pm 0.04$	$0.95 \pm 0.06$	$0.98 \pm 0.08$	$1.03 \pm 0.09$

Table 26:  $M_T$  peak Data/MC scale factors. The pre-veto SFs are applied to the  $t\bar{t} \rightarrow \ell\ell$  sample, while the post-veto SFs are applied to the single lepton samples. The veto SF is shown for comparison across channels. The raw MC is used for backgrounds from rare processes. The uncertainties are statistical only.

## 498 9.5 Uncertainty on extra jet radiation for dilepton background

499 As discussed in Section 5.3.1, the jet distribution in  $t\bar{t} \rightarrow$  dilepton MC is rescaled by the factors  $K_3$  and  
500  $K_4$  to make it agree with the data. The 3% uncertainties on  $K_3$  and  $K_4$  comes from data/MC statistics.  
501 This results directly in a 3% uncertainty on the dilepton background, which is by far the most important  
502 one.

## 503 9.6 Uncertainty from MC statistics

504 This affects mostly the  $t\bar{t} \rightarrow \ell\ell$  background estimate, which is taken from Monte Carlo with appropriate  
505 correction factors. This uncertainty is negligible in the low  $E_T^{\text{miss}}$  signal regions, and grows to about 15%  
506 in SRG.

## 507 9.7 Uncertainty on the $t\bar{t} \rightarrow \ell\ell$ Background

508 The  $t\bar{t}$  background prediction is obtained from MC, with corrections derived from control samples in data.  
509 The uncertainty associated with the  $t\bar{t}$  background is derived from the level of closure of the background  
510 prediction in CR4 (Table 17) and CR5 (Table 19). The results from these control region checks are shown  
511 in Figure 15. The uncertainties assigned to the  $t\bar{t} \rightarrow \ell\ell$  background prediction based on these tests are  
512 5% (SRA), 10% (SRB), 15% (SRC), 25% (SRD), 40% (SRE-G).

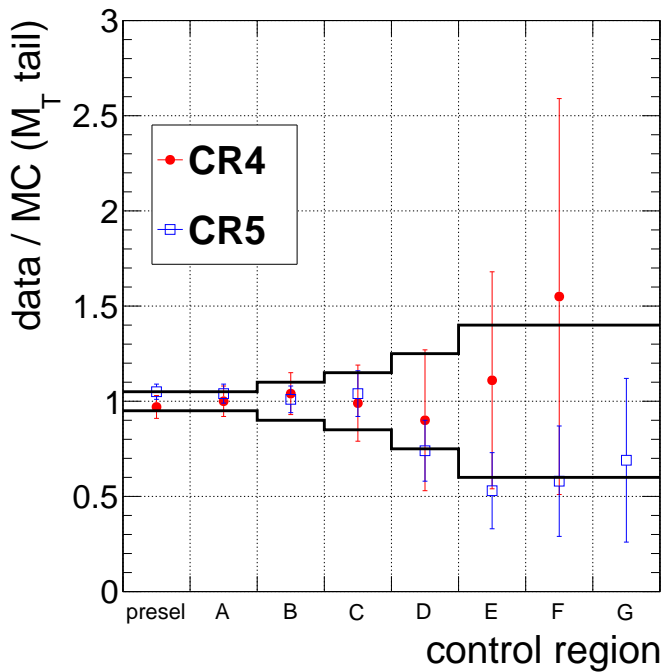


Figure 15: Results of the comparison of yields in the  $M_T$  tail comparing the MC prediction (after applying SFs) to data for CR4 and CR5 for all the signal region requirements considered (A-G). The bands indicate the systematic uncertainties assigned based on these tests, ranging from 5% for SRA to 40% for SRE-G.

513 **9.7.1 Check of the impact of Signal Contamination**

514 We examine the contribution of possible signal events in the  $t\bar{t} \rightarrow \ell\ell$  control regions (CR4 and CR5).  
 515 It should be emphasized that these regions are not used to apply data/MC SFs. They are used only  
 516 to quantify the level of data/MC agreement and assign a corresponding uncertainty. As a result, if  
 517 signal events were to populate these control regions this would not lead to an increase in the predicted  
 518 background.

519 To illustrate how much signal is expected to populate these control regions, we examine signal points  
 520 near the edge of the analysis sensitivity ( $m(\text{stop}) = 450$  m( $\chi^0$ ) = 0 for T2tt,  $m(\text{stop}) = 450$  m( $\chi^0$ ) =  
 521 0 for T2bw with  $x=0.75$  and  $m(\text{stop}) = 350$  m( $\chi^0$ ) = 0 for T2bw with  $x=0.5$ ). Table 27 compares the  
 522 expected signal yields and the raw total MC background prediction in the control regions with the  $E_T^{\text{miss}}$   
 523 and  $M_T$  requirements corresponding to SRB, SRC and SRD (these are the signal regions that dominate  
 524 the sensitivity). The signal contamination is smaller than the uncertainty on the dilepton background  
 525 and smaller than the signal/background in the signal regions, with the exception of the T2bw scenario  
 526 with  $x=0.5$ . However, based on the fact that the CR4 and CR5 are not used to extract data/MC scale  
 527 factors and that we do not observe evidence for signal contamination in these control regions (CR5, the  
 528 control region with larger statistical precision, actually shows a slight deficit of data w.r.t. MC), we do  
 529 not assign a correction for signal contamination in these control regions.

Sample		CR B	CR C	CR D
CR4	Raw MC	$168.2 \pm 4.5$	$51.5 \pm 2.5$	$19.6 \pm 1.5$
	T2tt $m(\text{stop}) = 450$ m( $\chi^0$ ) = 0	$2.6 \pm 0.3$ (2%)	$2.0 \pm 0.2$ (4%)	$1.4 \pm 0.2$ (7%)
	T2bw $x=0.75$ m( $\chi^0$ ) = 450 m( $\chi^0$ ) = 0	$10.5 \pm 0.4$ (6%)	$6.1 \pm 0.3$ (12%)	$3.1 \pm 0.2$ (16%)
	T2bw $x=0.5$ m( $\chi^0$ ) = 350 m( $\chi^0$ ) = 0	$32.1 \pm 1.5$ (19%)	$14.7 \pm 1.0$ (29%)	$5.5 \pm 0.6$ (28%)
CR5	Raw MC	$306.5 \pm 6.2$	$101.8 \pm 3.6$	$38.0 \pm 2.2$
	T2tt $m(\text{stop}) = 450$ m( $\chi^0$ ) = 0	$10.6 \pm 0.6$ (3%)	$7.8 \pm 0.5$ (8%)	$5.4 \pm 0.4$ (14%)
	T2bw $x=0.75$ m( $\chi^0$ ) = 450 m( $\chi^0$ ) = 0	$17.3 \pm 0.5$ (6%)	$11.3 \pm 0.4$ (11%)	$6.2 \pm 0.3$ (16%)
	T2bw $x=0.5$ m( $\chi^0$ ) = 350 m( $\chi^0$ ) = 0	$33.0 \pm 1.5$ (11%)	$14.4 \pm 1.0$ (14%)	$5.7 \pm 0.6$ (15%)
SIGNAL	Raw MC	$486.3 \pm 7.8$	$164.3 \pm 4.5$	$61.5 \pm 2.8$
	T2tt $m(\text{stop}) = 450$ m( $\chi^0$ ) = 0	$65.3 \pm 1.4$ (13%)	$48.8 \pm 1.2$ (30%)	$32.9 \pm 1.0$ (53%)
	T2bw $x=0.75$ m( $\chi^0$ ) = 450 m( $\chi^0$ ) = 0	$69.3 \pm 1.0$ (14%)	$47.3 \pm 0.8$ (29%)	$27.3 \pm 0.6$ (44%)
	T2bw $x=0.5$ m( $\chi^0$ ) = 350 m( $\chi^0$ ) = 0	$105.5 \pm 2.8$ (22%)	$44.6 \pm 1.8$ (27%)	$15.9 \pm 1.1$ (26%)

Table 27: Yields in  $M_T$  tail comparing the raw SM MC prediction to the yields for a few signal points on the edge of our sensitivity in the  $t\bar{t} \rightarrow \ell\ell$  control regions CR4, CR5 and in the corresponding signal region. The numbers in parenthesis are the expected signal yield divided by the total background. The uncertainties are statistical only.

530 **9.7.2 Check of the uncertainty on the  $t\bar{t} \rightarrow \ell\ell$  Background**

531 We check that the systematic uncertainty assigned to the  $t\bar{t} \rightarrow \ell\ell$  background prediction covers the  
 532 uncertainty associated with the theoretical modeling of the  $t\bar{t}$  production and decay by comparing the  
 533 background predictions obtained using alternative MC samples. It should be noted that the full analysis  
 534 is performed with the alternative samples under consideration, including the derivation of the various  
 535 data-to-MC scale factors. The variations considered are

- 536 • Top mass: The alternative values for the top mass differ from the central value by 6 GeV:  $m_{\text{top}} =$   
 537  $178.5$  GeV and  $m_{\text{top}} = 166.5$  GeV.
- 538 • Jet-parton matching scale: This corresponds to variations in the scale at which the Matrix Element  
 539 partons from Madgraph are matched to Parton Shower partons from Pythia. The nominal value is  
 540  $x_q > 20$  GeV. The alternative values used are  $x_q > 10$  GeV and  $x_q > 40$  GeV.
- 541 • Renormalization and factorization scale: The alternative samples correspond to variations in the  
 542 scale  $\times 2$  and  $\times 0.5$ . The nominal value for the scale used is  $Q^2 = m_{\text{top}}^2 + \sum_{\text{jets}} p_{\text{T}}^2$ .
- 543 • Alternative generators: Samples produced with different generators, Powheg (our default) and  
 544 Madgraph.

- 545 • Modeling of taus: The alternative sample does not include Tauola and is otherwise identical to the  
 546 Powheg sample. This effect was studied earlier using 7 TeV samples and found to be negligible.
- 547 • The PDF uncertainty is estimated following the PDF4LHC recommendations. The events are  
 548 reweighted using alternative PDF sets for CT10 and MSTW2008 and the uncertainties for each are  
 549 derived using the alternative eigenvector variations and the “master equation”. The NNPDF2.1 set  
 550 with 100 replicas is also used. The central value is determined from the mean and the uncertainty  
 551 is derived from the  $1\sigma$  range. The overall uncertainty is derived from the envelope of the alternative  
 552 predictions and their uncertainties. This effect was studied earlier using 7 TeV samples and found  
 553 to be negligible.

$\Delta/N [\%]$	Madgraph	Mass Up	Mass Down	Scale Up	Scale Down	Match Up	Match Down
SRA	2	2	5	12	7	0	2
SRB	6	0	6	5	12	5	6

Table 28: Relative difference in  $t\bar{t} \rightarrow \ell\ell$  predictions for alternative MC samples in the higher statistics regions SRA and SRB. These differences are based on the central values of the predictions. For a fuller picture of the situation, including statistical uncertainties, see Fig. 16.

554 In Fig. 16 we compare the alternate MC  $t\bar{t} \rightarrow \ell\ell$  background predictions for regions A through E. We  
 555 can make the following observations based on this Figure.

- 556 • In the tighter signal regions we are running out of statistics.  
 557 • Within the limited statistics, there is no evidence that the situation changes as we go from signal  
 558 region A to signal region E.  
 559 • In signal regions B and above, the uncertainties assigned in Section 9.7 fully cover the alternative  
 560 MC variations.  
 561 • In order to fully (as opposed as  $1\sigma$ ) cover the alternative MC variations in region A we would  
 562 have to take a systematic uncertainty of  $\approx 10\%$  instead of 5%. This would be driven by the scale  
 563 up/scale down variations, see Table 28.

Sample	K3	K4
Powheg	$1.01 \pm 0.03$	$0.93 \pm 0.04$
Madgraph	$1.01 \pm 0.04$	$0.92 \pm 0.04$
Mass Up	$1.00 \pm 0.04$	$0.92 \pm 0.04$
Mass Down	$1.06 \pm 0.04$	$0.99 \pm 0.05$
Scale Up	$1.14 \pm 0.04$	$1.23 \pm 0.06$
Scale Down	$0.89 \pm 0.03$	$0.74 \pm 0.03$
Match Up	$1.02 \pm 0.04$	$0.97 \pm 0.04$
Match Down	$1.02 \pm 0.04$	$0.91 \pm 0.04$

Table 29:  $E_T^{\text{miss}} > 100$  GeV: Data/MC scale factors used to account for differences in the fraction of events with additional hard jets from radiation in  $t\bar{t} \rightarrow \ell\ell$  events.

- 564 However, we have two pieces of information indicating that the scale up/scale down variations are incon-  
 565 sistent with the data. These are described below.  
 566 The first piece of information is that the jet multiplicity in the scale up/scale down sample is the most  
 567 inconsistent with the data. This is shown in Table 29, where we tabulate the  $K_3$  and  $K_4$  factors of  
 568 Section 5.3.1 for different  $t\bar{t}$  MC samples. The data/MC disagreement in the  $N_{\text{jets}}$  distribution for the  
 569 scale up/scale down samples is also shown in Fig. 17 and 18. This should be compared with the equivalent  
 570  $N_{\text{jets}}$  plots for the default Powheg MC, see Fig. 9, which agrees much better with data.

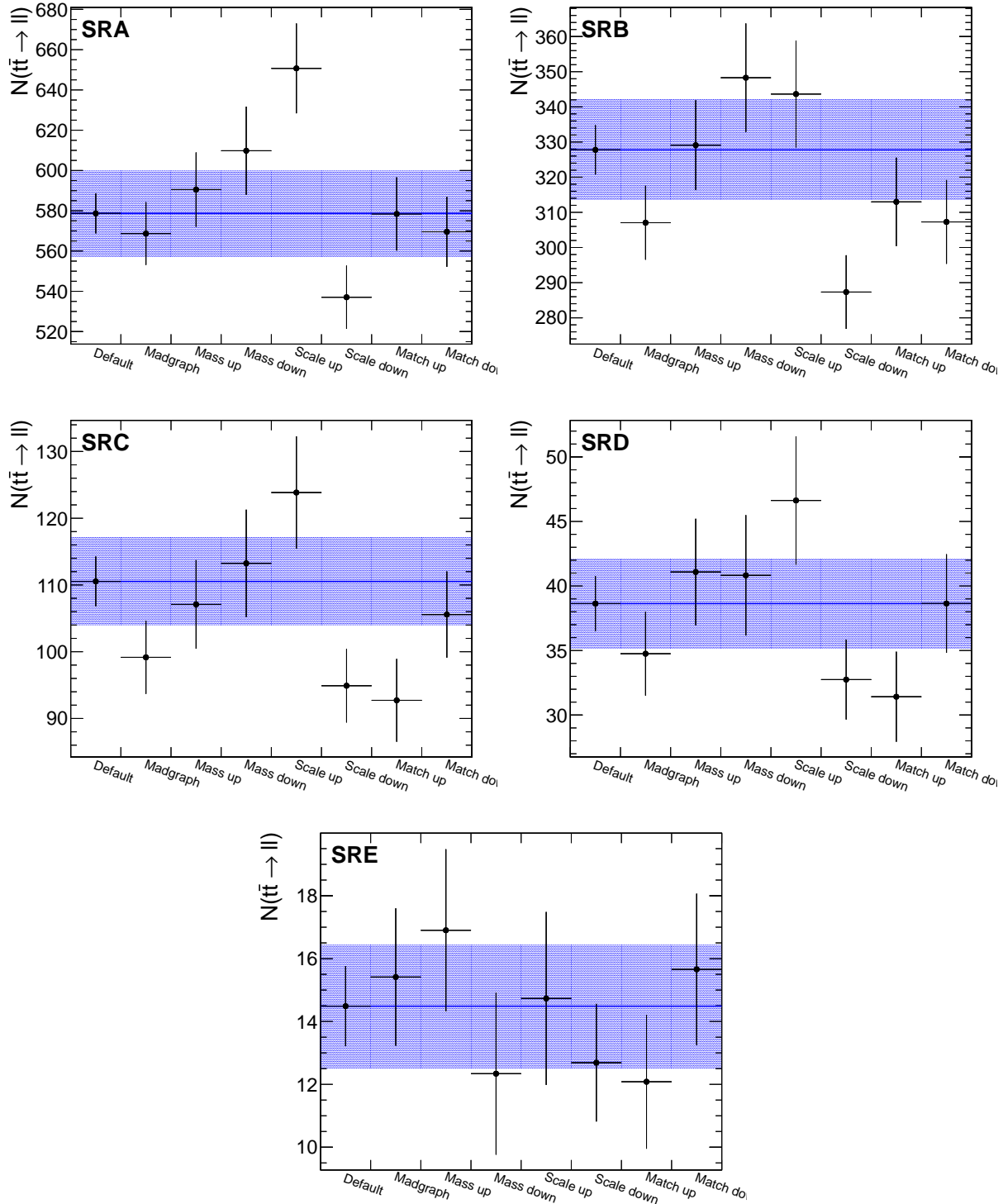


Figure 16: Comparison of the  $t\bar{t} \rightarrow \ell\ell$  central prediction with those using alternative MC samples. The blue band corresponds to the total statistical error for all data and MC samples. The alternative sample predictions are indicated by the datapoints. The uncertainties on the alternative predictions correspond to the uncorrelated statistical uncertainty from the size of the alternative sample only. Note the suppressed vertical scales.

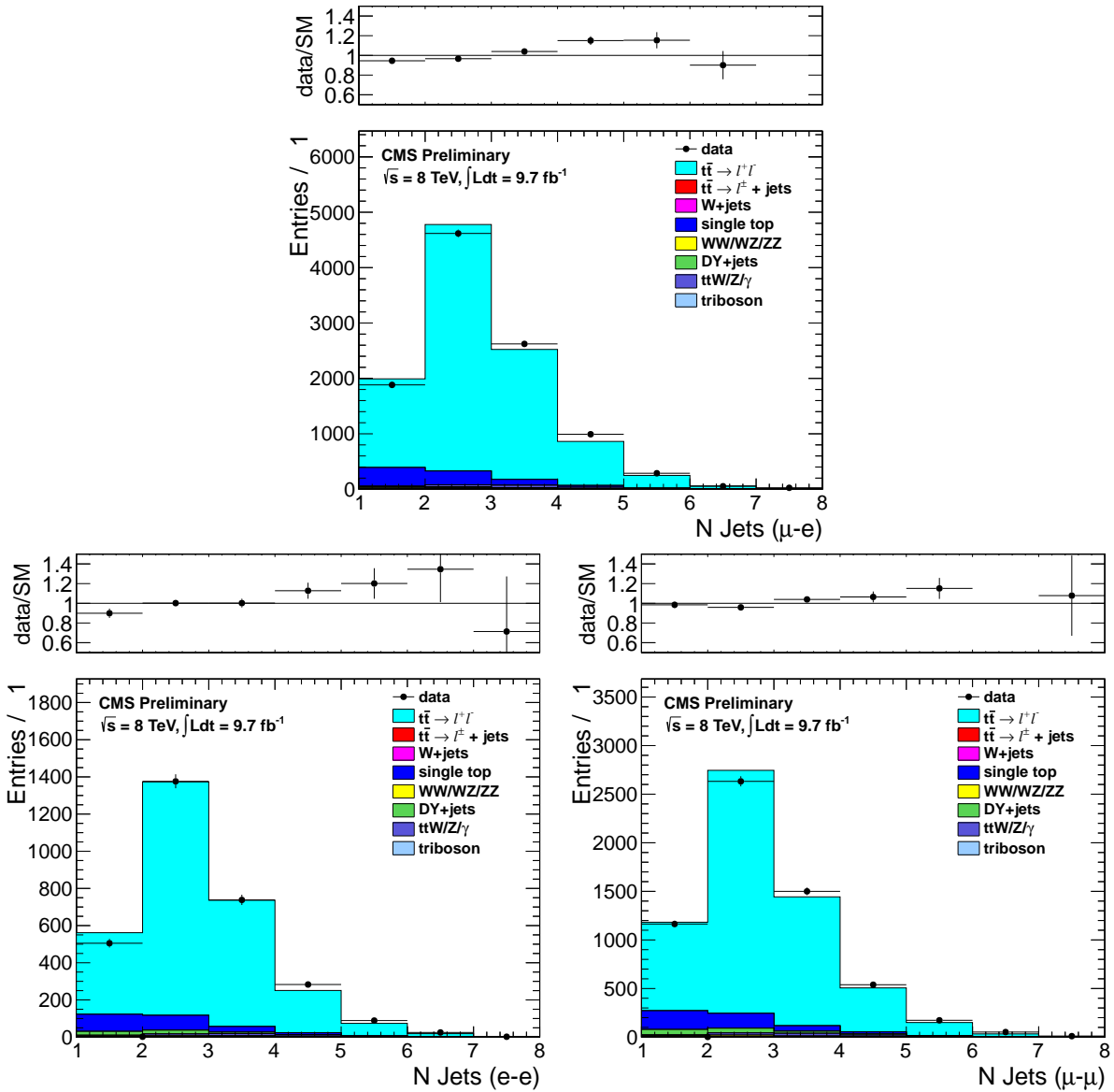


Figure 17: SCALE UP: Comparison of the jet multiplicity distribution in data and MC for dilepton events in the  $e\text{-}\mu$  (top),  $e\text{-}e$  (bottom left) and  $\mu\text{-}\mu$  (bottom right) channels.

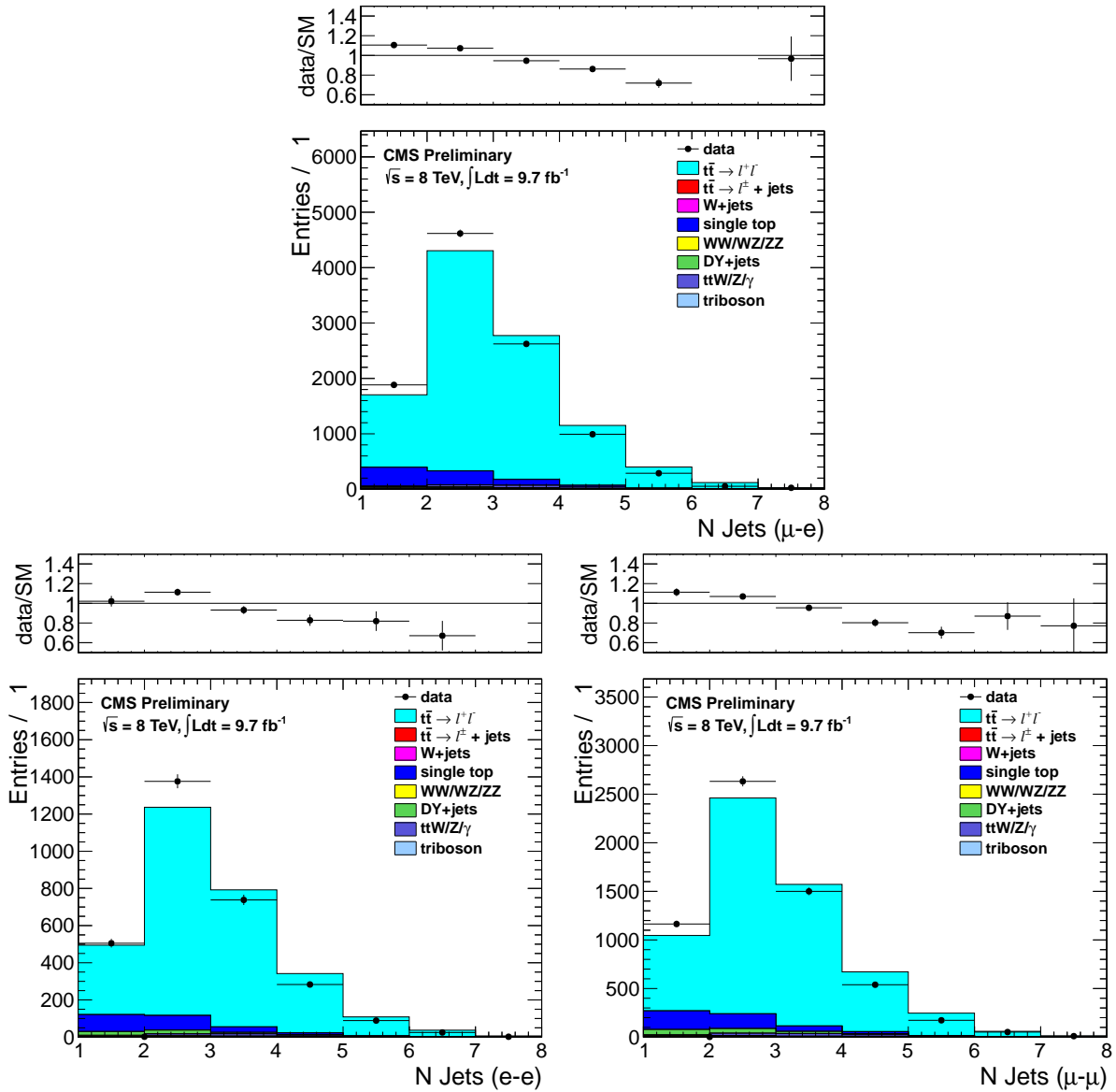


Figure 18: SCALE DOWN: Comparison of the jet multiplicity distribution in data and MC for dilepton events in the  $e\text{-}\mu$  (top),  $e\text{-}e$  (bottom left) and  $\mu\text{-}\mu$  (bottom right) channels.

571 The second piece of information is that we have performed closure tests in CR5 using the alternative MC  
 572 samples. These are exactly the same tests as the one performed in Section D.2 on the Powheg sample.  
 573 As we argued previously, this is a very powerful test of the background calculation. The results of this  
 574 test are summarized in Table 30. Concentrating on the relatively high statistics CR5A region, we see  
 575 for all  $t\bar{t}$  MC samples except scale up/scale down we obtain closure within  $1\sigma$ . The scale up/scale down  
 576 tests closes worse, only within  $2\sigma$ . This again is evidence that the scale up/scale down variations are in  
 577 disagreement with the data.

Sample	CR5PRESEL	CR5A	CR5B	CR5C	CR5D	CR5E
POWHEG						
$\mu$ Data/MC SF	$1.05 \pm 0.05$	$1.04 \pm 0.06$	$1.08 \pm 0.09$	$1.17 \pm 0.17$	$0.64 \pm 0.20$	$0.54 \pm 0.29$
e Data/MC SF	$1.06 \pm 0.06$	$1.04 \pm 0.07$	$0.93 \pm 0.09$	$0.89 \pm 0.16$	$0.86 \pm 0.25$	$0.52 \pm 0.28$
$\mu+e$ Data/MC SF	$1.05 \pm 0.04$	$1.04 \pm 0.05$	$1.01 \pm 0.07$	$1.04 \pm 0.12$	$0.74 \pm 0.16$	$0.53 \pm 0.20$
MADGRAPH						
$\mu$ Data/MC SF	$1.05 \pm 0.05$	$1.06 \pm 0.07$	$1.08 \pm 0.10$	$1.21 \pm 0.19$	$0.64 \pm 0.21$	$0.43 \pm 0.24$
e Data/MC SF	$1.06 \pm 0.06$	$1.04 \pm 0.08$	$0.97 \pm 0.10$	$0.97 \pm 0.18$	$1.10 \pm 0.34$	$0.68 \pm 0.38$
$\mu+e$ Data/MC SF	$1.06 \pm 0.04$	$1.05 \pm 0.05$	$1.03 \pm 0.07$	$1.10 \pm 0.13$	$0.83 \pm 0.18$	$0.53 \pm 0.21$
MASS UP						
$\mu$ Data/MC SF	$1.04 \pm 0.06$	$1.04 \pm 0.07$	$1.07 \pm 0.10$	$1.20 \pm 0.19$	$0.57 \pm 0.18$	$0.56 \pm 0.31$
e Data/MC SF	$1.04 \pm 0.06$	$1.05 \pm 0.08$	$1.01 \pm 0.11$	$1.12 \pm 0.22$	$1.02 \pm 0.33$	$0.61 \pm 0.34$
$\mu+e$ Data/MC SF	$1.04 \pm 0.04$	$1.04 \pm 0.05$	$1.04 \pm 0.07$	$1.17 \pm 0.15$	$0.74 \pm 0.17$	$0.58 \pm 0.23$
MASS DOWN						
$\mu$ Data/MC SF	$1.02 \pm 0.06$	$1.02 \pm 0.07$	$1.04 \pm 0.10$	$1.25 \pm 0.21$	$0.82 \pm 0.28$	$0.94 \pm 0.56$
e Data/MC SF	$1.06 \pm 0.06$	$1.02 \pm 0.08$	$0.95 \pm 0.11$	$0.91 \pm 0.18$	$1.07 \pm 0.35$	$0.59 \pm 0.33$
$\mu+e$ Data/MC SF	$1.04 \pm 0.04$	$1.02 \pm 0.05$	$1.00 \pm 0.07$	$1.09 \pm 0.14$	$0.94 \pm 0.22$	$0.72 \pm 0.30$
SCALE UP						
$\mu$ Data/MC SF	$0.94 \pm 0.05$	$0.94 \pm 0.07$	$0.99 \pm 0.10$	$1.24 \pm 0.21$	$0.71 \pm 0.24$	$0.69 \pm 0.39$
e Data/MC SF	$0.94 \pm 0.06$	$0.89 \pm 0.07$	$0.81 \pm 0.09$	$0.77 \pm 0.15$	$0.84 \pm 0.27$	$0.49 \pm 0.28$
$\mu+e$ Data/MC SF	$0.94 \pm 0.04$	$0.91 \pm 0.05$	$0.91 \pm 0.07$	$1.00 \pm 0.13$	$0.77 \pm 0.18$	$0.57 \pm 0.23$
SCALE DOWN						
$\mu$ Data/MC SF	$1.11 \pm 0.06$	$1.10 \pm 0.07$	$1.24 \pm 0.12$	$1.26 \pm 0.20$	$0.64 \pm 0.21$	$0.70 \pm 0.39$
e Data/MC SF	$1.16 \pm 0.07$	$1.20 \pm 0.09$	$1.00 \pm 0.11$	$1.02 \pm 0.19$	$1.02 \pm 0.32$	$0.53 \pm 0.29$
$\mu+e$ Data/MC SF	$1.13 \pm 0.04$	$1.14 \pm 0.06$	$1.13 \pm 0.08$	$1.15 \pm 0.14$	$0.80 \pm 0.18$	$0.60 \pm 0.23$
MATCH UP						
$\mu$ Data/MC SF	$1.06 \pm 0.06$	$1.06 \pm 0.07$	$1.20 \pm 0.11$	$1.42 \pm 0.23$	$0.70 \pm 0.23$	$0.63 \pm 0.35$
e Data/MC SF	$1.06 \pm 0.06$	$1.04 \pm 0.08$	$0.97 \pm 0.11$	$0.93 \pm 0.18$	$1.25 \pm 0.41$	$0.63 \pm 0.36$
$\mu+e$ Data/MC SF	$1.06 \pm 0.04$	$1.06 \pm 0.05$	$1.09 \pm 0.08$	$1.18 \pm 0.15$	$0.92 \pm 0.21$	$0.63 \pm 0.25$
MATCH DOWN						
$\mu$ Data/MC SF	$1.08 \pm 0.06$	$1.06 \pm 0.07$	$1.14 \pm 0.11$	$1.17 \pm 0.19$	$0.59 \pm 0.19$	$0.45 \pm 0.25$
e Data/MC SF	$1.05 \pm 0.06$	$0.99 \pm 0.08$	$0.86 \pm 0.09$	$0.78 \pm 0.15$	$0.79 \pm 0.25$	$0.50 \pm 0.28$
$\mu+e$ Data/MC SF	$1.07 \pm 0.04$	$1.03 \pm 0.05$	$1.00 \pm 0.07$	$0.98 \pm 0.12$	$0.68 \pm 0.15$	$0.48 \pm 0.18$

Table 30: Ratio of yields in  $M_T$  tail comparing the MC prediction (after applying SFs) to data. The uncertainties are statistical only.

578 Based on the two observations above, we argue that the MC scale up/scale down variations are too  
 579 extreme. We feel that a reasonable choice would be to take one-half of the scale up/scale down variations  
 580 in our MC. This factor of 1/2 would then bring the discrepancy in the closure test of Table 30 for the  
 581 scale up/scale down variations from about  $2\sigma$  to about  $1\sigma$ .  
 582 Then, going back to Table 28, and reducing the scale up/scale down variations by a factor 2, we can see  
 583 that a systematic uncertainty of 5% covers the range of reasonable variations from different MC models  
 584 in SRA and SRB. Note that this 5% is also consistent with the level at which we are able to test the  
 585 closure of the method with alternative samples in CR5 for the high statistics regions (Table 30). The  
 586 range of reasonable variations obtained with the alternative samples are consistent with the uncertainties  
 587 assigned for the  $t\bar{t} \rightarrow \ell\ell$  background based on the closure of the background predictions and data in CR4  
 588 and CR5.

## 589 9.8 Uncertainty from the isolated track veto

590 This is the uncertainty associated with how well the isolated track veto performance is modeled by the  
 591 Monte Carlo. This uncertainty only applies to the fraction of dilepton BG events that have a second  $e/\mu$   
 592 or a one prong  $\tau \rightarrow h$ , with  $P_T > 10$  GeV in  $|\eta| < 2.4$ . This fraction is about 1/3, see Table 31. The  
 593 uncertainty for these events is 6% and is obtained from tag-and-probe studies, see Section 9.8.1.

Sample	SRA	SRB	SRC	SRD	SRE	SRF	SRG
$\mu$ Frac. $t\bar{t} \rightarrow \ell\ell$ with true iso. trk.	$0.32 \pm 0.03$	$0.30 \pm 0.03$	$0.32 \pm 0.06$	$0.34 \pm 0.10$	$0.35 \pm 0.16$	$0.40 \pm 0.24$	$0.50 \pm 0.32$
e Frac. $t\bar{t} \rightarrow \ell\ell$ with true iso. trk.	$0.32 \pm 0.03$	$0.31 \pm 0.04$	$0.33 \pm 0.06$	$0.38 \pm 0.11$	$0.38 \pm 0.19$	$0.60 \pm 0.31$	$0.61 \pm 0.45$

Table 31: Fraction of  $t\bar{t} \rightarrow \ell\ell$  events with a true isolated track.

### 594 9.8.1 Isolated Track Veto: Tag and Probe Studies

595 In this section we compare the performance of the isolated track veto in data and MC using tag-and-  
 596 probe studies with samples of  $Z \rightarrow ee$  and  $Z \rightarrow \mu\mu$ . The purpose of these studies is to demonstrate that the  
 597 efficiency to satisfy the isolated track veto requirements is well-reproduced in the MC, since if this were  
 598 not the case we would need to apply a data-to-MC scale factor in order to correctly predict the  $t\bar{t} \rightarrow \ell\ell$   
 599 background.

600 This study addresses possible data vs. MC discrepancies for the **efficiency** to identify (and reject)  
 601 events with a second **genuine** lepton ( $e$ ,  $\mu$ , or  $\tau \rightarrow 1$ -prong). It does not address possible data vs.  
 602 MC discrepancies in the fake rate for rejecting events without a second genuine lepton; this is handled  
 603 separately in the top normalization procedure by scaling the  $t\bar{t} \rightarrow \ell + \text{jets}$  contribution to match the data  
 604 in the  $M_T$  peak after applying the isolated track veto.

605 Furthermore, we test the data and MC isolated track veto efficiencies for electrons and muons since we are  
 606 using a  $Z$  tag-and-probe technique, but we do not directly test the performance for hadronic tracks from  
 607  $\tau$  decays. The performance for hadronic  $\tau$  decay products may differ from that of electrons and muons  
 608 for two reasons. First, the  $\tau$  may decay to a hadronic track plus one or two  $\pi^0$ 's, which may decay to  
 609  $\gamma\gamma$  followed by a photon conversion. As shown in Figure 33, the isolation distribution for charged tracks  
 610 from  $\tau$  decays that are not produced in association with  $\pi^0$ 's are consistent with that from  $e$ s and  $\mu$ s.  
 611 Since events from single prong  $\tau$  decays produced in association with  $\pi^0$ 's comprise a small fraction of the  
 612 total sample, and since the kinematics of  $\tau$ ,  $\pi^0$  and  $\gamma \rightarrow e^+e^-$  decays are well-understood, we currently  
 613 demonstrate that the isolation is well-reproduced for electrons and muons only. Second, hadronic tracks  
 614 may undergo nuclear interactions and hence their tracks may not be reconstructed. As discussed above,  
 615 independent studies show that the MC reproduces the hadronic tracking efficiency within 4%, leading  
 616 to a total background uncertainty of less than 0.5% (after taking into account the fraction of the total  
 617 background due to hadronic  $\tau$  decays with  $p_T > 10$  GeV tracks), and we hence regard this effect as  
 618 negligible.

619 The tag-and-probe studies are performed in the full data sample, and compared with the DYJets mad-  
 620 graph sample. All events must contain a tag-probe pair (details below) with opposite-sign and satisfying  
 621 the  $Z$  mass requirement 76–106 GeV. We compare the distributions of absolute track isolation for probe  
 622 electrons/muons in data vs. MC. The contributions to this isolation sum are from ambient energy in the  
 623 event from underlying event, pile-up and jet activity, and hence do not depend on the  $p_T$  of the probe  
 624 lepton. We therefore restrict the probe  $p_T$  to be  $> 30$  GeV in order to suppress fake backgrounds with  
 625 steeply-falling  $p_T$  spectra. To suppress non- $Z$  backgrounds (in particular  $t\bar{t}$ ) we require  $E_T^{\text{miss}} < 30$  GeV  
 626 and 0 b-tagged events. The specific criteria for tags and probes for electrons and muons are:

- 627     • Electrons
  - 628         – Tag criteria
    - 629             \* Electron passes full analysis ID/iso selection
    - 630             \*  $p_T > 30$  GeV,  $|\eta| < 2.1$
    - 631             \* Matched to the single electron trigger HLT\_Ele27\_WP80\_v\*
  - 632         – Probe criteria

- \* Electron passes full analysis ID selection
- \*  $p_T > 30 \text{ GeV}$
- Muons
  - Tag criteria
    - \* Muon passes full analysis ID/iso selection
    - \*  $p_T > 30 \text{ GeV}, |\eta| < 2.1$
    - \* Matched to 1 of the 2 single muon triggers
      - HLT\_IsoMu30\_v\*
      - HLT\_IsoMu30\_eta2p1\_v\*
  - Probe criteria
    - \* Muon passes full analysis ID selection
    - \*  $p_T > 30 \text{ GeV}$

The absolute track isolation distributions for passing probes are displayed in Fig. 19. In general we observe good agreement between data and MC. To be more quantitative, we compare the data vs. MC efficiencies to satisfy absolute track isolation requirements varying from  $> 1 \text{ GeV}$  to  $> 5 \text{ GeV}$ , as summarized in Table 32. In the  $\geq 0$  and  $\geq 1$  jet bins where the efficiencies can be tested with statistical precision, the data and MC efficiencies agree within 6%, and we apply this as a systematic uncertainty on the isolated track veto efficiency. For the higher jet multiplicity bins the statistical precision decreases, but we do not observe any evidence for a data vs. MC discrepancy in the isolated track veto efficiency.

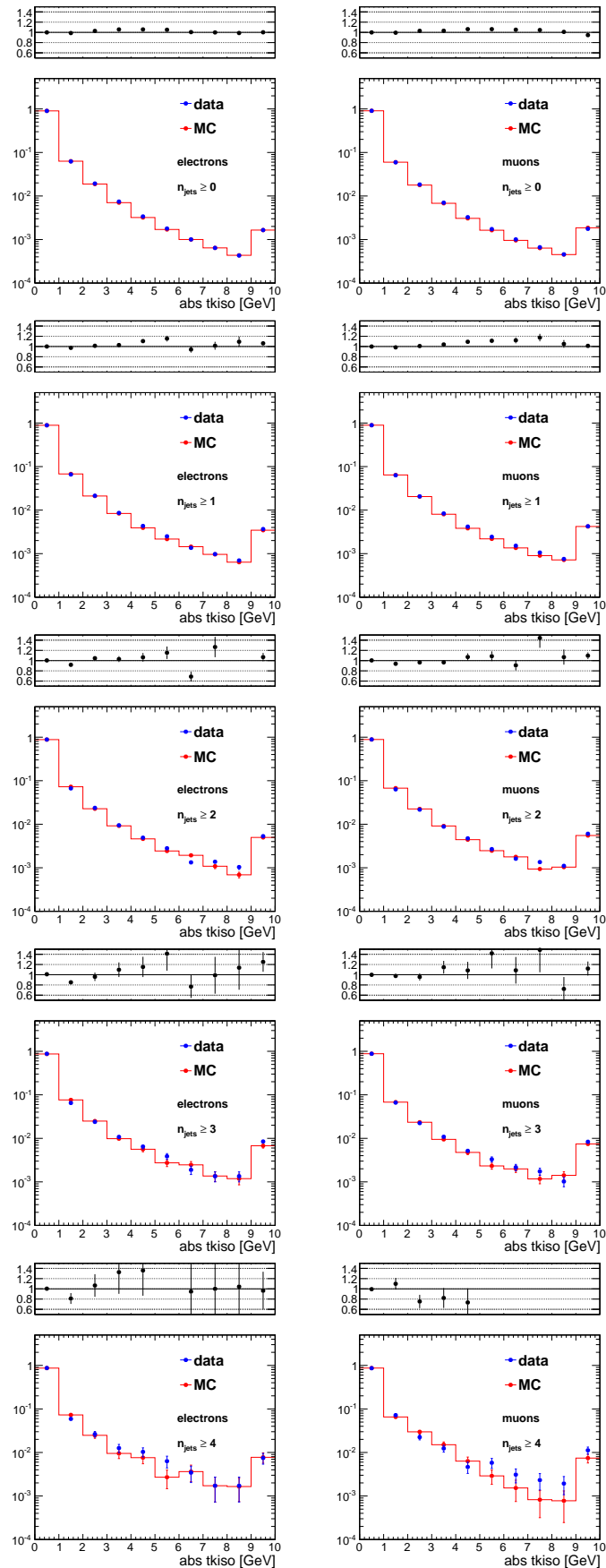


Figure 19: Comparison of the absolute track isolation in data vs. MC for electrons (left) and muons (right) for events with the  $N_{\text{jets}}$  requirement varied from  $N_{\text{jets}} \geq 0$  to  $N_{\text{jets}} \geq 4$ .

$e + \geq 0$ jets	$> 1$ GeV	$> 2$ GeV	$> 3$ GeV	$> 4$ GeV	$> 5$ GeV
data	$0.098 \pm 0.0002$	$0.036 \pm 0.0001$	$0.016 \pm 0.0001$	$0.009 \pm 0.0001$	$0.006 \pm 0.0000$
mc	$0.097 \pm 0.0002$	$0.034 \pm 0.0001$	$0.016 \pm 0.0001$	$0.009 \pm 0.0001$	$0.005 \pm 0.0000$
data/mc	$1.00 \pm 0.00$	$1.04 \pm 0.00$	$1.04 \pm 0.01$	$1.03 \pm 0.01$	$1.02 \pm 0.01$
$\mu + \geq 0$ jets	$> 1$ GeV	$> 2$ GeV	$> 3$ GeV	$> 4$ GeV	$> 5$ GeV
data	$0.094 \pm 0.0001$	$0.034 \pm 0.0001$	$0.016 \pm 0.0001$	$0.009 \pm 0.0000$	$0.006 \pm 0.0000$
mc	$0.093 \pm 0.0001$	$0.033 \pm 0.0001$	$0.015 \pm 0.0001$	$0.009 \pm 0.0000$	$0.006 \pm 0.0000$
data/mc	$1.01 \pm 0.00$	$1.03 \pm 0.00$	$1.03 \pm 0.01$	$1.03 \pm 0.01$	$1.02 \pm 0.01$
$e + \geq 1$ jets	$> 1$ GeV	$> 2$ GeV	$> 3$ GeV	$> 4$ GeV	$> 5$ GeV
data	$0.110 \pm 0.0005$	$0.044 \pm 0.0003$	$0.022 \pm 0.0002$	$0.014 \pm 0.0002$	$0.009 \pm 0.0002$
mc	$0.110 \pm 0.0005$	$0.042 \pm 0.0003$	$0.021 \pm 0.0002$	$0.013 \pm 0.0002$	$0.009 \pm 0.0001$
data/mc	$1.00 \pm 0.01$	$1.04 \pm 0.01$	$1.06 \pm 0.02$	$1.08 \pm 0.02$	$1.06 \pm 0.03$
$\mu + \geq 1$ jets	$> 1$ GeV	$> 2$ GeV	$> 3$ GeV	$> 4$ GeV	$> 5$ GeV
data	$0.106 \pm 0.0004$	$0.043 \pm 0.0003$	$0.023 \pm 0.0002$	$0.014 \pm 0.0002$	$0.010 \pm 0.0001$
mc	$0.106 \pm 0.0004$	$0.042 \pm 0.0003$	$0.021 \pm 0.0002$	$0.013 \pm 0.0002$	$0.009 \pm 0.0001$
data/mc	$1.00 \pm 0.01$	$1.04 \pm 0.01$	$1.06 \pm 0.01$	$1.08 \pm 0.02$	$1.07 \pm 0.02$
$e + \geq 2$ jets	$> 1$ GeV	$> 2$ GeV	$> 3$ GeV	$> 4$ GeV	$> 5$ GeV
data	$0.117 \pm 0.0012$	$0.050 \pm 0.0008$	$0.026 \pm 0.0006$	$0.017 \pm 0.0005$	$0.012 \pm 0.0004$
mc	$0.120 \pm 0.0012$	$0.048 \pm 0.0008$	$0.025 \pm 0.0006$	$0.016 \pm 0.0005$	$0.011 \pm 0.0004$
data/mc	$0.97 \pm 0.01$	$1.05 \pm 0.02$	$1.05 \pm 0.03$	$1.07 \pm 0.04$	$1.07 \pm 0.05$
$\mu + \geq 2$ jets	$> 1$ GeV	$> 2$ GeV	$> 3$ GeV	$> 4$ GeV	$> 5$ GeV
data	$0.111 \pm 0.0010$	$0.048 \pm 0.0007$	$0.026 \pm 0.0005$	$0.018 \pm 0.0004$	$0.013 \pm 0.0004$
mc	$0.115 \pm 0.0010$	$0.048 \pm 0.0006$	$0.025 \pm 0.0005$	$0.016 \pm 0.0004$	$0.012 \pm 0.0003$
data/mc	$0.97 \pm 0.01$	$1.01 \pm 0.02$	$1.04 \pm 0.03$	$1.09 \pm 0.04$	$1.09 \pm 0.04$
$e + \geq 3$ jets	$> 1$ GeV	$> 2$ GeV	$> 3$ GeV	$> 4$ GeV	$> 5$ GeV
data	$0.123 \pm 0.0031$	$0.058 \pm 0.0022$	$0.034 \pm 0.0017$	$0.023 \pm 0.0014$	$0.017 \pm 0.0012$
mc	$0.131 \pm 0.0030$	$0.055 \pm 0.0020$	$0.030 \pm 0.0015$	$0.020 \pm 0.0013$	$0.015 \pm 0.0011$
data/mc	$0.94 \pm 0.03$	$1.06 \pm 0.06$	$1.14 \pm 0.08$	$1.16 \pm 0.10$	$1.17 \pm 0.12$
$\mu + \geq 3$ jets	$> 1$ GeV	$> 2$ GeV	$> 3$ GeV	$> 4$ GeV	$> 5$ GeV
data	$0.121 \pm 0.0025$	$0.055 \pm 0.0018$	$0.033 \pm 0.0014$	$0.022 \pm 0.0011$	$0.017 \pm 0.0010$
mc	$0.120 \pm 0.0024$	$0.052 \pm 0.0016$	$0.029 \pm 0.0012$	$0.019 \pm 0.0010$	$0.014 \pm 0.0009$
data/mc	$1.01 \pm 0.03$	$1.06 \pm 0.05$	$1.14 \pm 0.07$	$1.14 \pm 0.08$	$1.16 \pm 0.10$
$e + \geq 4$ jets	$> 1$ GeV	$> 2$ GeV	$> 3$ GeV	$> 4$ GeV	$> 5$ GeV
data	$0.129 \pm 0.0080$	$0.070 \pm 0.0061$	$0.044 \pm 0.0049$	$0.031 \pm 0.0042$	$0.021 \pm 0.0034$
mc	$0.132 \pm 0.0075$	$0.059 \pm 0.0053$	$0.035 \pm 0.0041$	$0.025 \pm 0.0035$	$0.017 \pm 0.0029$
data/mc	$0.98 \pm 0.08$	$1.18 \pm 0.15$	$1.26 \pm 0.20$	$1.24 \pm 0.24$	$1.18 \pm 0.28$
$\mu + \geq 4$ jets	$> 1$ GeV	$> 2$ GeV	$> 3$ GeV	$> 4$ GeV	$> 5$ GeV
data	$0.136 \pm 0.0067$	$0.064 \pm 0.0048$	$0.041 \pm 0.0039$	$0.029 \pm 0.0033$	$0.024 \pm 0.0030$
mc	$0.130 \pm 0.0063$	$0.065 \pm 0.0046$	$0.035 \pm 0.0034$	$0.020 \pm 0.0026$	$0.013 \pm 0.0022$
data/mc	$1.04 \pm 0.07$	$0.99 \pm 0.10$	$1.19 \pm 0.16$	$1.47 \pm 0.25$	$1.81 \pm 0.37$

Table 32: Comparison of the data vs. MC efficiencies to satisfy the indicated requirements on the absolute track isolation, and the ratio of these two efficiencies. Results are indicated separately for electrons and muons and for various jet multiplicity requirements.

## 652 9.9 Summary of uncertainties

653 The contribution from each source to the total uncertainty on the background yield is given in Tables 33  
 654 and 34 for the relative and absolute uncertainties, respectively. In the low- $E_T^{\text{miss}}$  regions the dominant  
 655 uncertainty comes from the top tail-to-peak ratio,  $R_{\text{top}}$  (Section 7), while in the high- $E_T^{\text{miss}}$  regions the  
 656  $t\bar{t} \rightarrow \ell\ell$  systematic uncertainty dominates (Section 9.7).

Sample	SRA	SRB	SRC	SRD	SRE	SRF	SRG
Muon							
$W + \text{jets}$ cross-section	1.7%	2.3%	3.0%	3.7%	4.2%	4.2%	5.3%
rare cross-sections	2.0%	2.3%	3.4%	5.6%	8.8%	8.0%	10.4%
top tail-to-peak ratio	12.6%	8.7%	8.6%	6.7%	7.1%	8.6%	4.6%
$W + \text{jets}$ tail-to-peak ratio	6.5%	5.3%	5.8%	6.9%	8.9%	12.0%	13.6%
$t\bar{t} \rightarrow \ell\ell$ (stat)	1.1%	1.5%	2.8%	4.7%	6.7%	9.7%	12.2%
$K_3$ and $K_4$	1.9%	1.9%	2.0%	2.0%	1.9%	1.8%	1.8%
2nd lepton veto	1.2%	1.3%	1.3%	1.3%	1.2%	1.2%	1.2%
$t\bar{t} \rightarrow \ell\ell$ (CR4 and CR5 closure tests)	3.1%	6.5%	10.2%	16.9%	25.1%	23.8%	23.4%
$M_T$ peak data and MC (stat)	1.1%	2.1%	3.8%	6.0%	8.6%	13.1%	20.0%
total	15.0%	13.0%	16.1%	22.1%	31.3%	33.7%	37.9%
Electron							
$W + \text{jets}$ cross-section	1.7%	2.3%	2.9%	4.2%	4.4%	4.5%	4.6%
rare cross-sections	2.1%	2.1%	2.9%	3.7%	1.9%	3.2%	1.9%
top tail-to-peak ratio	12.4%	8.6%	8.3%	6.1%	8.7%	11.0%	8.8%
$W + \text{jets}$ tail-to-peak ratio	6.4%	5.2%	5.5%	6.3%	10.8%	15.4%	25.7%
$t\bar{t} \rightarrow \ell\ell$ (stat)	1.3%	1.8%	3.2%	5.6%	8.7%	13.6%	16.6%
$K_3$ and $K_4$	1.9%	2.0%	2.1%	2.1%	2.1%	2.0%	2.0%
2nd lepton veto	1.2%	1.3%	1.4%	1.4%	1.4%	1.3%	1.3%
$t\bar{t} \rightarrow \ell\ell$ (CR4 and CR5 closure tests)	3.1%	6.6%	10.4%	17.7%	28.1%	26.1%	26.6%
$M_T$ peak data and MC (stat)	1.4%	2.5%	4.3%	7.4%	11.5%	15.2%	22.5%
total	14.8%	13.0%	16.1%	22.7%	34.9%	38.7%	47.5%
Muon+Electron Combined							
$W + \text{jets}$ cross-section	1.7%	2.3%	3.0%	3.9%	4.3%	4.3%	5.1%
rare cross-sections	2.0%	2.2%	3.2%	4.9%	6.4%	6.2%	7.6%
top tail-to-peak ratio	12.5%	8.7%	8.5%	6.5%	7.7%	9.5%	6.0%
$W + \text{jets}$ tail-to-peak ratio	6.4%	5.2%	5.7%	6.6%	9.6%	13.3%	17.6%
$t\bar{t} \rightarrow \ell\ell$ (stat)	1.2%	1.6%	3.0%	5.1%	7.4%	11.1%	13.6%
$K_3$ and $K_4$	1.9%	2.0%	2.1%	2.1%	2.0%	1.9%	1.8%
2nd lepton veto	1.2%	1.3%	1.4%	1.4%	1.3%	1.2%	1.2%
$t\bar{t} \rightarrow \ell\ell$ (CR4 and CR5 closure tests)	3.1%	6.5%	10.3%	17.3%	26.1%	24.7%	24.5%
$M_T$ peak data and MC (stat)	0.9%	1.7%	2.9%	4.7%	7.0%	10.1%	15.4%
total	14.9%	12.9%	15.9%	21.8%	31.7%	34.2%	38.2%

Table 33: Contributions to the total relative uncertainties.

Sample	SRA	SRB	SRC	SRD	SRE	SRF	SRG
Muon							
$W$ +jets cross-section	9.0	6.5	2.6	1.2	0.6	0.3	0.2
rare cross-sections	10.4	6.6	3.0	1.9	1.3	0.5	0.4
top tail-to-peak ratio	67.1	24.8	7.6	2.2	1.0	0.5	0.2
$W$ +jets tail-to-peak ratio	34.5	14.9	5.1	2.3	1.3	0.7	0.5
$t\bar{t} \rightarrow \ell\ell$ (stat)	6.0	4.4	2.4	1.6	1.0	0.6	0.5
$K_3$ and $K_4$	9.9	5.5	1.8	0.7	0.3	0.1	0.1
2nd lepton veto	6.5	3.6	1.2	0.4	0.2	0.1	0.0
$t\bar{t} \rightarrow \ell\ell$ (CR4 and CR5 closure tests)	16.5	18.3	8.9	5.6	3.6	1.5	0.9
$M_T$ peak data and MC (stat)	6.0	6.1	3.4	2.0	1.2	0.8	0.8
total	79.8	36.8	14.2	7.3	4.5	2.1	1.4
Electron							
$W$ +jets cross-section	6.8	5.0	2.2	1.0	0.3	0.2	0.1
rare cross-sections	8.1	4.6	2.2	0.9	0.1	0.1	0.0
top tail-to-peak ratio	49.2	18.9	6.1	1.4	0.7	0.4	0.2
$W$ +jets tail-to-peak ratio	25.3	11.4	4.1	1.4	0.8	0.6	0.5
$t\bar{t} \rightarrow \ell\ell$ (stat)	5.2	3.9	2.4	1.3	0.7	0.5	0.3
$K_3$ and $K_4$	7.4	4.3	1.5	0.5	0.2	0.1	0.0
2nd lepton veto	4.9	2.9	1.0	0.3	0.1	0.0	0.0
$t\bar{t} \rightarrow \ell\ell$ (CR4 and CR5 closure tests)	12.4	14.4	7.7	4.0	2.2	1.0	0.5
$M_T$ peak data and MC (stat)	5.7	5.4	3.2	1.7	0.9	0.6	0.4
total	58.8	28.5	11.9	5.2	2.7	1.5	0.9
Muon+Electron Combined							
$W$ +jets cross-section	15.9	11.5	4.8	2.2	0.9	0.4	0.3
rare cross-sections	18.5	11.1	5.1	2.7	1.4	0.6	0.4
top tail-to-peak ratio	116.3	43.6	13.7	3.6	1.7	1.0	0.3
$W$ +jets tail-to-peak ratio	59.8	26.3	9.1	3.7	2.1	1.3	1.0
$t\bar{t} \rightarrow \ell\ell$ (stat)	11.2	8.3	4.8	2.9	1.7	1.1	0.8
$K_3$ and $K_4$	17.4	9.8	3.3	1.2	0.4	0.2	0.1
2nd lepton veto	11.5	6.5	2.2	0.8	0.3	0.1	0.1
$t\bar{t} \rightarrow \ell\ell$ (CR4 and CR5 closure tests)	28.9	32.8	16.6	9.7	5.8	2.5	1.4
$M_T$ peak data and MC (stat)	8.7	8.4	4.7	2.6	1.5	1.0	0.9
total	138.4	64.8	25.6	12.2	7.0	3.4	2.2

Table 34: Contributions to the total uncertainties.

## 657 10 Results

658 The results of the search are shown in Table 35, including both statistical and systematic uncertainties.  
 659 Agreement is observed between the data and the predicted background for all signal regions. The pre-  
 660 dicted and observed  $E_T^{\text{miss}}$  distribution for  $E_T^{\text{miss}} > 150 \text{ GeV}$  and  $M_T > 120 \text{ GeV}$  are shown in Figure 20,  
 661 obtained from the yields for SRB to SRG. Two signal points are shown for comparison, corresponding  
 662 to the low and high stop mass sensitivity boundaries for this search. This shows that the lower  $E_T^{\text{miss}}$   
 663 region is more sensitive to lighter stop signals, while the higher  $E_T^{\text{miss}}$  region is more sensitive to heavier  
 664 stops, for the T2tt signal model shown. The  $M_T$  distributions for increasing values of  $E_T^{\text{miss}}$  are shown  
 665 in Fig 21 and 22.

Sample	SRA	SRB	SRC	SRD	SRE	SRF	SRG
Muon							
$t\bar{t} \rightarrow \ell\ell$	$331 \pm 22$	$183 \pm 21$	$59.5 \pm 10.0$	$23 \pm 6$	$9.0 \pm 3.9$	$3.7 \pm 1.8$	$2.2 \pm 1.2$
$t\bar{t} \rightarrow \ell + \text{jets \& single top } (1\ell)$	$148 \pm 75$	$67.9 \pm 28.9$	$16.1 \pm 9.1$	$4.7 \pm 3.2$	$1.8 \pm 1.6$	$0.9 \pm 0.9$	$0.4 \pm 0.5$
$W + \text{jets}$	$19.2 \pm 4.5$	$10.0 \pm 2.2$	$3.11 \pm 0.98$	$1.2 \pm 0.6$	$0.6 \pm 0.4$	$0.4 \pm 0.3$	$0.2 \pm 0.2$
Rare	$33.2 \pm 16.6$	$22.7 \pm 11.4$	$9.00 \pm 4.50$	$4.8 \pm 2.4$	$2.9 \pm 1.5$	$1.2 \pm 0.6$	$1.0 \pm 0.5$
Total	$531 \pm 80$	$284 \pm 37$	$87.7 \pm 14.2$	$33 \pm 7$	$14 \pm 5$	$6.1 \pm 2.1$	$3.8 \pm 1.4$
Data	494	254	76	31	8	2	1
Electron							
$t\bar{t} \rightarrow \ell\ell$	$248 \pm 17$	$144 \pm 17$	$51.1 \pm 8.8$	$16 \pm 5$	$5.5 \pm 2.5$	$2.5 \pm 1.3$	$1.3 \pm 0.7$
$t\bar{t} \rightarrow \ell + \text{jets \& single top } (1\ell)$	$108 \pm 55$	$51.8 \pm 22.1$	$12.9 \pm 7.3$	$3.0 \pm 2.0$	$1.2 \pm 1.1$	$0.7 \pm 0.7$	$0.4 \pm 0.5$
$W + \text{jets}$	$14.3 \pm 3.3$	$7.50 \pm 1.66$	$2.43 \pm 0.77$	$0.8 \pm 0.4$	$0.4 \pm 0.3$	$0.3 \pm 0.2$	$0.1 \pm 0.2$
Rare	$25.8 \pm 12.9$	$15.8 \pm 7.9$	$7.10 \pm 3.55$	$2.9 \pm 1.5$	$0.7 \pm 0.4$	$0.3 \pm 0.2$	$0.1 \pm 0.1$
Total	$396 \pm 59$	$219 \pm 29$	$73.5 \pm 11.9$	$23 \pm 5$	$7.8 \pm 2.7$	$3.9 \pm 1.5$	$1.9 \pm 0.9$
Data	367	202	74	30	15	7	2
Muon+Electron Combined							
$t\bar{t} \rightarrow \ell\ell$	$579 \pm 38$	$328 \pm 37$	$111 \pm 18$	$39 \pm 10$	$14 \pm 6$	$6.2 \pm 2.9$	$3.5 \pm 1.8$
$t\bar{t} \rightarrow \ell + \text{jets \& single top } (1\ell)$	$256 \pm 131$	$120 \pm 51$	$29.0 \pm 16.4$	$7.7 \pm 5.1$	$3.1 \pm 2.7$	$1.7 \pm 1.6$	$0.8 \pm 1.0$
$W + \text{jets}$	$33.5 \pm 8.2$	$17.5 \pm 4.5$	$5.54 \pm 1.98$	$2.0 \pm 1.0$	$1.0 \pm 0.7$	$0.7 \pm 0.6$	$0.3 \pm 0.4$
Rare	$59.0 \pm 29.5$	$38.5 \pm 19.3$	$16.1 \pm 8.1$	$7.7 \pm 3.9$	$3.6 \pm 1.8$	$1.5 \pm 0.8$	$1.1 \pm 0.6$
Total	$927 \pm 138$	$504 \pm 65$	$161 \pm 26$	$56 \pm 12$	$22 \pm 7$	$10 \pm 3$	$5.7 \pm 2.2$
Data	861	456	150	61	23	9	3

Table 35: The result of the search.

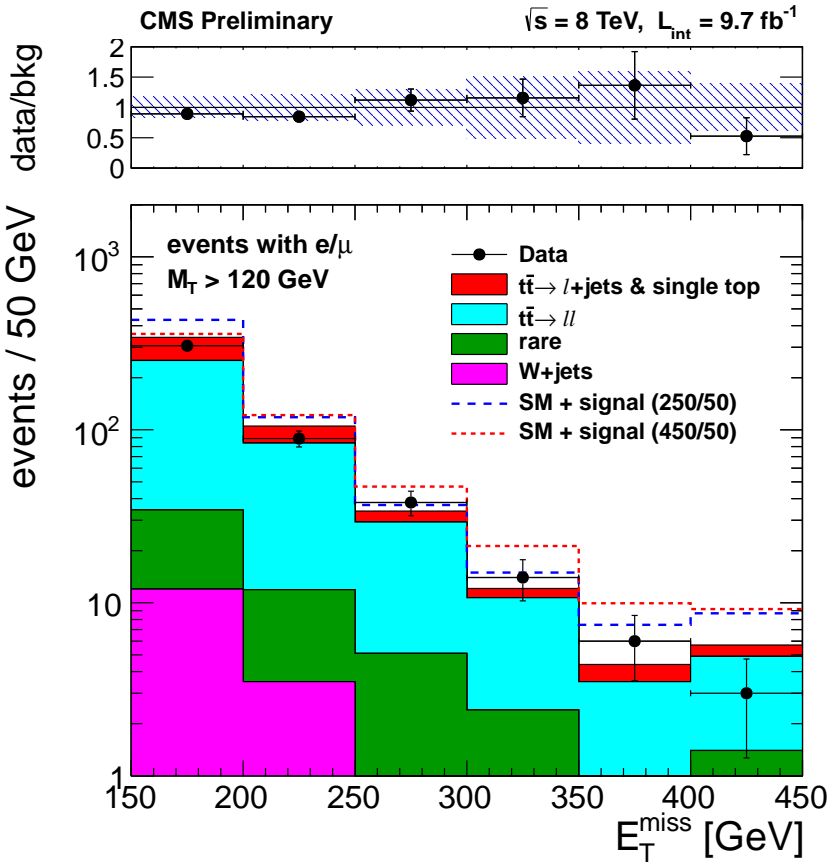


Figure 20: Predicted and observed  $E_T^{\text{miss}}$  for  $M_T > 120$  GeV, obtained from the yields for SRB to SRG. Note SRB corresponds to the integral of the distribution, while subsequent signal regions SRC to SRG correspond to integrals from subsequent bins. The band on the ratio (above) corresponds to the full relative background uncertainty.

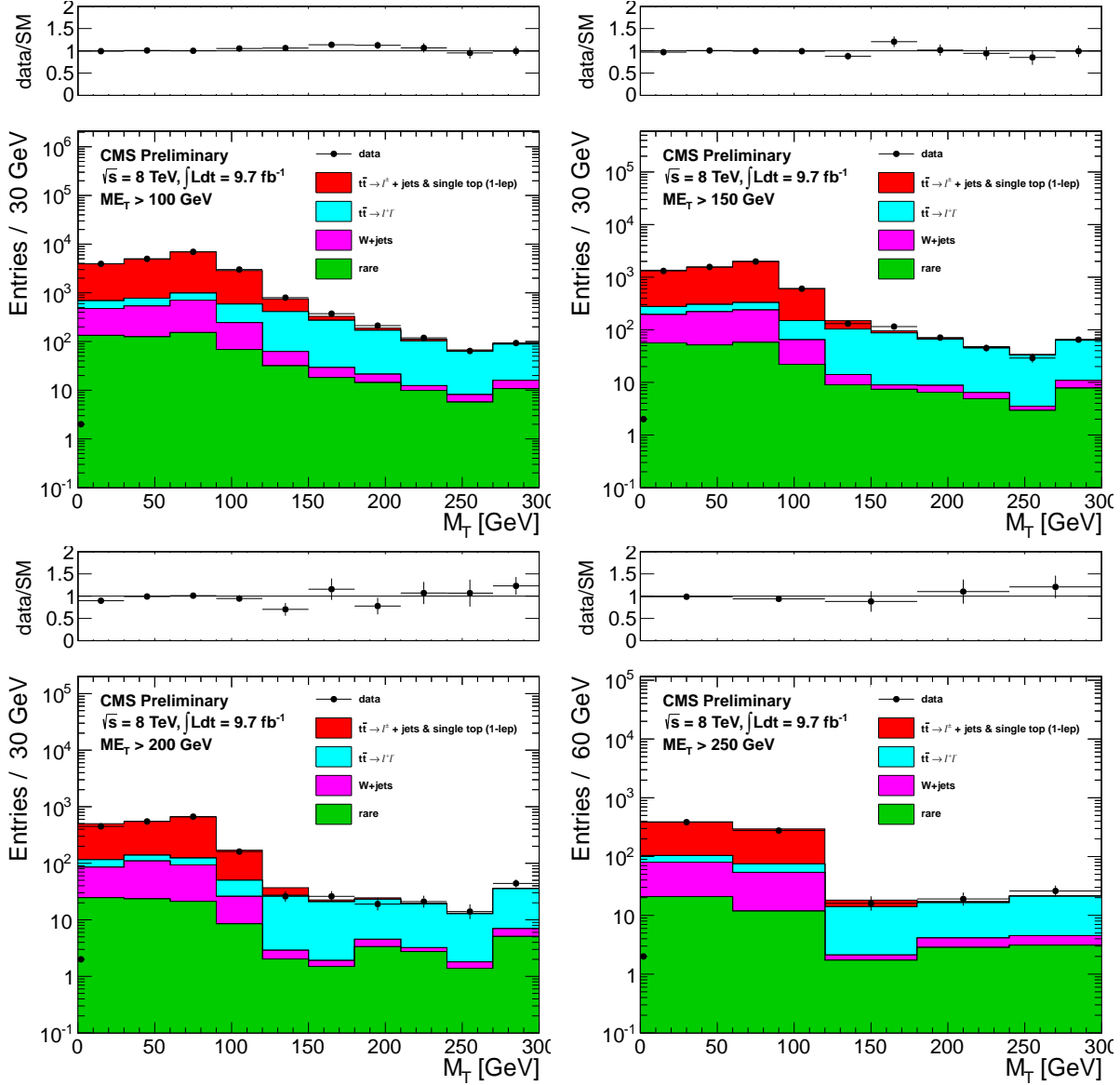


Figure 21:  $M_T$  in the data compared to SM Monte Carlo, for increasing values of  $E_T^{\text{miss}}$ . Only statistical uncertainties are shown. Note that the MC tails have not been rescaled at this point.

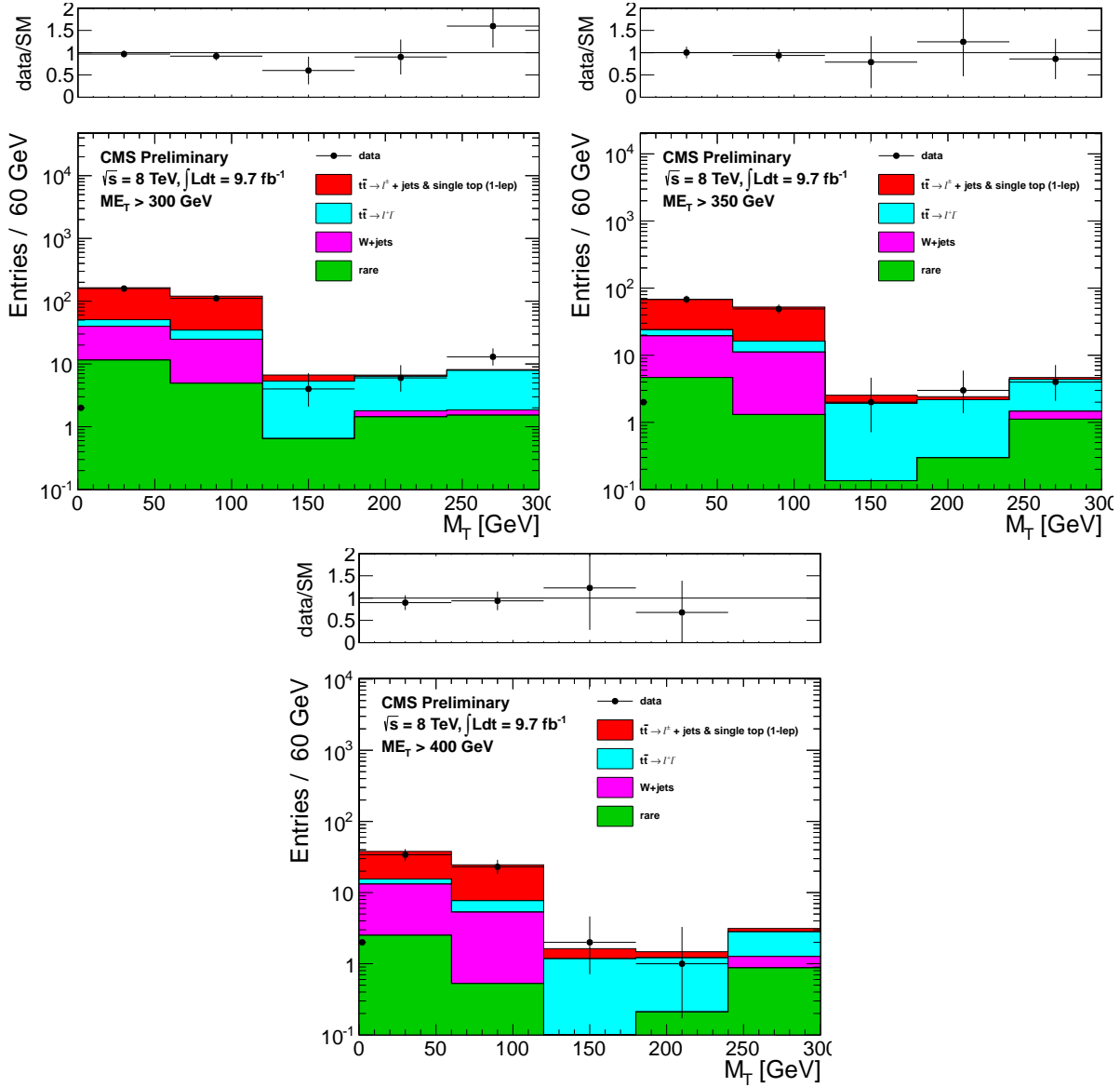


Figure 22:  $M_T$  in the data compared to SM Monte Carlo, for increasing values of  $E_T^{\text{miss}}$ . Only statistical uncertainties are shown. Note that the MC tails have not been rescaled at this point.

## 666 11 Limits

667 In this Section, we interpret the results of this search in terms of the T2tt and T2bw simplified models,  
 668 see Figure 23. The branching fractions for the stop decay are assumed to be 100% for each model. The  
 669 signal samples are normalized to cross sections calculated at NLO in  $\alpha_S$ , including the resummation of  
 670 soft gluon emission at next-to-leading-logarithmic accuracy (NLO+NLL).

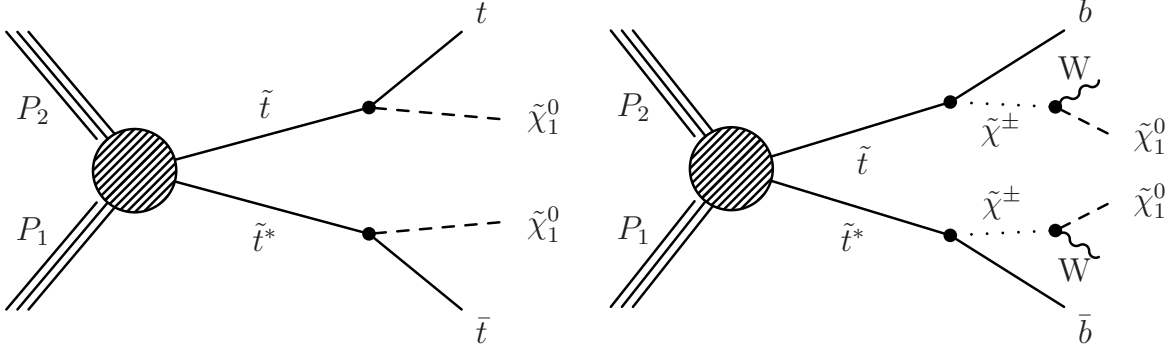


Figure 23: Diagram for the T2tt (left) and T2bw (right) simplified models.

671 The exclusion is performed using the results from the counting experiments in the signal regions defined  
 672 by  $E_T^{\text{miss}}$  and  $M_T$  and listed in Table 4. The cross section upper limit calculation is performed with the  
 673 LandS software using the LHC-type CLs criterion.

674 The signal efficiency uncertainties include the luminosity (4.4%), lepton ID and isolation efficiency (2%),  
 675 and trigger efficiency (3%). The uncertainty from JES is assessed for each scan point following the POG-  
 676 recommended procedure, by varying the jet energies by the  $p_T$ - and  $\eta$ - dependent uncertainties, and  
 677 propagating this to the jet multiplicity,  $E_T^{\text{miss}}$  and  $M_T$ . The official b-tagging scale-factors for CSVm are  
 678 used to compute scale factors for the signal. The results are nearly constant across the model parameter  
 679 space, and an overall scale factor of  $(98 \pm 2)\%$  is used.

680 The signal efficiency in the stop vs LSP mass plane for T2tt is shown for each signal region in Figures 24,  
 681 25 and 26 (left). The corresponding distributions for T2bw are shown in Figures 27 and 28 (left) for  
 682  $x=0.75$  and in Figure 29 (left) for  $x=0.5$ . The current analysis is not sensitive to the  $x=0.25$  scenario  
 683 (Figure 31, bottom).

684 These distributions show how challenging it is to have sensitivity near the kinematical boundaries. The  
 685 cross section upper limits, along with the observed and expected exclusion contours, are also shown in  
 686 Figures 24, 25 and 26 for T2tt, in Figures 27 and 28 for T2bw with  $x=0.75$ , and in Figure 29 for T2bw with  
 687  $x=0.5$  (right). The complementarity of the different signal regions is readily apparent. The sensitivity to  
 688 low (high) stop masses comes from the low (high)  $E_T^{\text{miss}}$  signal regions.

689 A combined result is obtained using the observed limit from the signal region with the best expected limit  
 690 for each scan point. The combined cross section upper limits, with the observed and expected exclusion  
 691 contours, are shown in Figure 30 for T2tt and Figure 31 for T2bw (left). The signal region with the best  
 692 expected limit for each scan point is also shown in Figure 30 for T2tt and Figure 31 for T2bw (right).  
 693 For the T2tt scenario, these results exclude stops with masses in the range of approximately 230 – 460  
 694 GeV, for LSP masses up to about 120 GeV. In the T2bw scenario with  $x=0.75$ , this search excludes stops  
 695 with masses in the range of approximately 150 – 430 GeV, for LSP masses up to about 140 GeV. The  
 696 sensitivity is reduced in the  $x=0.5$  scenario, where the results exclude stops with masses in the range of  
 697 approximately 250 – 360 GeV, for LSP masses less than approximately 100 GeV.

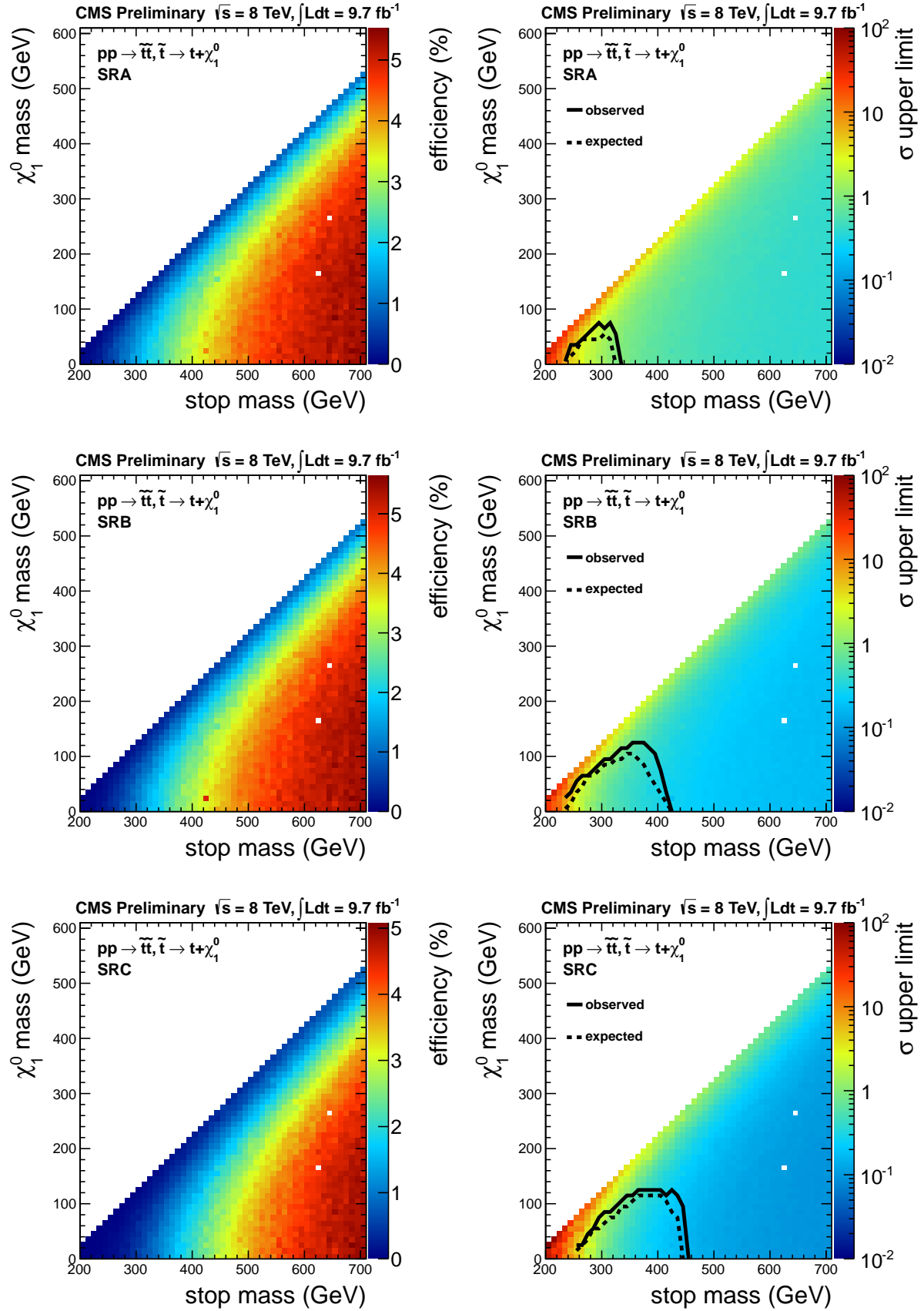


Figure 24: Signal efficiency (left) and cross section upper limit (right) for the T2tt model, showing both the expected and observed exclusion contours. The results for signal regions SRA (top), SRB (middle) and SRC (bottom) are shown separately.

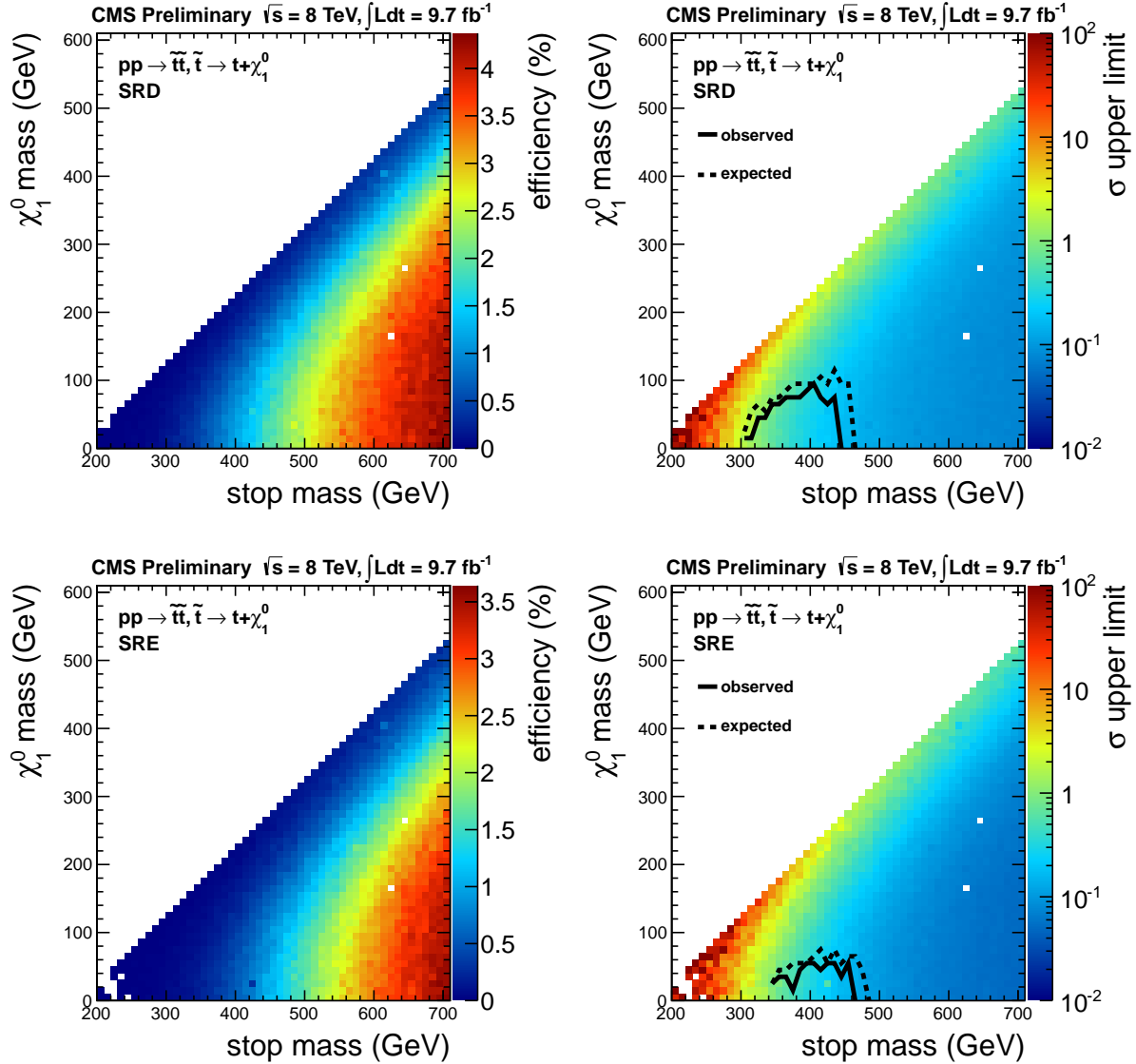


Figure 25: Signal efficiency (left) and cross section upper limit (right) for the T2tt model, showing both the expected and observed exclusion contours. The results for signal regions SRD (top), and SRE (bottom) are shown separately.

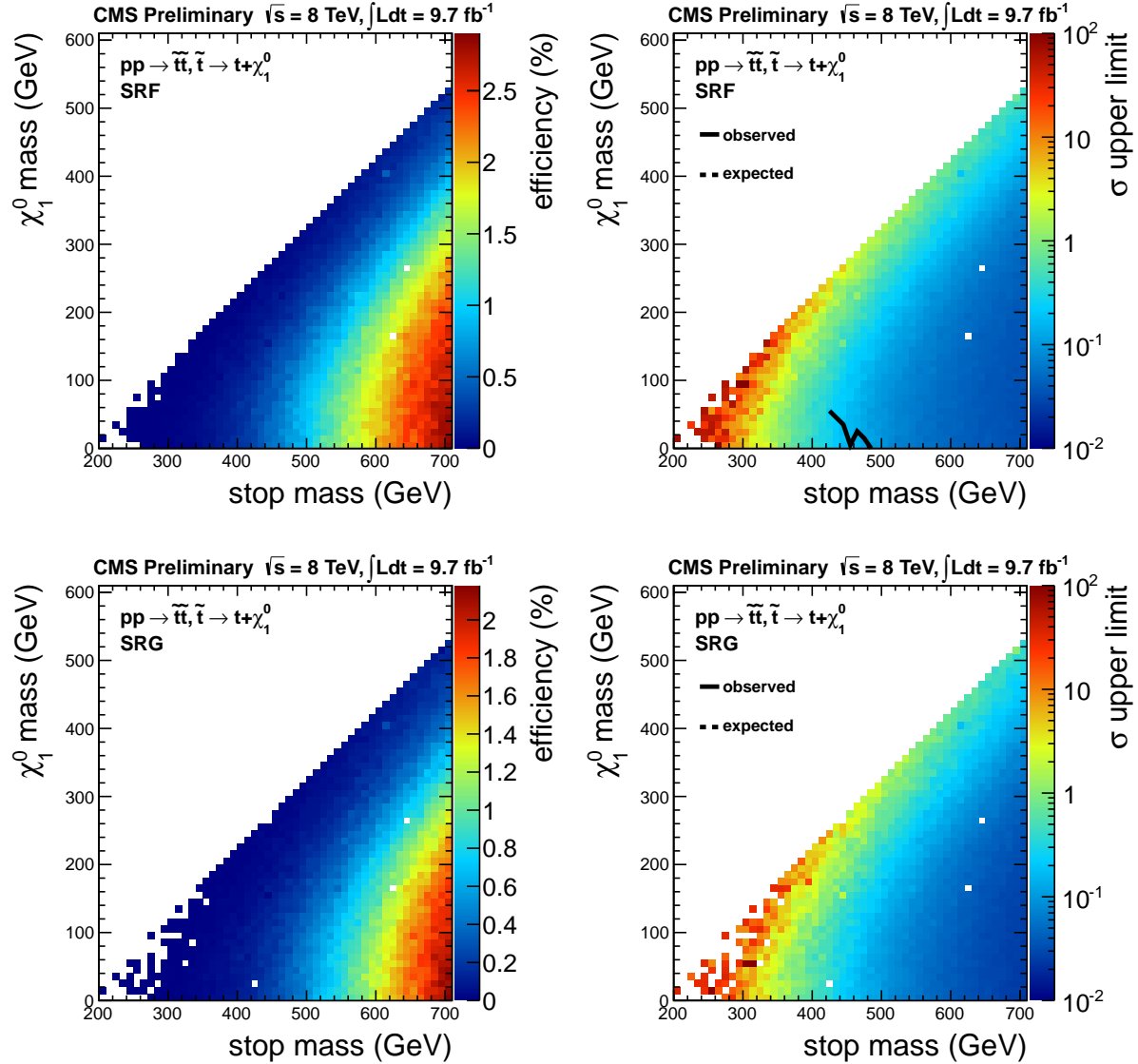


Figure 26: Signal efficiency (left) and cross section upper limit (right) for the T2tt model, showing both the expected and observed exclusion contours. The results for signal regions SRF (top) and SRG (bottom) are shown separately.

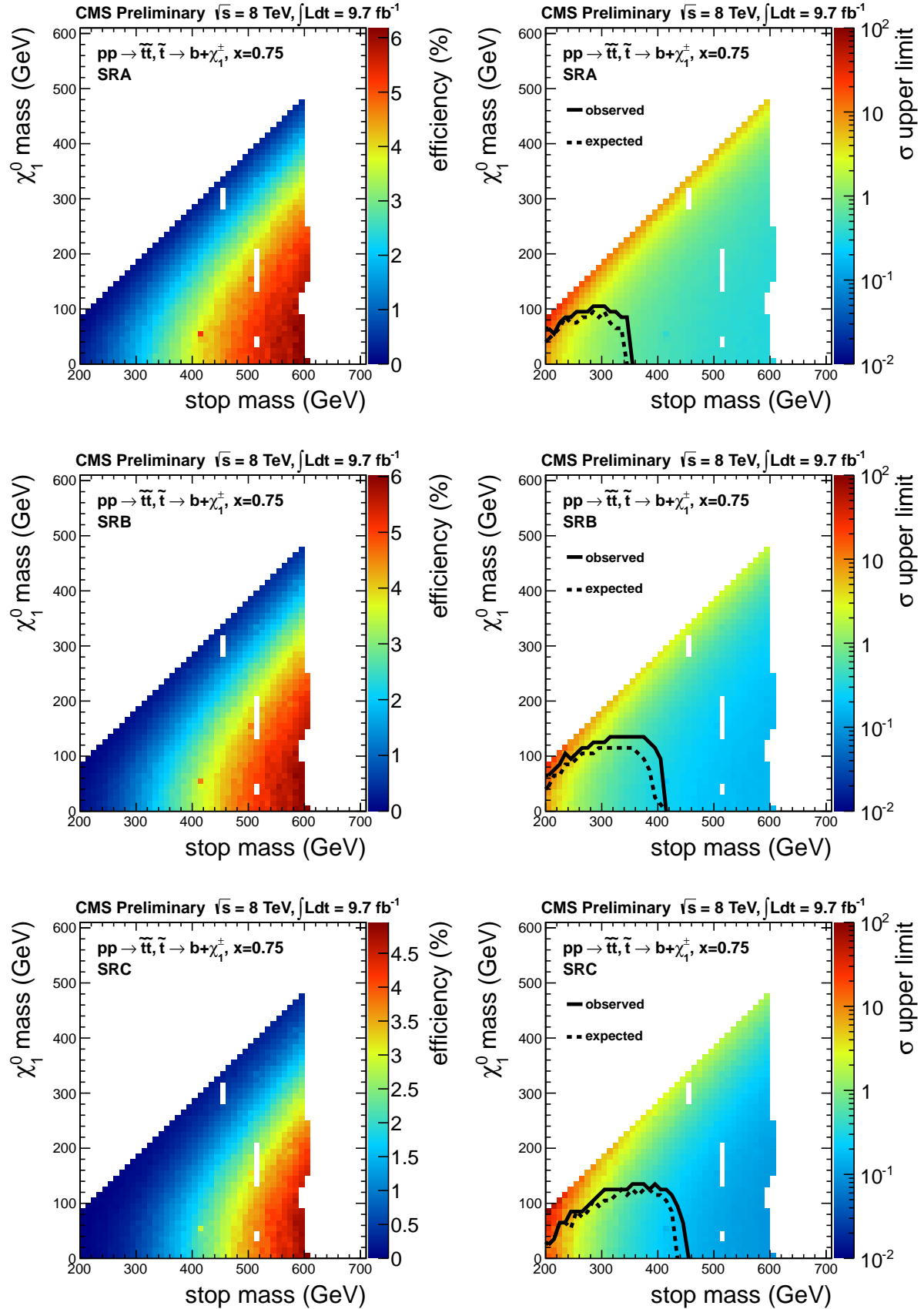


Figure 27: Signal efficiency (left) and cross section upper limit (right) for the T2bw model with  $x=0.75$ , showing both the expected and observed exclusion contours. The results for signal regions SRA (top), SRB (middle) and SRC (bottom) are shown separately.

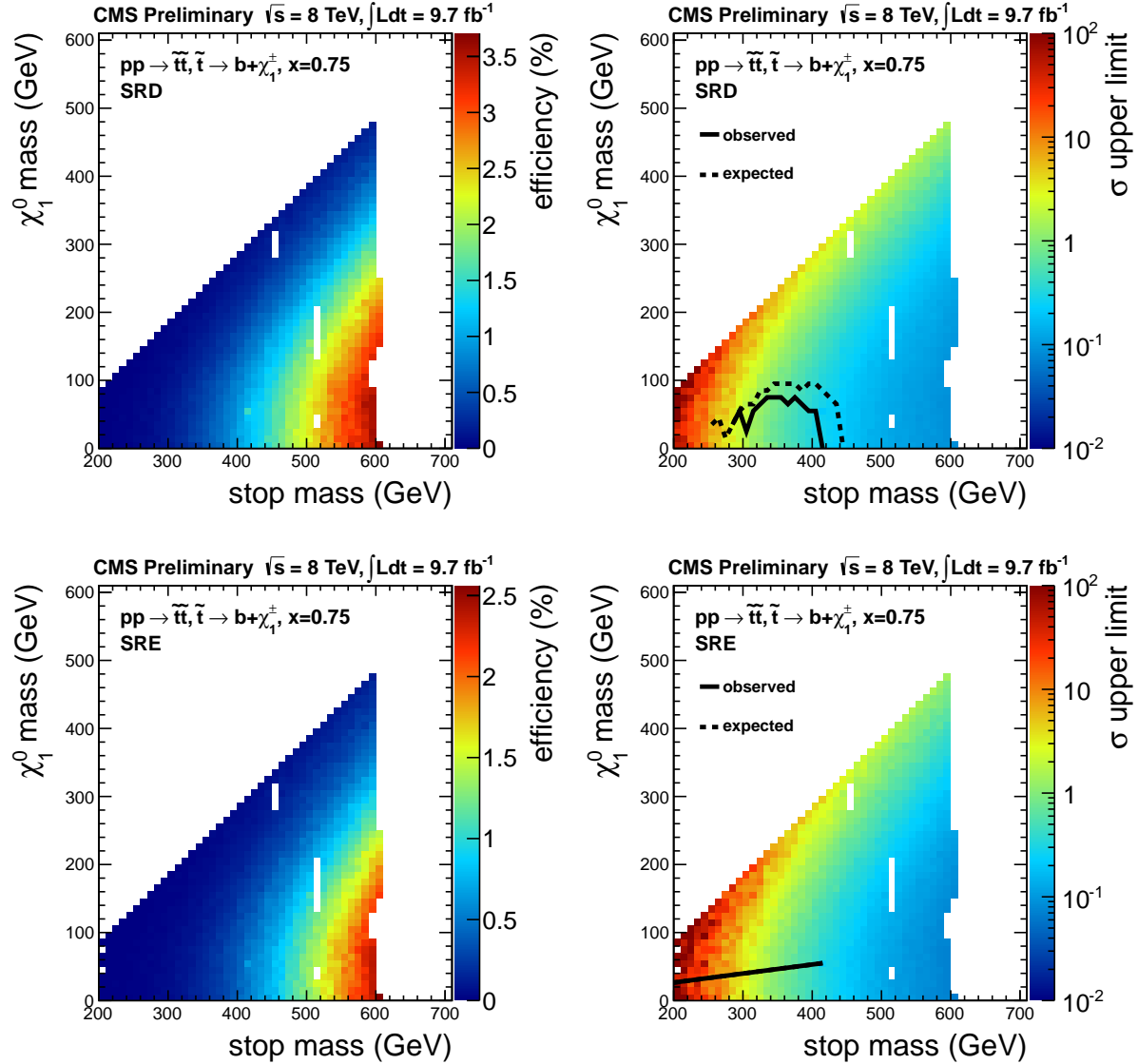


Figure 28: Signal efficiency (left) and cross section upper limit (right) for the T2bw model with  $x=0.75$ , showing both the expected and observed exclusion contours. The results for signal regions SRD (top), and SRE (bottom) are shown separately.

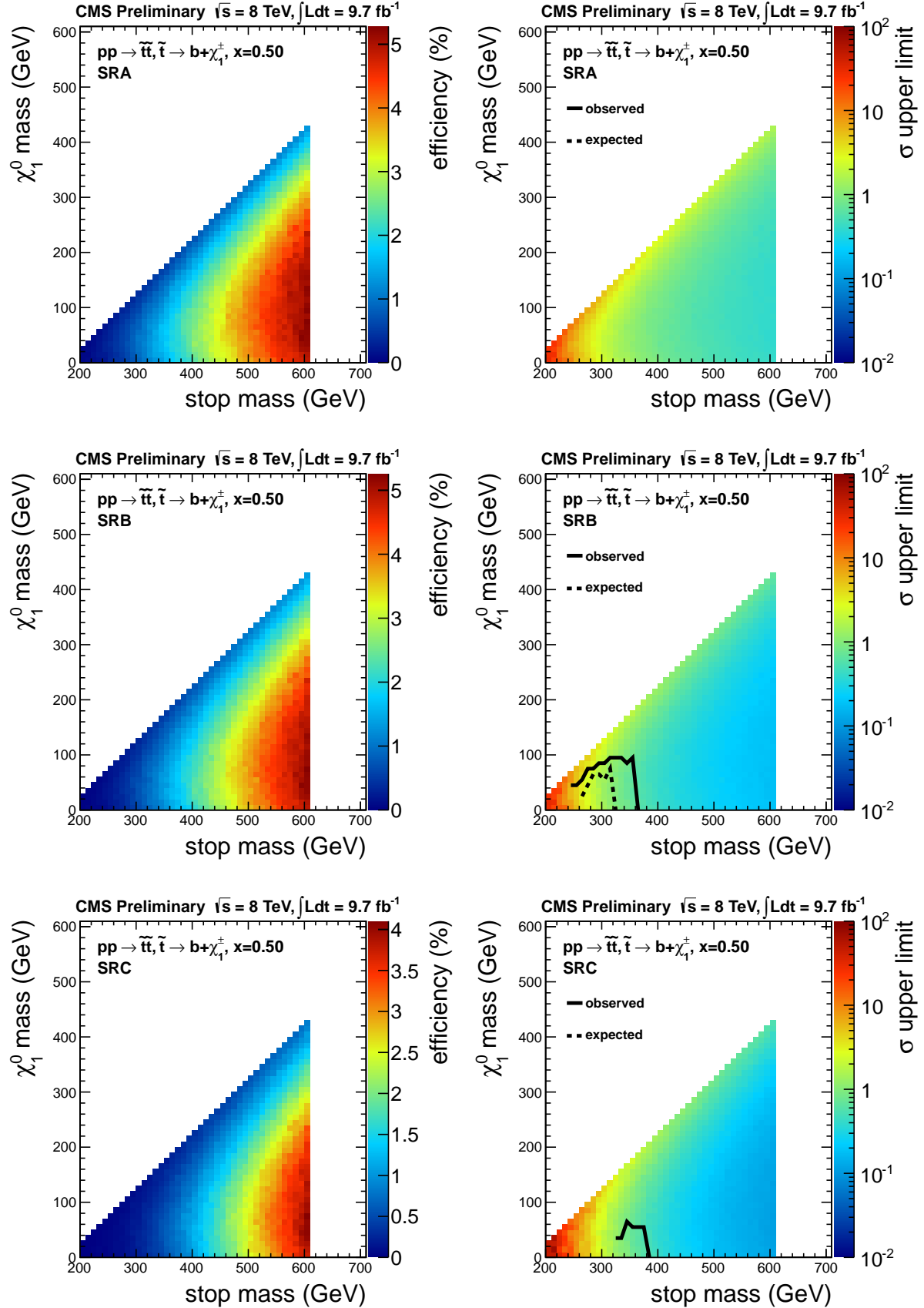


Figure 29: Signal efficiency (left) and cross section upper limit (right) for the T2bw model with  $x=0.5$ , showing both the expected and observed exclusion contours. The results for signal regions SRA (top), SRB (middle) and SRC (bottom) are shown separately.

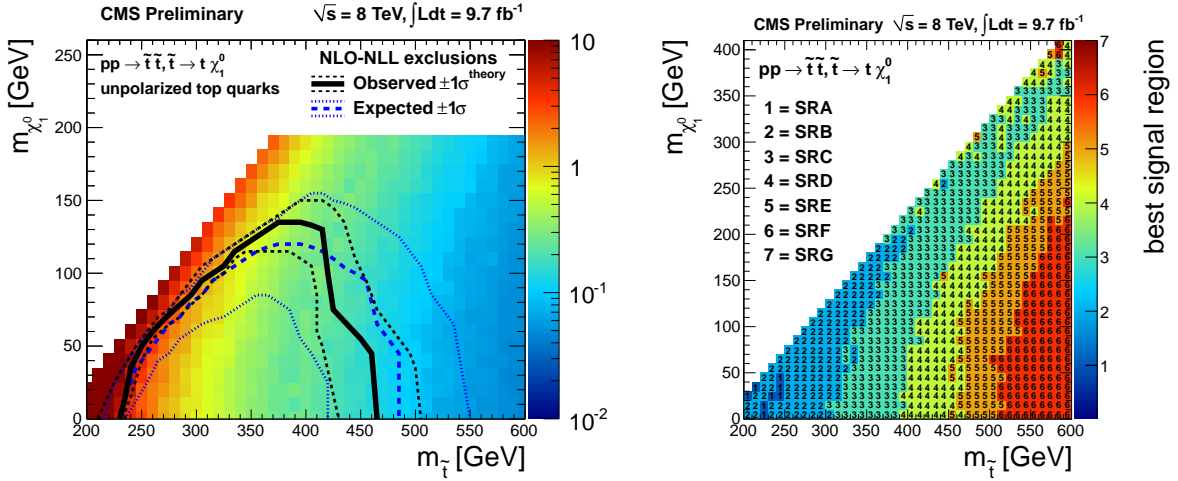


Figure 30: Upper limit on the cross section for the T2tt model in the plane of stop vs. LSP mass, showing both the expected (dashed) and observed (solid curve) exclusion contours (left). The observed limit is selected from the signal region with the best expected limit (shown on right). All uncertainties are included and the dotted contours around the dashed expected limit correspond to the  $\pm 1\sigma$  result.

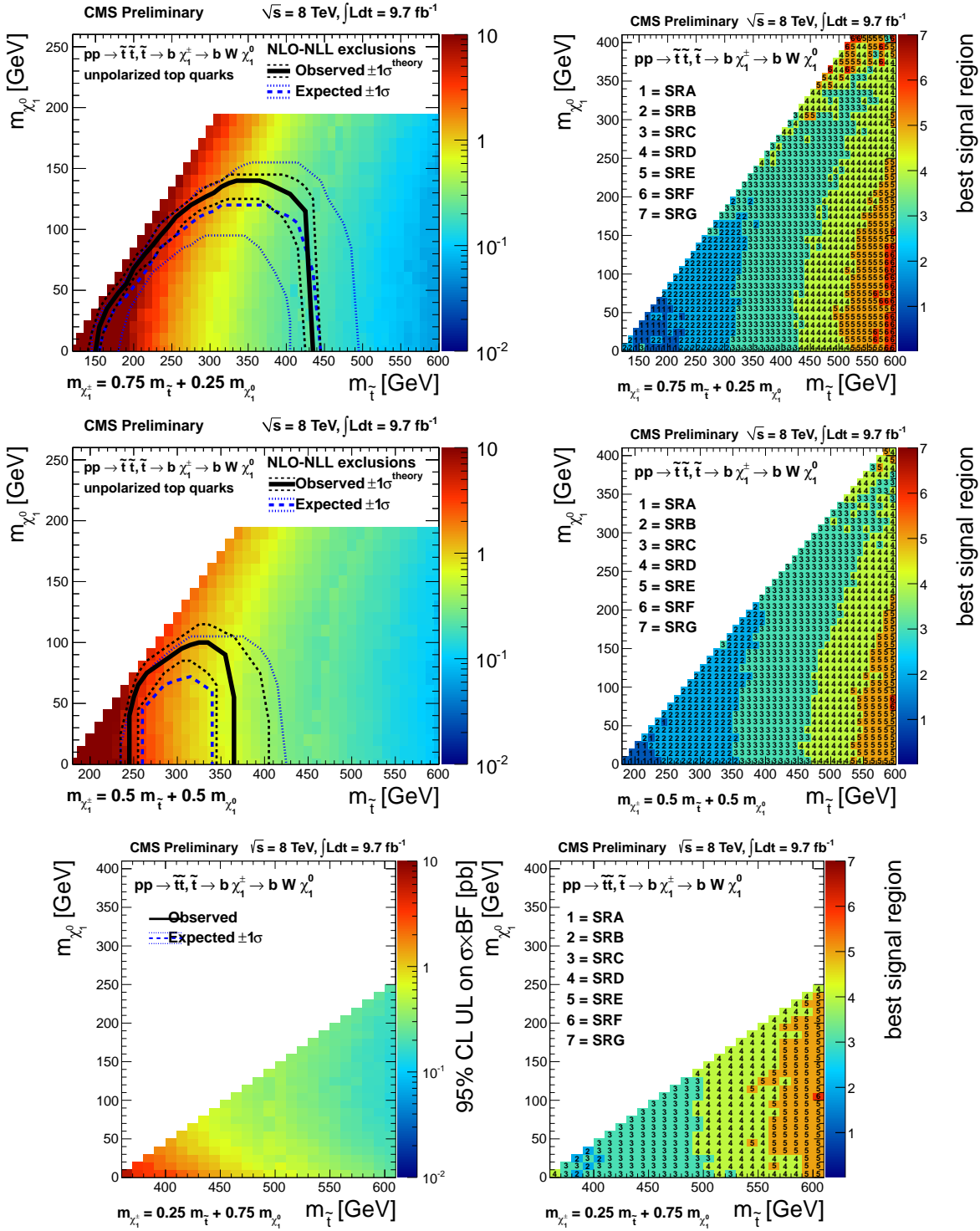


Figure 31: Upper limit on the cross section for the T2bw model for  $x=0.7$  (top),  $x=0.5$  (middle) and  $x=0.25$  (bottom) in the plane of stop vs. LSP mass, showing both the expected (dashed) and observed (solid curve) exclusion contours (left). The observed limit is selected from the signal region with the best expected limit (shown on right). All uncertainties are included and the dotted contours around the dashed expected limit correspond to the  $\pm 1\sigma$  result.

## 698 12 Conclusion

699 This note presents a search for the production of stop quark pairs in events with a single isolated lepton,  
700 several jets, missing transverse energy, and large transverse mass. The dataset used corresponds to an  
701 integrated luminosity of  $9.7 \text{ fb}^{-1}$  at center-of-mass energy of 8 TeV. Seven signal regions are defined, based  
702 on  $E_T^{\text{miss}}$  and  $M_T$  requirements. Agreement is observed between the data and the predicted backgrounds  
703 for all signal regions. The results are interpreted in the context of simplified SUSY models where the  
704 stops decay to top-neutralino or b-chargino and are used to place constraints on the stop mass.

## 705 References

- 706 [1] <https://twiki.cern.ch/twiki/bin/view/LHCPhysics/SUSYCrossSections8TeVstopsbottom>
- 707 [2] T. Plenh *et al.*, JHEP 1208(2012) 091.
- 708 [3] These are measured by the Florida group in the context of the same sign and ewk-ino analyses.
- 709 [4] M. Perelstein, A. Weiler, arXiv:0811.1024v2 [hep-ph]

## 710 A Performance of the Isolation Requirement

711 The last requirement used in the analysis is an isolated track veto. This selection criteria rejects events  
 712 containing a track of  $p_T > 10$  GeV with relative track isolation  $\sum p_T/p_T(\text{trk})$  in a cone of size  $R = 0.3 <$   
 713 0.1. It may be noted that only tracks consistent with the vertex with highest  $\sum p_T^2$  are considered in  
 714 order to reduce the impact of spurious tracks, for example from pileup interactions. This requirement  
 715 has very good performance. Figure 32 shows the efficiency for rejecting dilepton events compared to the  
 716 efficiency for selecting single lepton events for various cone sizes and cut values. The chosen working  
 717 point provides a signal efficiency of  $\epsilon(\text{sig}) = 92\%$  for a background rejection of  $\epsilon(\text{bkg}) = 53\%$  in MC.  
 718 With "signal" ("background") we are referring to  $t\bar{t} \rightarrow \ell + \text{jets}$  ( $t\bar{t} \rightarrow \ell\ell$ ).

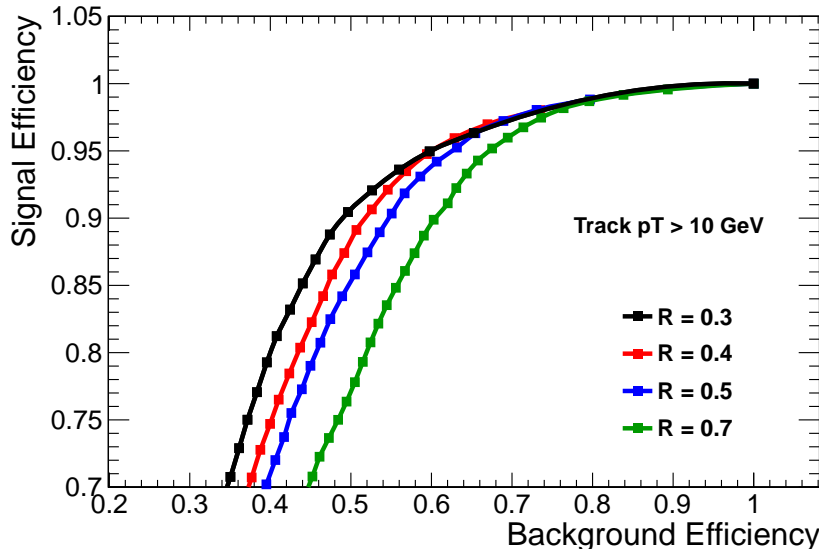


Figure 32: Comparison of the performance in terms of signal (single lepton events) efficiency and background (dilepton events) rejection for various cone sizes and cut values. The current isolation requirement uses a cone of size  $\Delta R = 0.3$  and a cut value of 0.1, corresponding to  $\epsilon(\text{sig}) = 92\%$  for  $\epsilon(\text{bkg}) = 53\%$ .

719 It should be emphasized that the isolated track veto has a different impact on the samples with a single  
 720 lepton (mainly  $t\bar{t} \rightarrow \ell + \text{jets}$  and  $W + \text{jets}$ ) and that with two leptons (mainly  $t\bar{t} \rightarrow \ell\ell$ ). For the dilepton  
 721 background, the veto rejects events which have a genuine second lepton. Thus the performance may  
 722 be understood as an efficiency  $\epsilon_{iso, trk}$  to identify the isolated track. In the case of the single lepton  
 723 background, the veto rejects events which do not have a genuine second lepton, but rather which contain  
 724 a "fake" isolated track. The isolated track veto thus effectively scales the single lepton sample by  $(1 -$   
 725  $\epsilon_{fake})$ , where  $\epsilon_{fake}$  is the probability to identify an isolated track with  $p_T > 10$  GeV in events which contain  
 726 no genuine second lepton. It is thus necessary to study the isolated track efficiency  $\epsilon(trk)$  and  $\epsilon_{fake}$  in  
 727 order to fully characterize the veto performance.

728 The veto efficiency for dilepton events is calculated using the tag and probe method in Z events. A good  
 729 lepton satisfying the full ID and isolation criteria and matched to a trigger object serves as the tag. The  
 730 probe is defined as a track with  $p_T > 10$  GeV that has opposite charge to the tag and has an invariant  
 731 mass with the probe consistent with the Z mass.

732 The variable used to study the performance of the veto is the absolute track isolation, since it removes  
 733 the dependence of the isolation variable on the  $p_T$  of the object under consideration. This is particularly  
 734 useful because the underlying  $p_T$  distribution is different for second leptons in  $t\bar{t} \rightarrow \ell\ell$  events compared to  
 735 Z events, particularly due to the presence of  $\tau$ s that have softer decay products. As shown in Figure 33,  
 736 the absolute isolation is consistent between Z + 4 jet events and  $t\bar{t} \rightarrow \ell\ell$  events, including leptons from W  
 737 and  $\tau$  decays. This supports the notion that the isolation, defined as the energy surrounding the object  
 738 under consideration, depends only on the environment of the object and not on the object itself. The  
 739 isolation is thus sensitive to the ambient pileup and jet activity in the event, which is uncorrelated with  
 740 the lepton  $p_T$ . It is thus justified to use tag and probe in Z + 4 jet events, where the jet activity is similar  
 741 to  $t\bar{t} \rightarrow \ell\ell$  events in our  $N_{\text{jets}} > 4$  signal region, in order to estimate the performance of the isolation  
 742 requirement for the various leptonic categories of  $t\bar{t} \rightarrow \ell\ell$  events.

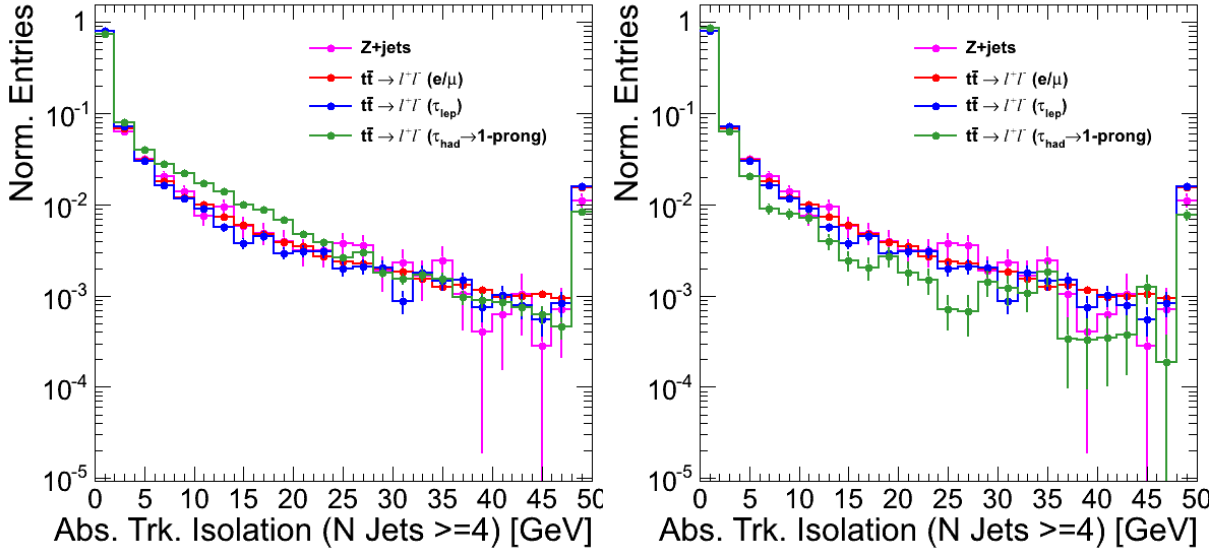


Figure 33: Comparison of absolute track isolation for track probes in Z + 4 jet and  $t\bar{t} \rightarrow \ell\ell$  events for different lepton types. The isolation variables agree across samples, except for single prong  $\tau$ s, that tend to be slightly less isolated (left). The agreement across isolation distributions is recovered after removing single prong  $\tau$  events produced in association with  $\pi^0$ s from the sample (right).

## 743 B Example BG prediction calculation

744 The calculation of the background prediction is a bit complicated. Here we walk the reader through a  
 745 concrete example.

746 **NB: the numbers in this section corresponded to the numbers in V3 of the analysis note.**  
 747 **They will not be updated, because this is meant as an illustration only..**

748 The main background is  $t\bar{t}$ . The main idea is to normalize to the  $M_T$  peak region ( $50 < M_T < 80$  GeV).  
 749 This eliminates dependence on  $t\bar{t}$  cross-section, luminosity, trigger efficiency, JES, lepton ID, etc. This  
 750 gets a bit complicated because the  $M_T$  peak region, while dominantly  $t\bar{t}$  lepton + jets, also includes some  
 751  $W+jets$ ,  $t\bar{t} \rightarrow \ell\ell$ , rare processes, etc. Also, we want to minimize our need to understand the effect of the  
 752 isolated track veto on  $t\bar{t} \rightarrow \ell + jets$ . As a result we actually define two  $M_T$  peak regions: one before and  
 753 one after applying the isolated track veto. Then the  $t\bar{t} \rightarrow \ell\ell$  background is normalized the the “before  
 754 veto” region, and the  $t\bar{t} \rightarrow \ell + jets$  and  $W+jets$  background are normalized to the “post veto” region.

755 This complex procedure is important for the high statistics signal regions with relatively low  $E_T^{\text{miss}}$   
 756 requirements, eg, SRA. For these SRs we want to keep the systematics low in order to be sensitive to low  
 757 mass stop; for the signal regions with hard cuts on  $E_T^{\text{miss}}$  this is less important. However, we apply the  
 758 same procedure to all SRs.

759 For concreteness, we show the calculation for SRA, electron channel. The MC and data event counts used  
 760 in the background calculation are collected in Table 36. Note that the background uncertainties have  
 761 already been described in Section 9. The one tricky point to keep in mind is that when the  $W+jets$  and  
 762 rare cross-sections are changed by their assumed uncertainties (50% each), the whole calculation described  
 763 below is repeated in order to take care of all the correlations properly.

Sample	$M_T$ peak, before trk veto	$M_T$ peak, after trk veto	Signal Region A
$t\bar{t} \rightarrow \ell\ell$	$290 \pm 6$	$116 \pm 4$	$261 \pm 6$
$t\bar{t} \rightarrow \ell + jets$ ( $1\ell$ )	$2899 \pm 19$	$2595 \pm 18$	not used
$W+jets$	$252 \pm 28$	$236 \pm 28$	not used
Rare	$89 \pm 5$	$62 \pm 4$	$26 \pm 2$
Total	$3530 \pm 35$	$3009 \pm 34$	not used
Data	3358	2787	not used

Table 36: Data and MC event counts used to predict the background in SRA, for electron events. Uncertainties are statistical only. The trigger efficiency has been applied to the MC samples. In the case of  $t\bar{t} \rightarrow \ell\ell$  the  $K_3$  and  $K_4$  factors of Section 5.3.1 have also been applied.

### 764 B.1 Central value of dilepton background

765 A “before veto” scale factor is defined from the second column in Table 36 as the factor by which all MC  
 766 except the “rare” need to be scaled up in order to have data/MC agreement. This is

$$767 SF_{\text{pre}} = (3358 - 89) / (2899 + 252 + 290) = 0.950.$$

768 Then the  $t\bar{t} \rightarrow \ell\ell$  background prediction is the number of events predicted by the MC in SRA (261 from  
 769 the last column of SRA), rescaled by  $SF_{\text{pre}}$ . The result for the central value is 248 events.

### 770 B.2 Central value of the $t\bar{t} \rightarrow \ell + jets$ background

771 A “post veto” scale factor is defined from the third column in Table 36 as the factor by which the  
 772  $t\bar{t} \rightarrow \ell + jets$  and the  $W+jets$  backgrounds need to be scaled to have data/MC agreement.

$$773 SF_{\text{post}} = (2787 - 62 - SF_{\text{pre}} \cdot 116) / (2595 + 236) = 0.924.$$

774 Then the  $t\bar{t} \rightarrow \ell + jets$  background is obtained as the product of the following three factors

- 775 •  $SF_{\text{post}} = 0.924$  as obtained above

- 776 • 2595, from the third column of Table 36

<sub>777</sub> • The tail-to-peak ratio  $R_{top} = 0.045$  from Table 21

<sub>778</sub> The result for the central value is 108 events.

### <sub>779</sub> **B.3 Central value for the $W+jets$ background**

<sub>780</sub> It is calculated as the product of

<sub>781</sub> •  $SF_{post} = 0.924$  from Section B.2

<sub>782</sub> • 236, from the third column of Table 36

<sub>783</sub> • The tail-to-peak ratio  $R_{wjet} = 0.066$  from Table 21

<sub>784</sub> The result for the central value is 14.3 events.

### <sub>785</sub> **B.4 Central value for the rare backgrounds**

<sub>786</sub> This is 26 events from Table 36

## 787 C Additional CR Data and MC Comparisons

788 This appendix shows some additional comparisons of the data and MC background samples for various  
 789 CRs. Figure 34 shows some additional components of the  $M_T$ , the lepton  $p_T$  and the azimuthal angle  
 790 between the lepton and the  $E_T^{\text{miss}}$  for CR1 (Section D.3). Figure 35 shows the equivalent distributions  
 791 for CR2 (Section 5.2), the positive lepton  $p_T$  and the angle between this lepton and the pseudo- $E_T^{\text{miss}}$ .  
 792 Similarly, figure 38 shows the lepton  $p_T$  and the azimuthal angle between the lepton and the  $E_T^{\text{miss}}$   
 793 for CR5 (Section D.2). Figures 36 and 37 provide some data and MC comparisons of the  $t\bar{t} \rightarrow \ell\ell$  control  
 794 sample CR4 (Section 5.3) for various kinematic distributions: leading lepton  $p_T$  and eta, as well as the  
 795 angles between the two leptons and between the leading lepton and the  $E_T^{\text{miss}}$ . These distributions show  
 796 quite good agreement between data and MC. More quantitative information is included in the section  
 797 discussing each control region.

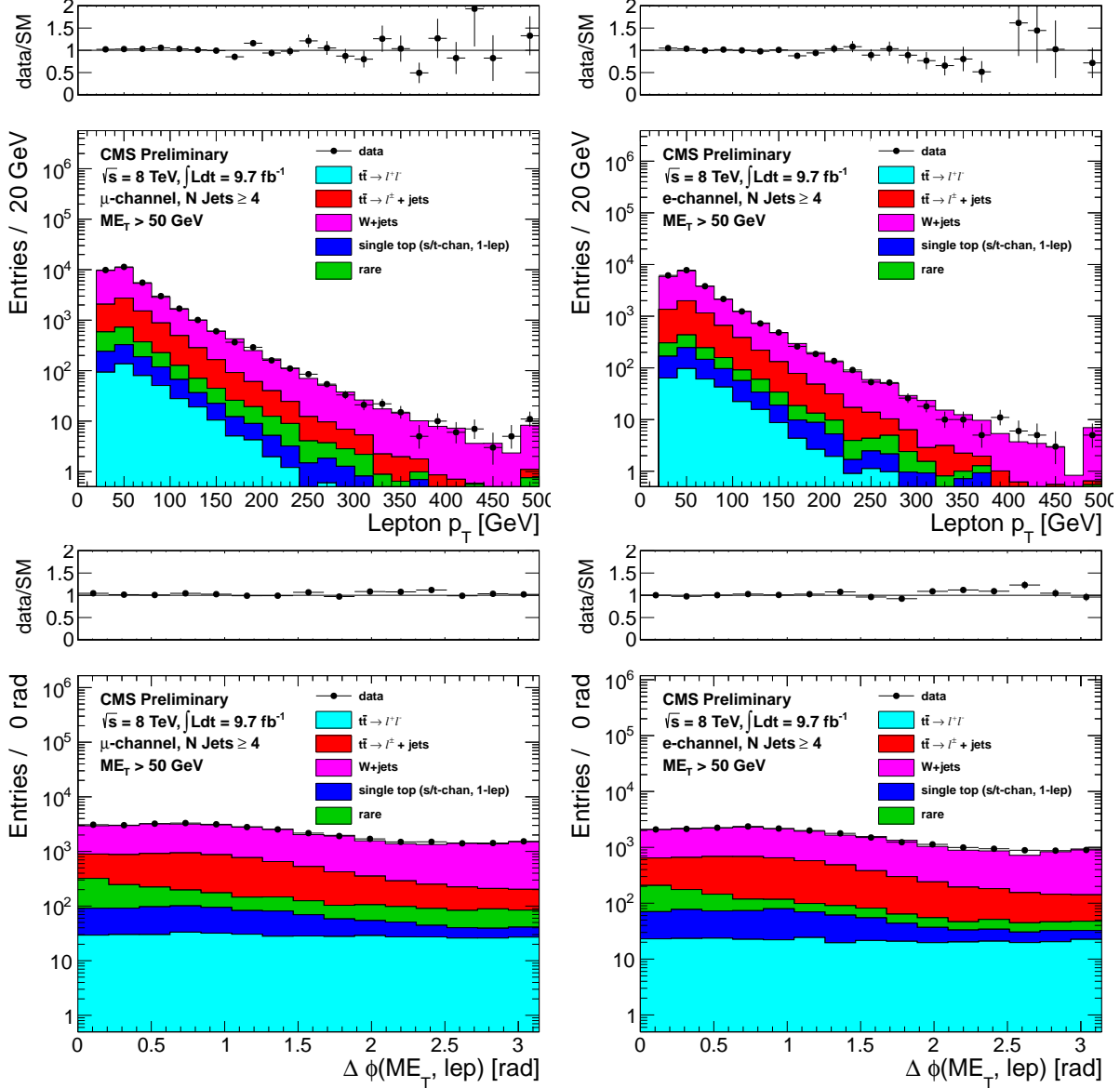


Figure 34: Comparison of the lepton  $p_T$  (top) and azimuthal angle between the  $E_T^{\text{miss}}$  and the lepton (bottom) for data vs. MC for events with a leading muon (left) and leading electron (right) satisfying the requirements of CR1.

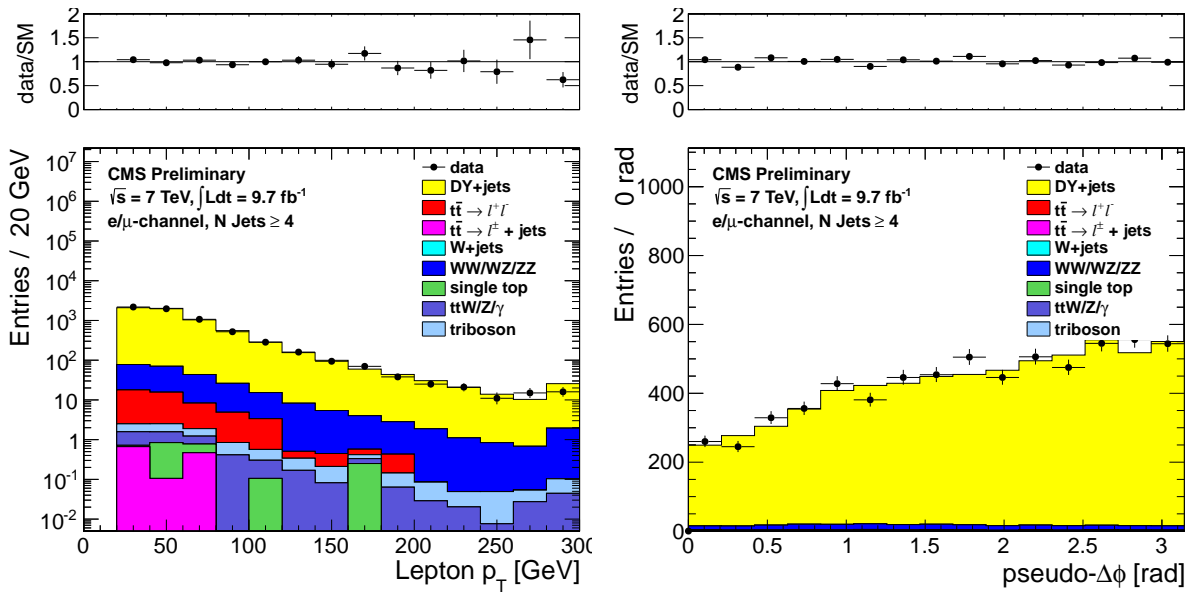


Figure 35: Comparison of the positive lepton  $p_T$  (left) and the azimuthal angle between this lepton and the pseudo- $E_T^{\text{miss}}$  (right) distributions in data vs. MC for events satisfying the requirements of CR2, combining both the muon and electron channels.

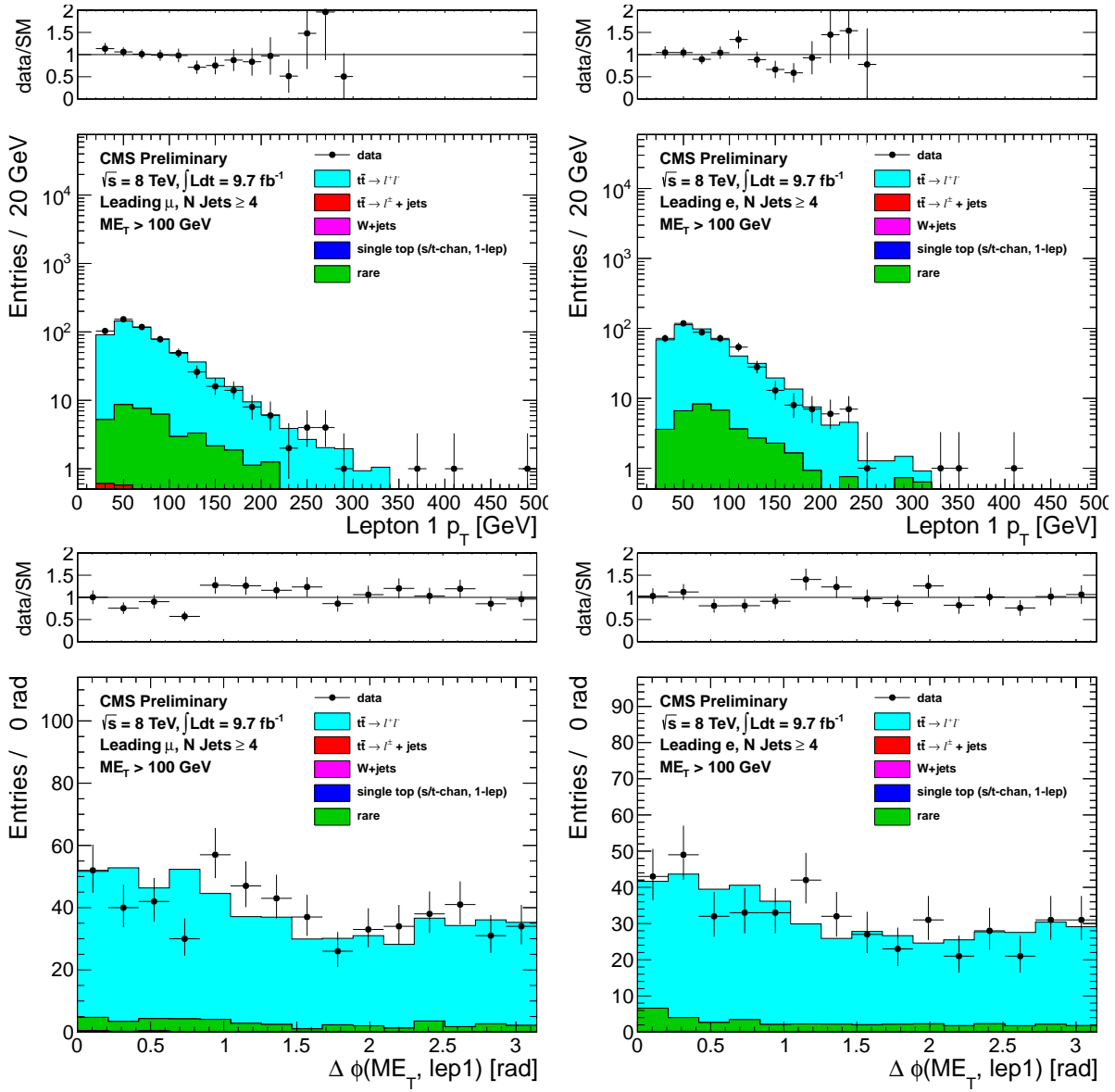


Figure 36: Comparison of the leading lepton  $p_T$  (top) and azimuthal angle between the leading lepton and the  $E_T^{\text{miss}}$  for  $E_T^{\text{miss}} > 100$  GeV distributions in data vs. MC for events with a leading muon (left) and leading electron (right) satisfying the requirements of CR4.

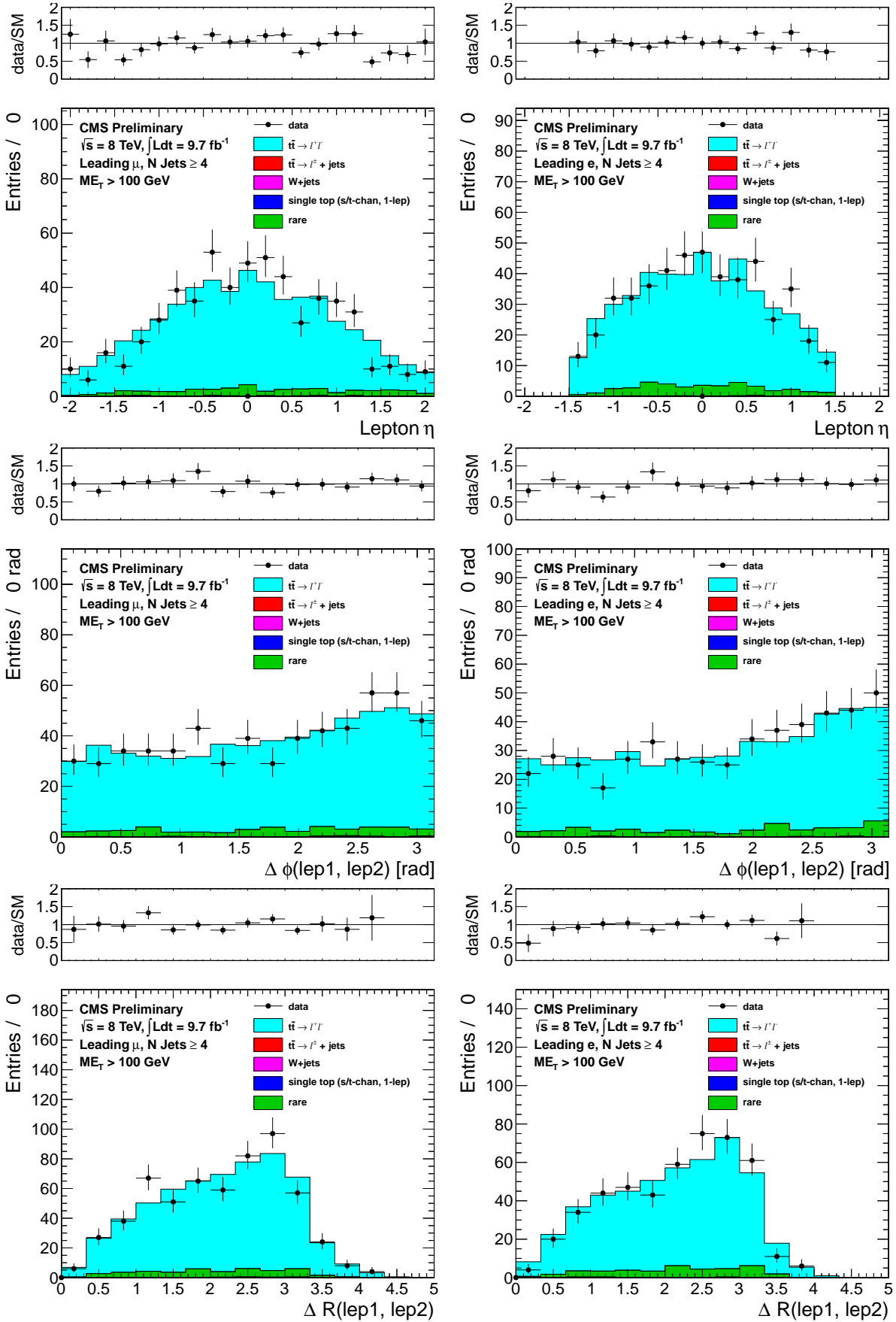


Figure 37: Comparison of the leading lepton eta (top), difference in the azimuthal angle (center) and  $\Delta R$  separation (bottom) between the two leptons for  $E_T^{\text{miss}} > 100 \text{ GeV}$  distributions in data vs. MC for events with a leading muon (left) and leading electron (right) satisfying the requirements of CR4.

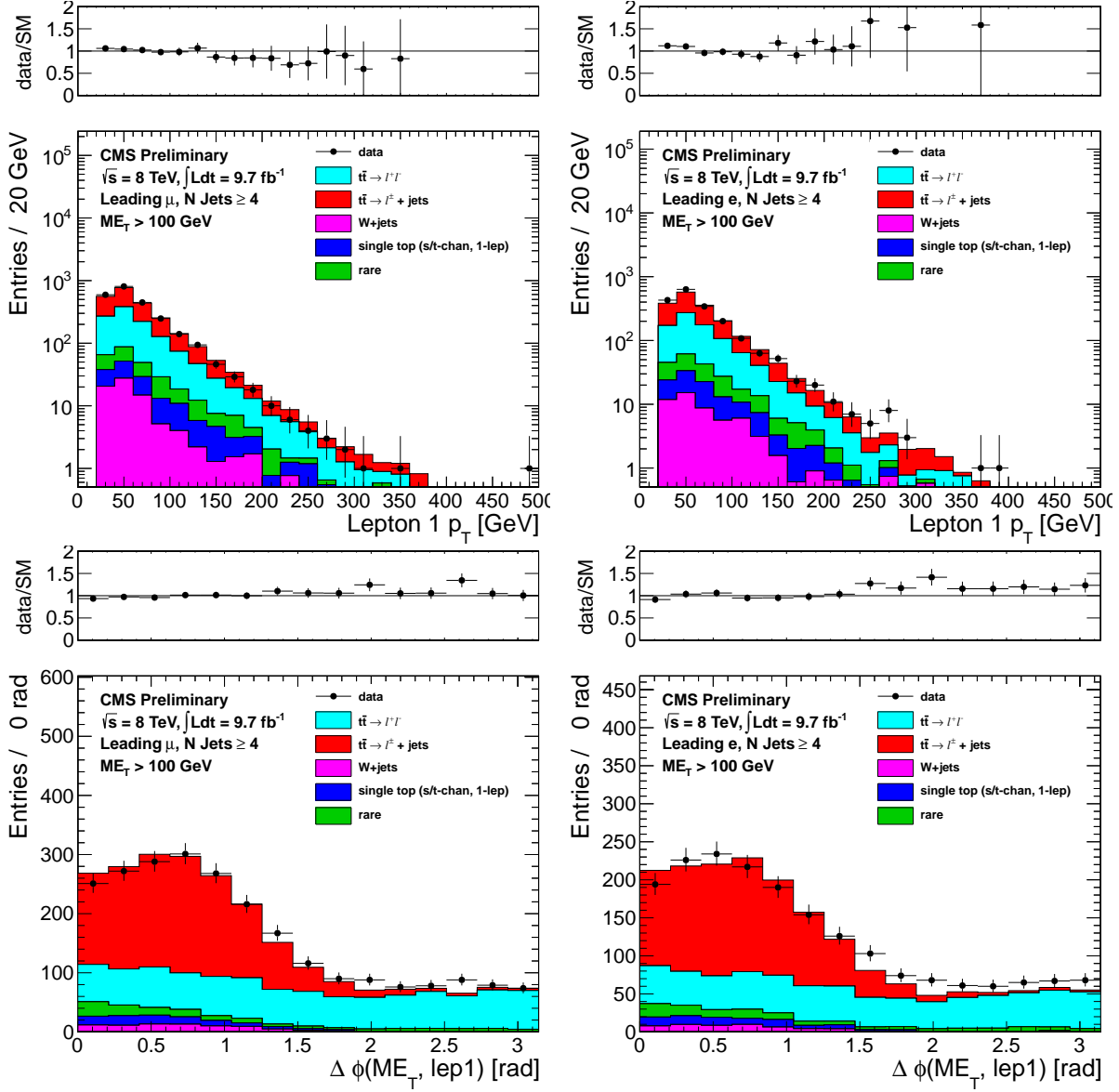


Figure 38: Comparison of the lepton  $p_T$  (top) and azimuthal angle between the  $E_{\text{T}}^{\text{miss}}$  and the lepton (bottom) for data vs. MC for  $E_{\text{T}}^{\text{miss}} > 100 \text{ GeV}$  for events with a leading muon (left) and leading electron (right) satisfying the requirements of CR5.

## 798 D Control Region Plots Summary

799 This appendix includes distributions from the various control regions used in the analysis used to validate  
 800 the MC modeling of the  $E_T^{\text{miss}}$  and  $M_T$  distributions in data and derive systematic uncertainties on the  
 801 background predictions. The distributions are shown in both log and linear scale.

### 802 D.1 CR4: $\geq 1$ b-tag, exactly 2 leptons

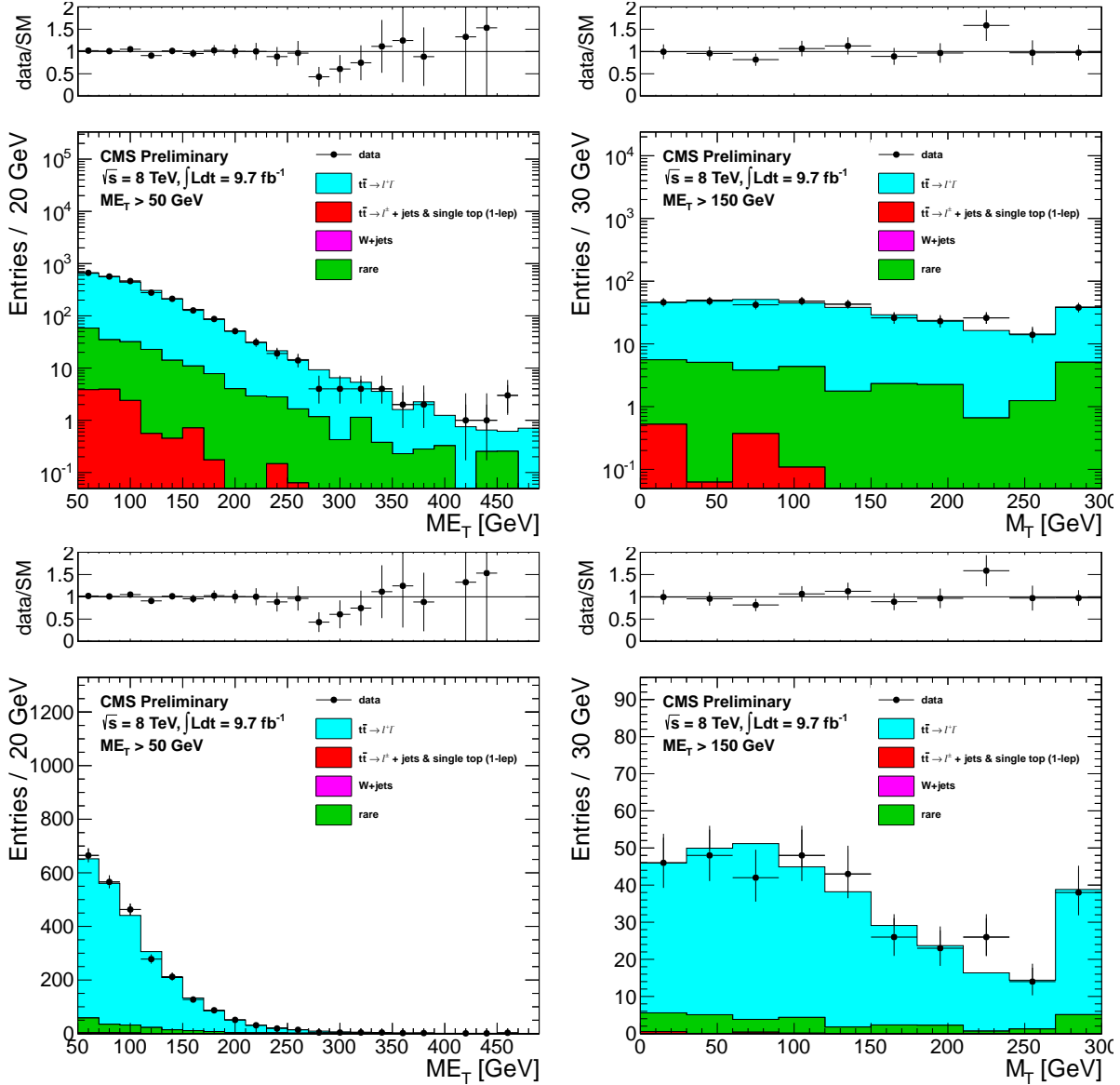


Figure 39: Comparison of the  $E_T^{\text{miss}}$  distribution (left) and  $M_T$  distribution for events satisfying  $E_T^{\text{miss}} > 150$  GeV (right) in data vs. MC for CR4.

803 D.2 CR5:  $\geq 1$  b-tag, 1 lepton + 1 isolated track

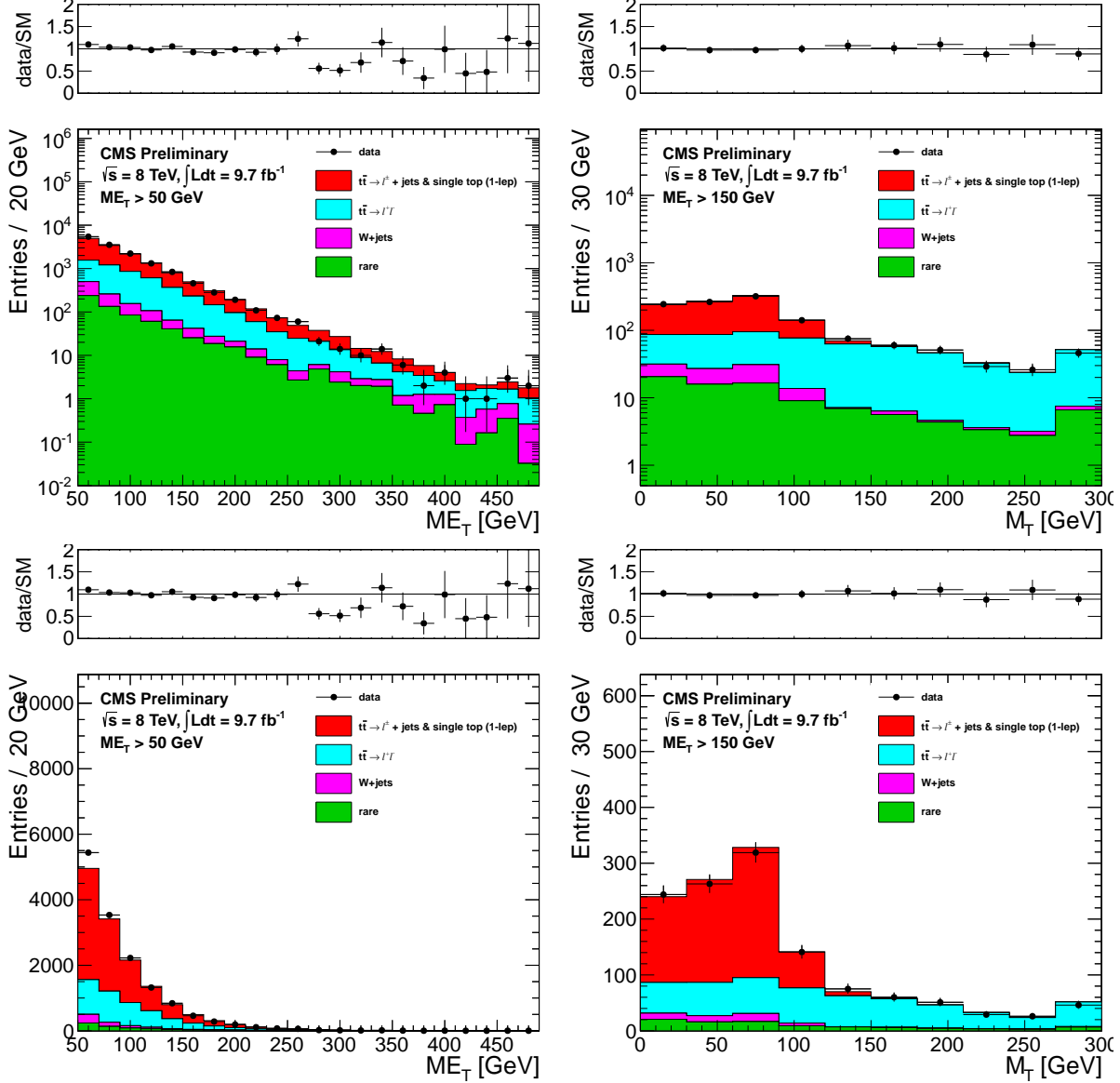


Figure 40: Comparison of the  $E_T^{\text{miss}}$  distribution (left) and  $M_T$  distribution for events satisfying  $E_T^{\text{miss}} > 150 \text{ GeV}$  (right) in data vs. MC for CR5.

804 D.3 CR1: 0 b-tags, exactly 1 lepton

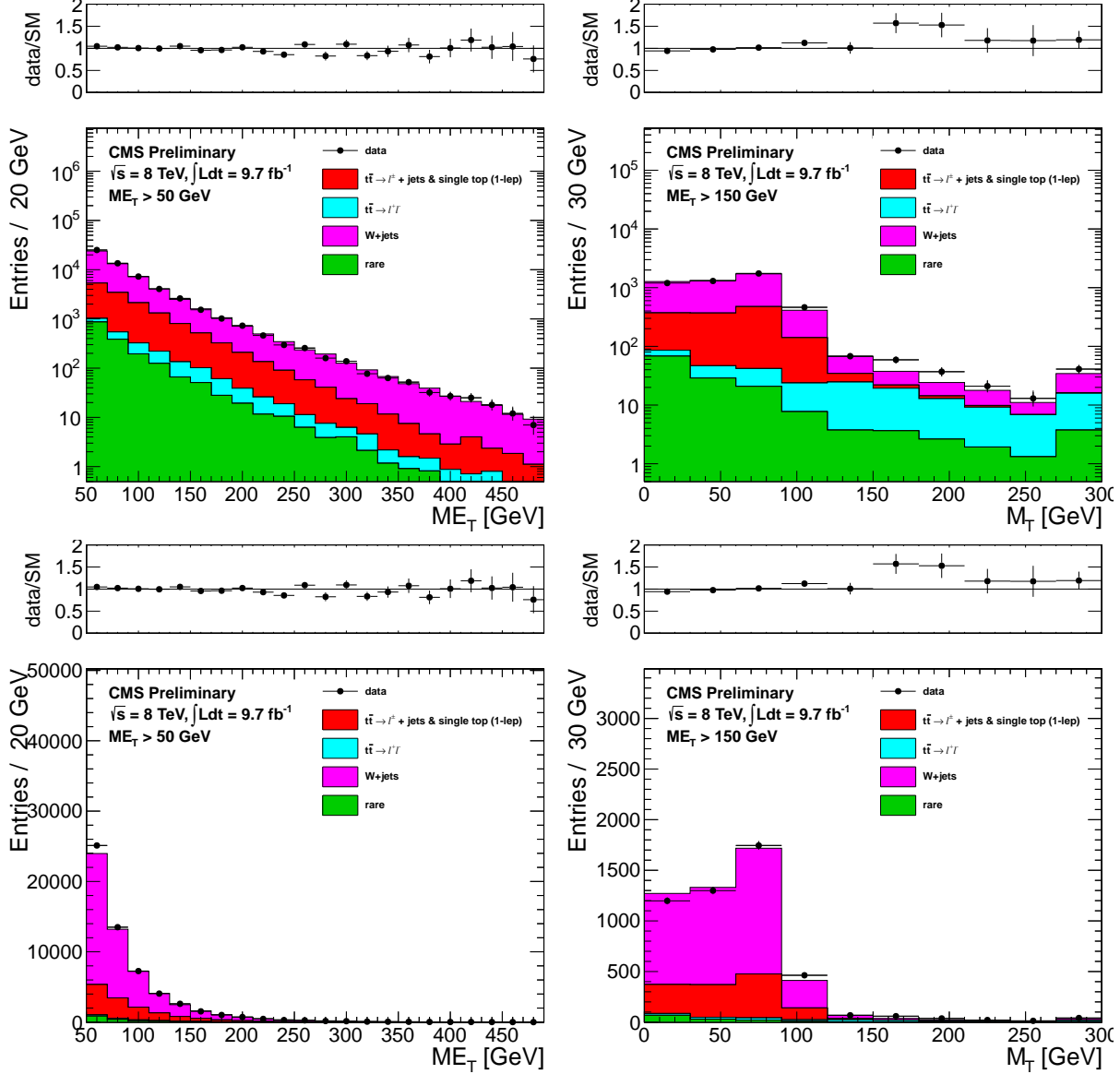


Figure 41: Comparison of the  $E_T^{\text{miss}}$  distribution (left) and the  $M_T$  distribution after a  $E_T^{\text{miss}} > 150 \text{ GeV}$  requirement (right) in data vs. MC for events satisfying the requirements of CR1.

805 D.4 CR2: 0 b-tags, exactly 2 leptons

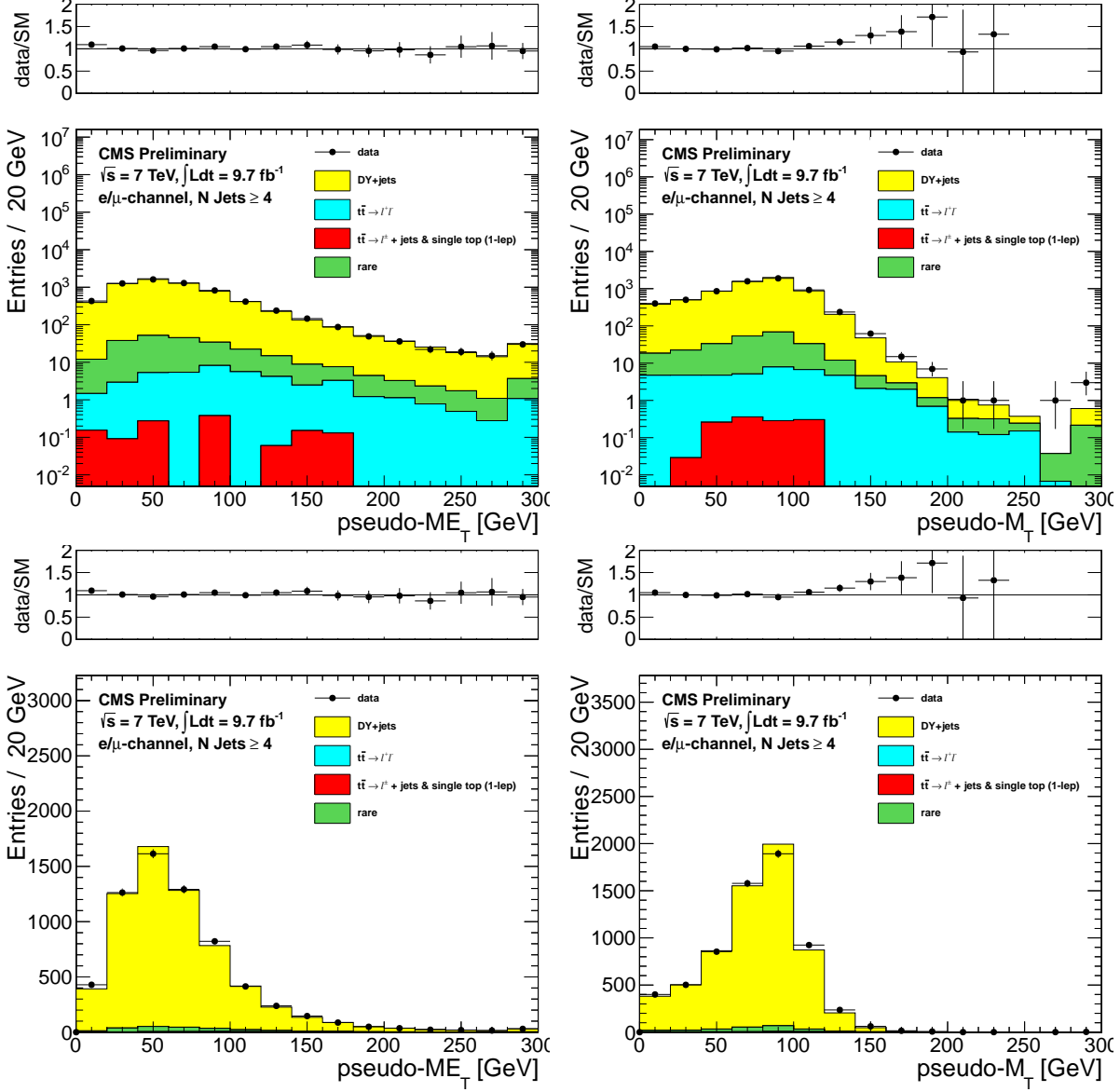


Figure 42: Comparison of the pseudo- $E_T^{\text{miss}}$  distribution (left) and the pseudo- $M_T$  distribution (right) in data vs. MC for CR2.

## 806 E Signal Kinematics

807 This appendix includes some kinematic distributions for a few signal points in the T2tt (Figure 43) and  
 808 T2bw (Figure 44) models. The parameter values shown correspond to the edge of the sensitivity of the  
 809 analysis and reflect the range of kinematics of the signal. The lower  $M(\tilde{t})$  samples have softer  $E_T^{\text{miss}}$  and  
 810  $M_T$  distributions and are thus better targeted by the signal regions with looser requirements. The higher  
 811  $M(\tilde{t})$  samples are harder in  $E_T^{\text{miss}}$  and  $M_T$  and the signal regions with tighter requirements provide higher  
 812 sensitivity to these models.

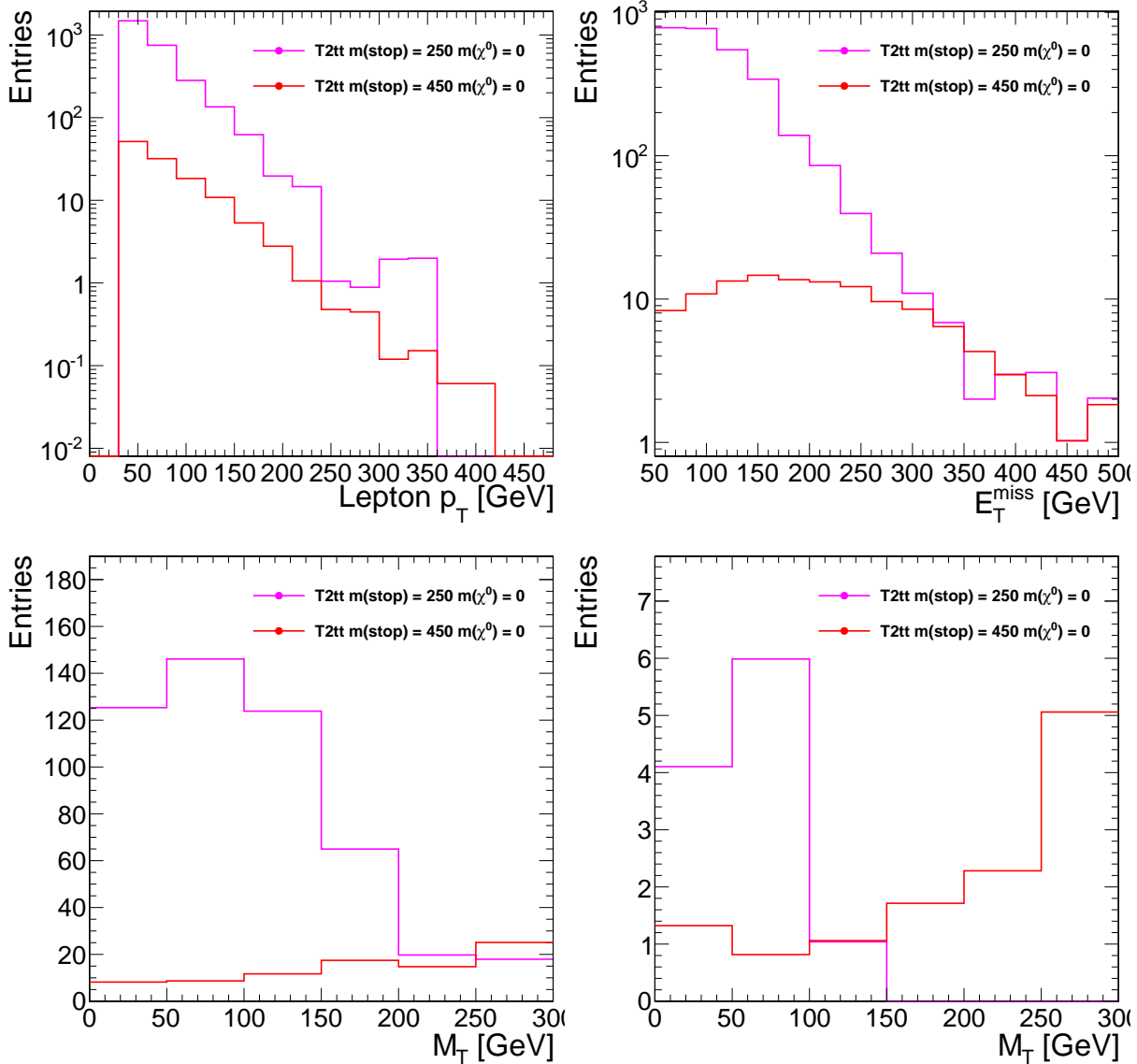


Figure 43: Signal kinematics for two signal points in the T2tt model: the lepton  $p_T$  (top, left), the  $E_T^{\text{miss}}$  (top, right) and the  $M_T$  for two values of the  $E_T^{\text{miss}}$  requirement,  $E_T^{\text{miss}} > 150 \text{ GeV}$  (bottom, left) and  $E_T^{\text{miss}} > 350 \text{ GeV}$  (bottom, right).

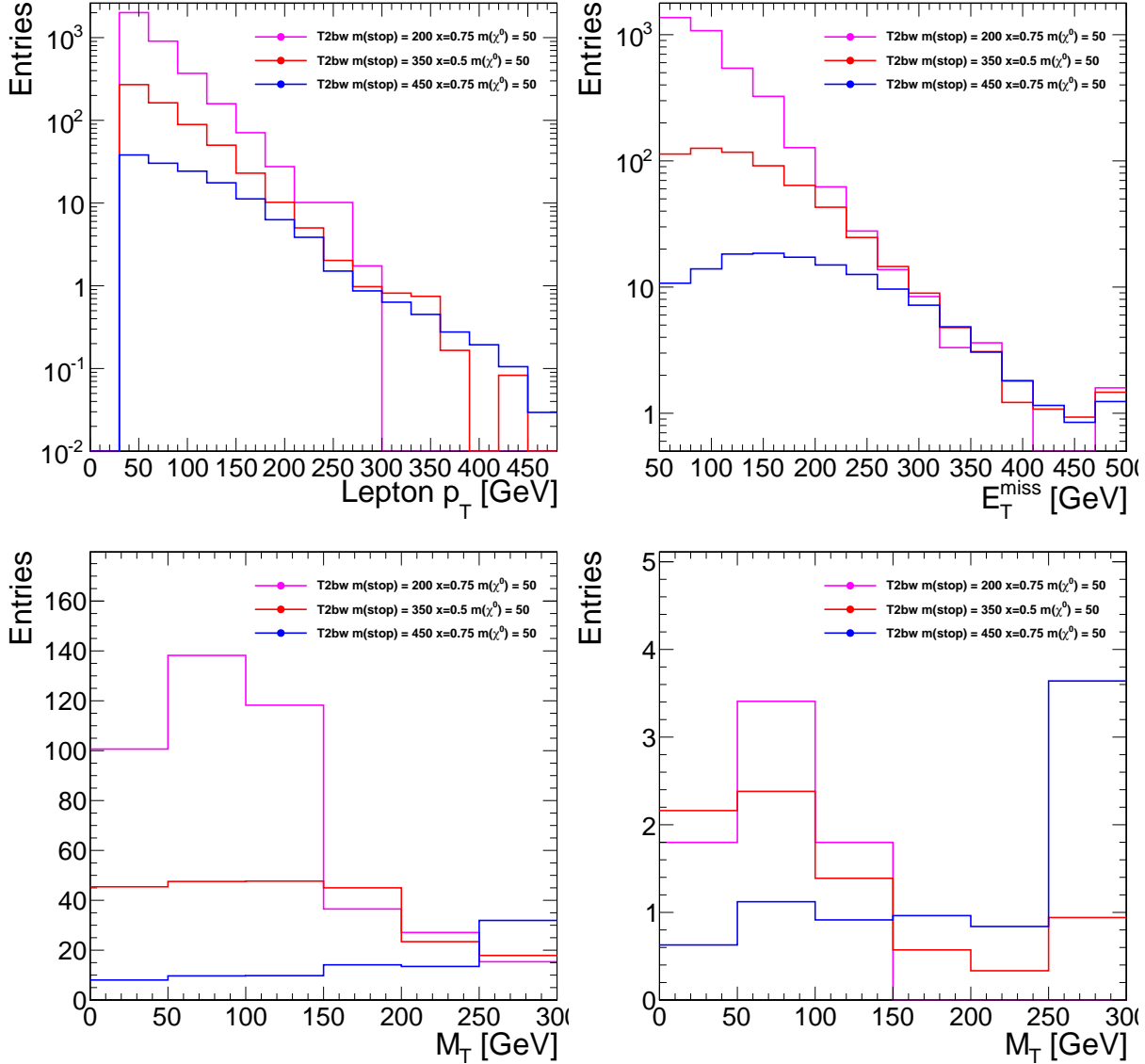


Figure 44: Signal kinematics for three signal points in the T2bw model: the lepton  $p_T$  (top, left), the  $E_T^{\text{miss}}$  (top, right) and the  $M_T$  for two values of the  $E_T^{\text{miss}}$  requirement,  $E_T^{\text{miss}} > 150$  GeV (bottom, left) and  $E_T^{\text{miss}} > 350$  GeV (bottom, right).

## 813 F Model dependence of the signal acceptance

814 The signal acceptance for T2tt events has a significant dependence on the model parameters, particularly  
 815 the mixing angle of left- and right-handed stops. Depending on the choice of mixing angle, the top quarks  
 816 produced in the decay can have a polarization anywhere between  $+p_{\chi_1^0}/E_{\chi^0}$  and  $-p_{\chi_1^0}/E_{\chi^0}$  [4], which for  
 817 a massless  $\chi_1^0$  becomes  $\pm 1$ . For right-handed top quarks, the charged lepton is emitted preferentially in  
 818 the direction parallel to the top velocity, resulting in larger lepton  $p_T$  and  $M_T$ .

819 The default signal MC used in this analysis has unpolarized top quarks. We estimate the impact of the  
 820 top polarization on our signal acceptance by reweighting our signal MC events to match the expected  
 821 distribution of the charged lepton decay angle ( $\theta^*$ ) corresponding to the choice of top polarizations of  
 822  $\pm 1$ . The default and reweighted  $\cos \theta^*$  distributions are shown in Figure 45. Note that this is only an  
 823 approximate study, because the angular distribution is in fact triply differential. We attempt to account  
 824 for the dominant effect.

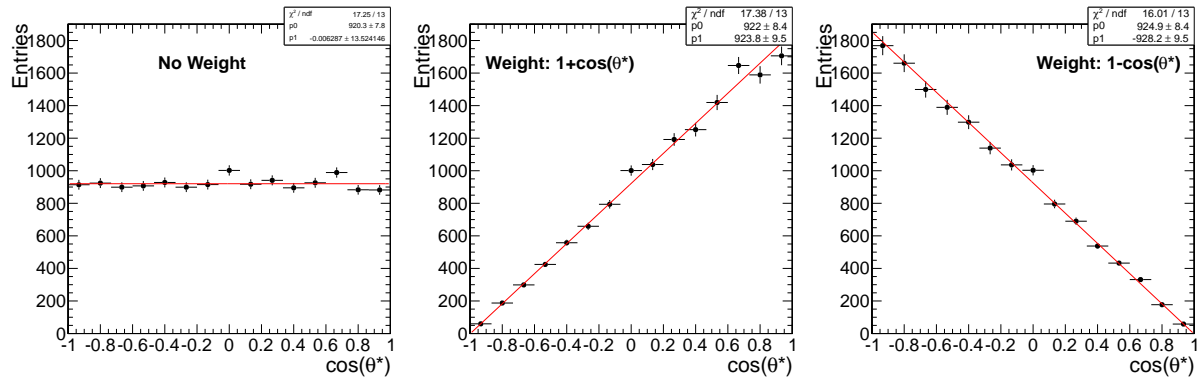


Figure 45: The default and reweighted  $\cos \theta^*$  distributions. The  $1 \pm \cos \theta^*$  weightings correspond to top polarizations of  $\pm 1$ .

825 We find that reweighting to resemble a top polarization of  $+1$  increases the signal acceptance by ap-  
 826 proximately 20-25% relative to the default MC, while using a top polarization of  $-1$  decreases the signal  
 827 acceptance by a similar amount.

## 828 G Glossary of abbreviations

829  $R_{wjet}^{MC}, R_{wjet}$

830 Monte Carlo and corrected ratios of  $W+jets$  events in the  $M_T$  tail to the  $M_T$  peak.

831  $R_{top}^{MC}, R_{top}$

832 Monte Carlo and corrected ratios of  $t\bar{t}$  or single-top  $\ell+jets$  events in the  $M_T$  tail to the  $M_T$  peak.

833  $SFR_{wjet}$

834 Data/MC scale factor for  $R_{wjet}^{MC}$

835

836  $SFR_{top}$

837 Data/MC scale factor for  $R_{top}^{MC}$  (not used)

838

839  $K_3$  and  $K_4$

840 Scale factors for  $t\bar{t} \rightarrow \ell\ell$  events with one or two extra jets from radiation

841

842  $SF_{pre}$  and  $SF_{post}$

843 Scale factors to be applied to MC to normalize to the yields in the  $M_T$  control region before and after  
 844 the application of the isolated track veto.